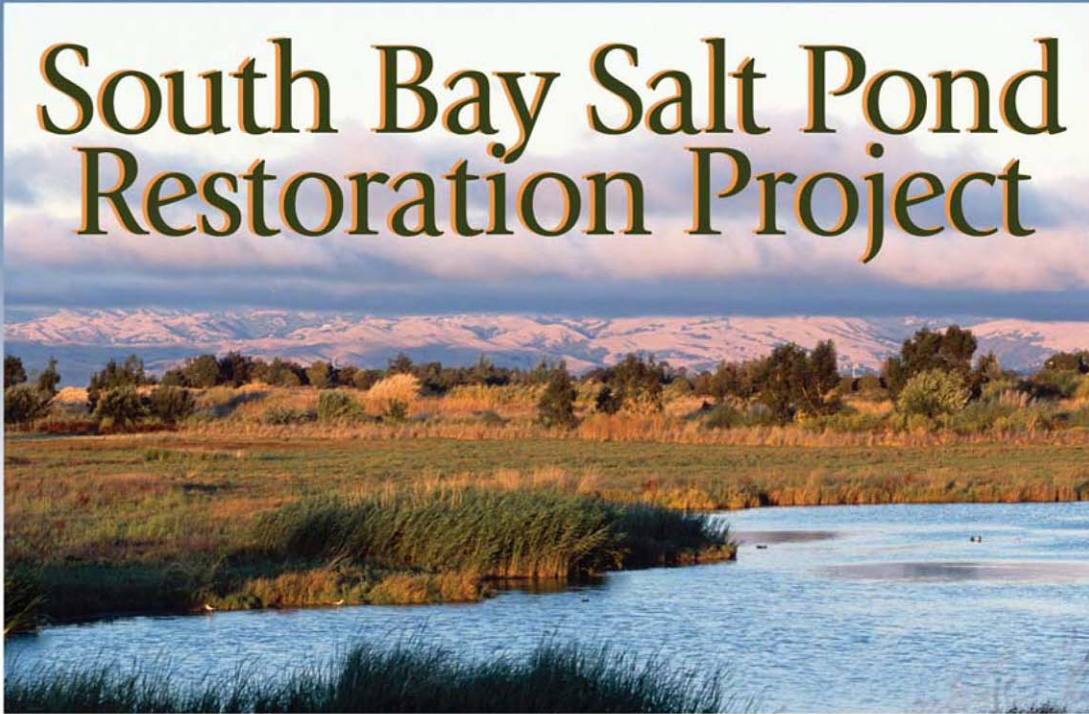


South Bay Salt Pond Restoration Project



Hydrodynamic Modeling Report: Alternatives Analyses

Submitted to:
California State Coastal Conservancy
U.S. Fish & Wildlife Service
California Department of Fish and Game

Prepared by:
PWA (Philip Williams & Associates, Ltd.)

October 2006

TABLE OF CONTENTS

	Page
INTRODUCTION	2-1
1.1 Modeling Objectives	2-1
1.2 Restoration Alternatives	2-1
1.3 NEPA/CEQA Baseline	2-2
1.4 Report Organization	2-3
2. MODELING CONTEXT	2-1
2.1 Model Development	2-1
2.2 Programmatic Modeling Simulations	2-2
2.3 Major Assumptions and Uncertainties	2-3
2.3.1 Phasing	2-4
2.3.2 Level of Detail	2-4
2.3.3 Managed Pond Discharges	2-4
2.3.4 Sediment Transport and Geomorphic Modeling	2-5
2.3.5 Grid Resolution	2-5
2.3.6 Two-dimensional Model Approach	2-6
2.3.7 Long-term Bathymetric Change	2-6
3. RESTORATION SCENARIO MODEL SET-UP	3-1
3.1 Baseline Conditions	3-1
3.1.1 Island Ponds	3-1
3.1.2 Eden Landing Ecological Reserve	3-1
3.1.3 Boundary and Initial Conditions	3-2
3.1.4 Potential Tidal Prism	3-6
3.2 Alternative C – Tidal Habitat Emphasis, Year 0	3-6
3.2.1 Breach Sizes and Locations	3-6
3.2.2 Boundary and Initial Conditions	3-7
3.2.3 Potential Tidal Prism	3-9
3.3 Alternative A – No Action, Year 50	3-9
3.3.1 Ponds	3-10
3.3.2 Tidal Sloughs	3-10
3.3.3 South Bay Bathymetry	3-13
3.3.4 Boundary and Initial Conditions	3-14
3.4 Alternative C – Tidal Habitat Emphasis, Year 50	3-14
3.4.1 Ponds	3-15
3.4.2 Tidal Sloughs	3-15
3.4.3 South Bay Bathymetry	3-16
3.4.4 Boundary and Initial Conditions	3-17
4. ALTERNATIVE C, YEAR 0, SUMMER CONDITIONS	4-1

4.1	Water Levels.....	4-1
4.1.1	South Bay	4-1
4.1.2	Tidal Sloughs	4-3
4.1.3	Ponds	4-5
4.2	Tidal Prism	4-6
4.3	Salinity	4-10
4.3.1	South Bay	4-10
4.3.2	Tidal Sloughs	4-11
4.4	Circulation.....	4-13
4.4.1	Current Velocity	4-14
4.4.2	Residual Circulation	4-16
4.5	Bed Shear Stress.....	4-17
4.5.1	South Bay	4-18
4.5.2	Tidal Sloughs	4-19
5.	ALTERNATIVE C, YEAR 0, WINTER CONDITIONS	5-1
5.1	Water Levels.....	5-1
5.1.1	South Bay	5-1
5.1.2	Tidal Sloughs	5-3
5.1.3	Ponds	5-5
5.2	Tidal Prism	5-7
5.3	Salinity	5-9
5.3.1	South Bay	5-10
5.3.2	Tidal Sloughs	5-10
5.4	Circulation.....	5-13
5.4.1	Current Velocity	5-14
5.4.2	Residual Circulation	5-16
5.5	Bed Shear Stress.....	5-17
5.5.1	South Bay	5-17
5.5.2	Tidal Sloughs	5-18
6.	ALTERNATIVE A, YEAR 50, SUMMER CONDITIONS	6-1
6.1	Water Levels.....	6-1
6.1.1	South Bay	6-1
6.1.2	Tidal Sloughs	6-2
6.2	Tidal Prism	6-4
6.3	Salinity	6-7
6.3.1	South Bay	6-7
6.3.2	Tidal Sloughs	6-8
6.4	Circulation.....	6-10
6.4.1	Current Velocity	6-11
6.4.2	Residual Circulation	6-12
6.5	Bed Shear Stress.....	6-13

6.5.1	South Bay	6-13
6.5.2	Tidal Sloughs	6-14
7. ALTERNATIVE C, YEAR 50, SUMMER CONDITIONS		7-1
7.1	Water Levels	7-1
7.1.1	South Bay	7-1
7.1.2	Tidal Sloughs	7-3
7.2	Tidal Prism	7-5
7.3	Salinity	7-8
7.3.1	South Bay	7-8
7.3.2	Tidal Sloughs	7-9
7.4	Circulation	7-11
7.4.1	Current Velocity	7-12
7.4.2	Residual Circulation	7-14
7.5	Bed Shear Stress	7-15
7.5.1	South Bay	7-15
7.5.2	Tidal Sloughs	7-15
8. REFERENCES		8-1
9. LIST OF PREPARERS		9-1
10. APPENDIX A – MODEL CALIBRATION SUMMARY		10-1
10.1	GSFB Model Calibration and Validation Summary	10-1
10.2	South Bay Model Calibration and Validation Summary	10-2

TABLES

Table 2-1.	Hydrodynamic Model Runs
Table 3-1.	Input and Boundary Condition Data Sources
Table 3-2.	Potential Tidal Prism of ISP Project Areas
Table 3-3.	Potential Tidal Prism of SBSP Alternative C Project Areas
Table 3-4.	Long-term Increase in Tidal Prism, Alternative A
Table 3-5.	Long-term Increase in Channel Depth, Alternative A
Table 3-6.	Long-term Increase in Tidal Prism, Alternative C
Table 3-7.	Long-term Increase in Channel Depth, Alternative C
Table 4-1.	South Bay Tidal Water Surface Elevation and Phase Differences under Alt C, Year 0, Summer
Table 4-2.	Tidal Slough Water Surface Elevation and Phase Differences under Alt C, Year 0, Summer
Table 4-3.	Comparison of Previous Estimates of Tidal Prism with DELFT3D Baseline Estimates
Table 4-4.	Comparison of Tidal Prism between Baseline and Alternative C, year 0, Summer
Table 4-5.	South Bay Salinity Differences under Alt C, Year 0, Summer
Table 4-6.	Tidal Slough Salinity Differences under Alt C, Year 0, Summer

Table 4-7. South Bay Peak Velocity Magnitude Comparisons: Alt C, Year 0, Summer vs. Baseline, Summer

Table 4-8. Tidal Slough Peak Velocity Comparisons: Alt C, Year 0, Summer vs. Baseline, Summer

Table 5-1. South Bay Tidal Water Surface Elevation and Phase Differences under Alt C, Year 0, Winter

Table 5-2. Tidal Slough Water Surface Elevation and Phase Differences under Alt C, Year 0, Winter

Table 5-3. Comparison of Tidal Prism between Baseline and Alternative C, Year 0, Winter

Table 5-4. South Bay Salinity Differences under Alt C, Year 0, Winter

Table 5-5. Tidal Slough Salinity Differences under Alt C, Year 0, Winter

Table 5-6. South Bay Peak Velocity Magnitude Comparisons: Alternative C, Winter, Year 0 vs. Baseline, Winter

Table 5-7. Tidal Slough Peak Velocity Comparisons: Alternative C, Winter, Year 0 vs. Baseline, Winter

Table 6-1. South Bay Tidal Water Surface Elevation and Phase Differences under Alt A, Year 50, Summer

Table 6-2. Tidal Slough Water Surface Elevation and Phase Differences under Alt A, Year 50, Summer

Table 6-3. Comparison of Tidal Prism between Baseline and Alternative A, year 50, summer

Table 6-4. South Bay Salinity Differences under Alt A, Year 50, Summer

Table 6-5. Tidal Slough Salinity Differences under Alt A, Year 50, Summer

Table 6-6. South Bay Peak Velocity Magnitude Comparisons: Alt A, Year 50, Summer vs. Baseline, Summer

Table 6-7. Tidal Slough Peak Velocity Magnitude Comparisons: Alt A, Year 50, Summer vs. Baseline, Summer

Table 7-1. South Bay Water Surface Elevation and Phase Differences under Alt C, Year 50, Summer

Table 7-2. South Bay Tidal Datums Differences under Alt C, Year 50, Summer and Alt A, Year 50, Summer

Table 7-3. Tidal Slough Water Surface Elevation and Phase Differences under Alt C, Year 50, Summer

Table 7-4. Comparison of Tidal Prism between Baseline and Alternative C, year 50, summer

Table 7-5. South Bay Salinity Differences under Alt C, Year 50, Summer

Table 7-6. Tidal Slough Salinity Differences under Alt C, Year 50, Summer

Table 7-7. South Bay Peak Velocity Magnitude Comparisons: Alt C, Year 50, Summer vs. Baseline, Summer

Table 7-8. Tidal Slough Peak Velocity Magnitude Comparisons: Alt C, Year 50, Summer vs. Baseline, Summer

FIGURES

Figure 2-1. Greater San Francisco Bay Model Extent and Bathymetry

Figure 2-2. Greater San Francisco Bay Model Grid Resolution

Figure 2-3. South Bay Model Extent and Bathymetry

Figure 2-4. South Bay Model Grid Resolution

Figure 3-1. Baseline, Eden Landing

Figure 3-2. Baseline, Alviso

Figure 3-3. Baseline, Ravenswood

Figure 3-4. Model Bathymetry, Island Ponds
Figure 3-5. Model Bathymetry, Eden Landing Restoration
Figure 3-6. Model Open Boundary, Water Level and Salinity, May-June 2001
Figure 3-7. Alternative C: Tidal Habitat Emphasis, Eden Landing, Year 0
Figure 3-8. Alternative C: Tidal Habitat Emphasis, Alviso, Year 0
Figure 3-9. Alternative C: Tidal Habitat Emphasis, Ravenswood, Year 0
Figure 3-10. Station Locations
Figure 3-11. South Bay Model Open Boundary Comparison
Figure 3-12. GSFB Model Water Level Comparisons
Figure 3-13. GSFB and South Bay Model Tidal Prism Comparisons
Figure 3-14. South Bay Model Water Level Comparisons
Figure 3-15. Eden Landing Breach Locations
Figure 3-16. Alviso Breach Locations
Figure 3-17. Ravenswood Breach Locations
Figure 3-18. Alternative A: No Action, Eden Landing, Year 50
Figure 3-19. Alternative A: No Action, Alviso, Year 50
Figure 3-20. Alternative A: No Action, Ravenswood, Year 50
Figure 4-1. South Bay Stations
Figure 4-2. Eden Landing Stations
Figure 4-3. Ravenswood Stations
Figure 4-4. Alviso Stations
Figure 4-5. Time Series Snapshot Points
Figure 4-6. Water Levels, San Mateo Bridge, Alt C, Year 0, Summer
Figure 4-7. Water Levels, Dumbarton Bridge, Alt C, Year 0, Summer
Figure 4-8. Water Levels, Channel Marker 17, Alt C, Year 0, Summer
Figure 4-9. Changes in MLLW, Alt C, Year 0, Summer
Figure 4-10. Changes in MHHW, Alt C, Year 0, Summer
Figure 4-11. Changes in Tidal Propagation, Alt C, Year 0, Summer
Figure 4-12. Water Levels, ACFCC Downstream, Alt C, Year 0, Summer
Figure 4-13. Water Levels, ACFCC Upstream, Alt C, Year 0, Summer
Figure 4-14. Water Levels, Old Alameda Creek Downstream, Alt C, Year 0, Summer
Figure 4-15. Water Levels, Old Alameda Creek Upstream, Alt C, Year 0, Summer
Figure 4-16. Water Levels, Coyote Creek Power Tower, Alt C, Year 0, Summer
Figure 4-17. Water Levels, Coyote Creek Railroad Bridge, Alt C, Year 0, Summer
Figure 4-18. Water Levels, Coyote Creek/Island Ponds, Year 0, Summer
Figure 4-19. Water Levels, Coyote Creek Upstream, Year 0, Summer
Figure 4-20. Water Levels, Mud Slough Downstream, Alt C, Year 0, Summer
Figure 4-21. Water Levels, Mud Slough Upstream, Alt C, Year 0, Summer
Figure 4-22. Water Levels, Alviso Slough Downstream, Alt C, Year 0, Summer
Figure 4-23. Water Levels, Alviso Slough Upstream, Alt C, Year 0, Summer
Figure 4-24. Water Levels, Guadalupe Slough Downstream, Alt C, Year 0, Summer
Figure 4-25. Water Levels, Guadalupe Slough Upstream, Alt C, Year 0, Summer
Figure 4-26. Water Levels, Moffett Channel, Alt C, Year 0, Summer

Figure 4-27. Water Levels, Steven Creek Downstream, Alt C, Year 0, Summer
Figure 4-28. Water Levels, Stevens Creek Upstream, Alt C, Year 0, Summer
Figure 4-29. Water Levels, Mountain View Slough Downstream, Alt C, Year 0, Summer
Figure 4-30. Water Levels, Mountain View Slough Upstream, Alt C, Year 0, Summer
Figure 4-31. Water Levels, Charleston Slough Downstream, Alt C, Year 0, Summer
Figure 4-32. Water Levels, Charleston Slough Upstream, Alt C, Year 0, Summer
Figure 4-33. Water Levels, Ravenswood Slough Downstream, Alt C, Year 0, Summer
Figure 4-34. Water Levels, Ravenswood Slough Upstream, Alt C, Year 0, Summer
Figure 4-35. Water Levels, Pond A20, Alt C, Year 0, Summer
Figure 4-36. Water Levels, ELER North, Alt C, Year 0, Summer
Figure 4-37. Water Levels, ELER South, Alt C, Year 0, Summer
Figure 4-38. Water Levels, Pond E6B, Alt C, Year 0, Summer
Figure 4-39. Water Levels, Pond A7, Alt C, Year 0, Summer
Figure 4-40. Water Levels, Pond A8, Alt C, Year 0, Summer
Figure 4-41. South Bay Tidal Prism Cross-Section Locations
Figure 4-42. Eden Landing Tidal Prism Cross-Section Locations
Figure 4-43. Alviso Tidal Prism Cross-Section Locations
Figure 4-44. Ravenswood Tidal Prism Cross-Section Locations
Figure 4-45. Tidal Prism, San Mateo and Dumbarton Bridges, Alt C, Year 0, Summer
Figure 4-46. Tidal Prism, Channel Marker 17 and Calaveras Point, Alt C, Year 0, Summer
Figure 4-47. Tidal Prism, ACFCC and Old Alameda Creek, Alt C, Year 0, Summer
Figure 4-48. Tidal Prism, Coyote Creek, Alt C, Year 0, Summer
Figure 4-49. Tidal Prism, Alviso and Guadalupe Sloughs, Alt C, Year 0, Summer
Figure 4-50. Tidal Prism, Stevens Creek and, Mountain View Sloughs, Alt C, Year 0, Summer
Figure 4-51. Tidal Prism, Charleston and Ravenswood Sloughs, Alt C, Year 0, Summer
Figure 4-52. Salinity at Spring HHW Jun – Aug, Alt C, Year 0, Summer
Figure 4-53. Salinity, San Mateo Bridge, Alt C, Year 0, Summer
Figure 4-54. Salinity, Dumbarton Bridge, Alt C, Year 0, Summer
Figure 4-55. Salinity, Channel Marker 17, Alt C, Year 0, Summer
Figure 4-56. Salinity at Spring HHW, Alt C, Year 0, Summer
Figure 4-57. Salinity at Spring LLW, Alt C, Year 0, Summer
Figure 4-58. Salinity, ACFCC Downstream, Alt C, Year 0, Summer
Figure 4-59. Salinity, ACFCC Upstream, Alt C, Year 0, Summer
Figure 4-60. Salinity, Old Alameda Creek Downstream, Alt C, Year 0, Summer
Figure 4-61. Salinity, Old Alameda Creek Upstream, Alt C, Year 0, Summer
Figure 4-62. Salinity at Spring HHW, Eden Landing, Alt C, Year 0, Summer
Figure 4-63. Salinity at Spring LLW, Eden Landing, Alt C, Year 0, Summer
Figure 4-64. Salinity, Coyote Creek Power Tower, Alt C, Year 0, Summer
Figure 4-65. Salinity, Coyote Creek Railroad Bridge, Alt C, Year 0, Summer
Figure 4-66. Salinity, Coyote Creek/Island Ponds, Year 0, Summer
Figure 4-67. Salinity, Coyote Creek Upstream, Year 0, Summer
Figure 4-68. Salinity, Mud Slough Downstream, Alt C, Year 0, Summer
Figure 4-69. Salinity, Mud Slough Upstream, Alt C, Year 0, Summer

Figure 4-70. Salinity, Alviso Slough Downstream, Alt C, Year 0, Summer Summer
Figure 4-71. Salinity, Alviso Slough Upstream, Alt C, Year 0, Summer Summer
Figure 4-72. Salinity, Guadalupe Slough Downstream, Alt C, Year 0, Summer Summer
Figure 4-73. Salinity, Guadalupe Slough Upstream, Alt C, Year 0, Summer Summer
Figure 4-74. Salinity, Moffett Channel, Alt C, Year 0, Summer Summer
Figure 4-75. Salinity, Steven Creek Downstream, Alt C, Year 0, Summer Summer
Figure 4-76. Salinity, Stevens Creek Upstream, Alt C, Year 0, Summer Summer
Figure 4-77. Salinity, Mountain View Slough Downstream, Alt C, Year 0, Summer Summer
Figure 4-78. Salinity, Mountain View Slough Upstream, Alt C, Year 0, Summer Summer
Figure 4-79. Salinity, Charleston Slough Downstream, Alt C, Year 0, Summer Summer
Figure 4-80. Salinity, Charleston Slough Upstream, Alt C, Year 0, Summer Summer
Figure 4-81. Salinity at Spring HHW, Alt C, Alviso, Year 0, Summer Summer
Figure 4-82. Salinity at Spring LLW, Alt C, Alviso, Year 0, Summer Summer
Figure 4-83. Salinity, Ravenswood Slough Downstream, Ravenswood, Alt C, Year 0, Summer Summer
Figure 4-84. Salinity, Ravenswood Slough Upstream, Ravenswood, Alt C, Year 0, Summer Summer
Figure 4-85. Salinity at Spring HHW, Ravenswood, Alt C, Year 0, Summer
Figure 4-86. Salinity at Spring LLW, Ravenswood, Alt C, Year 0, Summer
Figure 4-87. Velocity, San Mateo Bridge, Alt C, Year 0, Summer
Figure 4-88. Velocity, Dumbarton Bridge, Alt C, Year 0, Summer
Figure 4-89. Velocity, Channel Marker 17, Alt C, Year 0, Summer
Figure 4-90. Velocity at Spring Flood, Alt C, Year 0, Summer
Figure 4-91. Velocity at Spring Ebb, Alt C, Year 0, Summer
Figure 4-92. Velocity, ACFCC Downstream, Alt C, Year 0, Summer
Figure 4-93. Velocity, Old Alameda Creek Downstream, Alt C, Year 0, Summer
Figure 4-94. Velocity at Spring Flood, Eden Landing, Alt C, Year 0, Summer
Figure 4-95. Velocity at Spring Ebb, Eden Landing, Alt C, Year 0, Summer
Figure 4-96. Velocity, Coyote Creek Power Tower, Alt C, Year 0, Summer
Figure 4-97. Velocity, Coyote Creek Railroad Bridge, Alt C, Year 0, Summer
Figure 4-98. Velocity, Coyote Creek/Island Ponds, Year 0, Summer
Figure 4-99. Velocity, Mud Slough Downstream, Alt C, Year 0, Summer
Figure 4-100. Velocity, Alviso Slough Downstream, Alt C, Year 0, Summer
Figure 4-101. Velocity, Guadalupe Slough Downstream, Alt C, Year 0, Summer
Figure 4-102. Velocity, Moffett Channel, Alt C, Year 0, Summer
Figure 4-103. Velocity, Steven Creek Downstream, Alt C, Year 0, Summer
Figure 4-104. Velocity, Mountain View Slough Downstream, Alt C, Year 0, Summer
Figure 4-105. Velocity, Charleston Slough Downstream, Alt C, Year 0, Summer
Figure 4-106. Velocity at Spring Flood, Alviso, Alt C, Year 0, Summer
Figure 4-107. Velocity at Spring Ebb, Alviso, Alt C, Year 0, Summer
Figure 4-108. Velocity, Ravenswood Slough Downstream, Alt C, Year 0, Summer
Figure 4-109. Velocity at Spring Flood, Ravenswood, Alt C, Year 0, Summer
Figure 4-110. Velocity at Spring Ebb, Ravenswood, Alt C, Year 0, Summer
Figure 4-111. South Bay Residual Circulation, Baseline, Summer
Figure 4-112. South Bay Residual Circulation, Alt C, Year 0, Summer

Figure 4-113. South Bay Residual Circulation, Difference, Year 0, Summer
Figure 4-114. Far South Bay Residual Circulation, Baseline, Summer
Figure 4-115. Far South Bay Residual Circulation, Alt C, Year 0, Summer
Figure 4-116. Far South Bay Residual Circulation, Difference, Year 0, Summer
Figure 4-117. Tidal Bed Shear Stress, South Bay, Alt C, Year 0, Summer
Figure 4-118. Tidal Bed Shear Stress, Eden Landing, Alt C, Year 0, Summer
Figure 4-119. Tidal Bed Shear Stress, Alviso, Alt C, Year 0, Summer
Figure 4-120. Tidal Bed Shear Stress, Ravenswood, Alt C, Year 0, Summer
Figure 4-121. Total Bed Shear Stress, South Bay, Alt C, Year 0, Summer
Figure 4-122. Total Bed Shear Stress, Eden Landing, Alt C, Year 0, Summer
Figure 4-123. Total Bed Shear Stress, Alviso, Alt C, Year 0, Summer
Figure 4-124. Total Bed Shear Stress, Ravenswood, Alt C, Year 0, Summer
Figure 5-1. Water Levels, San Mateo Bridge, Alt C, Year 0, Winter
Figure 5-2. Water Levels, Dumbarton Bridge, Alt C, Year 0, Winter
Figure 5-3. Water Levels, Channel Marker 17, Alt C, Year 0, Winter
Figure 5-4. Changes in MLLW, Alt C, Year 0, Winter
Figure 5-5. Changes in MHHW, Alt C, Year 0, Winter
Figure 5-6. Changes in Tidal Propagation, Alt C, Year 0, Winter
Figure 5-7. Water Levels, ACFCC Downstream, Alt C, Year 0, Winter
Figure 5-8. Water Levels, ACFCC Upstream, Alt C, Year 0, Winter
Figure 5-9. Water Levels, Old Alameda Creek Downstream, Alt C, Year 0, Winter
Figure 5-10. Water Levels, Old Alameda Creek Upstream, Alt C, Year 0, Winter
Figure 5-11. Water Levels, Coyote Creek Power Tower, Alt C, Year 0, Winter
Figure 5-12. Water Levels, Coyote Creek Railroad Bridge, Alt C, Year 0, Winter
Figure 5-13. Water Levels, Coyote Creek/Island Ponds, Year 0, Winter
Figure 5-14. Water Levels, Coyote Creek Upstream, Year 0, Winter
Figure 5-15. Water Levels, Mud Slough Downstream, Alt C, Year 0, Winter
Figure 5-16. Water Levels, Mud Slough Upstream, Alt C, Year 0, Winter
Figure 5-17. Water Levels, Alviso Slough Downstream, Alt C, Year 0, Winter
Figure 5-18. Water Levels, Alviso Slough Upstream, Alt C, Year 0, Winter
Figure 5-19. Water Levels, Guadalupe Slough Downstream, Alt C, Year 0, Winter
Figure 5-20. Water Levels, Guadalupe Slough Upstream, Alt C, Year 0, Winter
Figure 5-21. Water Levels, Moffett Channel, Alt C, Year 0, Winter
Figure 5-22. Water Levels, Steven Creek Downstream, Alt C, Year 0, Winter
Figure 5-23. Water Levels, Stevens Creek Upstream, Alt C, Year 0, Winter
Figure 5-24. Water Levels, Mountain View Slough Downstream, Alt C, Year 0, Winter
Figure 5-25. Water Levels, Mountain View Slough Upstream, Alt C, Year 0, Winter
Figure 5-26. Water Levels, Charleston Slough Downstream, Alt C, Year 0, Winter
Figure 5-27. Water Levels, Charleston Slough Upstream, Alt C, Year 0, Winter
Figure 5-28. Water Levels, Ravenswood Slough Downstream, Alt C, Year 0, Winter
Figure 5-29. Water Levels, Ravenswood Slough Upstream, Alt C, Year 0, Winter
Figure 5-30. Water Levels, Pond A20, Alt C, Year 0, Winter
Figure 5-31. Water Levels, ELER North, Alt C, Year 0, Winter

Figure 5-32. Water Levels, ELER South, Alt C, Year 0, Winter
Figure 5-33. Water Levels, Pond E6B, Alt C, Year 0, Winter
Figure 5-34. Water Levels, Pond A7, Alt C, Year 0, Winter
Figure 5-35. Water Levels, Pond A8, Alt C, Year 0, Winter
Figure 5-36. Tidal Prism, San Mateo and Dumbarton Bridges, Alt C, Year 0, Winter
Figure 5-37. Tidal Prism, Channel Marker 17 and Calaveras Point, Alt C, Year 0, Winter
Figure 5-38. Tidal Prism, ACFCC and Old Alameda Creek, Alt C, Year 0, Winter
Figure 5-39. Tidal Prism, Coyote Creek, Alt C, Year 0, Winter
Figure 5-40. Tidal Prism, Alviso and Guadalupe Sloughs, Alt C, Year 0, Winter
Figure 5-41. Tidal Prism, Stevens Creek and, Mountain View Sloughs, Alt C, Year 0, Winter
Figure 5-42. Tidal Prism, Charleston and Ravenswood Sloughs, Alt C, Year 0, Winter
Figure 5-43. Salinity, San Mateo Bridge, Alt C, Year 0, Winter
Figure 5-44. Salinity, Dumbarton Bridge, Alt C, Year 0, Winter
Figure 5-45. Salinity, Channel Marker 17, Alt C, Year 0, Winter
Figure 5-46. Salinity at Spring HHW, Alt C, Year 0, Winter
Figure 5-47. Salinity at Spring LLW, Alt C, Year 0, Winter
Figure 5-48. Salinity, ACFCC Downstream, Alt C, Year 0, Winter
Figure 5-49. Salinity, ACFCC Upstream, Alt C, Year 0, Winter
Figure 5-50. Salinity, Old Alameda Creek Downstream, Alt C, Year 0, Winter
Figure 5-51. Salinity, Old Alameda Creek Upstream, Alt C, Year 0, Winter
Figure 5-52. Salinity at Spring HHW, Eden Landing, Alt C, Year 0, Winter
Figure 5-53. Salinity at Spring LLW, Eden Landing, Alt C, Year 0, Winter
Figure 5-54. Salinity, Coyote Creek Power Tower, Alt C, Year 0, Winter
Figure 5-55. Salinity, Coyote Creek Railroad Bridge, Alt C, Year 0, Winter
Figure 5-56. Salinity, Coyote Creek/Island Ponds, Year 0, Winter
Figure 5-57. Salinity, Coyote Creek Upstream, Year 0, Winter
Figure 5-58. Salinity, Mud Slough Downstream, Alt C, Year 0, Winter
Figure 5-59. Salinity, Mud Slough Upstream, Alt C, Year 0, Winter
Figure 5-60. Salinity, Alviso Slough Downstream, Alt C, Year 0, Winter
Figure 5-61. Salinity, Alviso Slough Upstream, Alt C, Year 0, Winter
Figure 5-62. Salinity, Guadalupe Slough Downstream, Alt C, Year 0, Winter
Figure 5-63. Salinity, Guadalupe Slough Upstream, Alt C, Year 0, Winter
Figure 5-64. Salinity, Moffett Channel, Alt C, Year 0, Winter
Figure 5-65. Salinity, Steven Creek Downstream, Alt C, Year 0, Winter
Figure 5-66. Salinity, Stevens Creek Upstream, Alt C, Year 0, Winter
Figure 5-67. Salinity, Mountain View Slough Downstream, Alt C, Year 0, Winter
Figure 5-68. Salinity, Mountain View Slough Upstream, Alt C, Year 0, Winter
Figure 5-69. Salinity, Charleston Slough Downstream, Alt C, Year 0, Winter
Figure 5-70. Salinity, Charleston Slough Upstream, Alt C, Year 0, Winter
Figure 5-71. Salinity at Spring HHW, Alt C, Alviso, Year 0, Winter
Figure 5-72. Salinity at Spring LLW, Alt C, Alviso, Year 0, Winter
Figure 5-73. Salinity, Ravenswood Slough Downstream, Ravenswood, Alt C, Year 0, Winter
Figure 5-74. Salinity, Ravenswood Slough Upstream, Ravenswood, Alt C, Year 0, Winter

Figure 5-75. Salinity at Spring HHW, Ravenswood, Alt C, Year 0, Winter
 Figure 5-76. Salinity at Spring LLW, Ravenswood, Alt C, Year 0, Winter
 Figure 5-77. Velocity, San Mateo Bridge, Alt C, Year 0, Winter
 Figure 5-78. Velocity, Dumbarton Bridge, Alt C, Year 0, Winter
 Figure 5-79. Velocity, Channel Marker 17, Alt C, Year 0, Winter
 Figure 5-80. Velocity at Spring Flood, Alt C, Year 0, Winter
 Figure 5-81. Velocity at Spring Ebb, Alt C, Year 0, Winter
 Figure 5-82. Velocity, ACFCC Downstream, Alt C, Year 0, Winter
 Figure 5-83. Velocity, Old Alameda Creek Downstream, Alt C, Year 0, Winter
 Figure 5-84. Velocity at Spring Flood, Eden Landing, Alt C, Year 0, Winter
 Figure 5-85. Velocity at Spring Ebb, Eden Landing, Alt C, Year 0, Winter
 Figure 5-86. Velocity, Coyote Creek Power Tower, Alt C, Year 0, Winter
 Figure 5-87. Velocity, Coyote Creek Railroad Bridge, Alt C, Year 0, Winter
 Figure 5-88. Velocity, Coyote Creek/Island Ponds, Year 0, Winter
 Figure 5-89. Velocity, Mud Slough Downstream, Alt C, Year 0, Winter
 Figure 5-90. Velocity, Alviso Slough Downstream, Alt C, Year 0, Winter
 Figure 5-91. Velocity, Guadalupe Slough Downstream, Alt C, Year 0, Winter
 Figure 5-92. Velocity, Moffett Channel, Alt C, Year 0, Winter
 Figure 5-93. Velocity, Steven Creek Downstream, Alt C, Year 0, Winter
 Figure 5-94. Velocity, Mountain View Slough Downstream, Alt C, Year 0, Winter
 Figure 5-95. Velocity, Charleston Slough Downstream, Alt C, Year 0, Winter
 Figure 5-96. Velocity at Spring Flood, Alviso, Alt C, Year 0, Winter
 Figure 5-97. Velocity at Spring Ebb, Alviso, Alt C, Year 0, Winter
 Figure 5-98. Velocity, Ravenswood Slough Downstream, Alt C, Year 0, Winter
 Figure 5-99. Velocity at Spring Flood, Ravenswood, Alt C, Year 0, Winter
 Figure 5-100. Velocity at Spring Ebb, Ravenswood, Alt C, Year 0, Winter
 Figure 5-101. South Bay Residual Circulation, Baseline, Winter
 Figure 5-102. South Bay Residual Circulation, Alt C, Year 0, Winter
 Figure 5-103. South Bay Residual Circulation, Difference, Year 0, Winter
 Figure 5-104. Far South Bay Residual Circulation, Baseline, Winter
 Figure 5-105. Far South Bay Residual Circulation, Alt C, Year 0, Winter
 Figure 5-106. Far South Bay Residual Circulation, Difference, Year 0, Winter
 Figure 5-107. Tidal Bed Shear Stress, South Bay, Alt C, Year 0, Winter
 Figure 5-108. Tidal Bed Shear Stress, Eden Landing, Alt C, Year 0, Winter
 Figure 5-109. Tidal Bed Shear Stress, Alviso, Alt C, Year 0, Winter
 Figure 5-110. Tidal Bed Shear Stress, Ravenswood, Alt C, Year 0, Winter
 Figure 5-111. Total Bed Shear Stress, South Bay, Alt C, Year 0, Winter
 Figure 5-112. Total Bed Shear Stress, Eden Landing, Alt C, Year 0, Winter
 Figure 5-113. Total Bed Shear Stress, Alviso, Alt C, Year 0, Winter
 Figure 5-114. Total Bed Shear Stress, Ravenswood, Alt C, Year 0, Winter
 Figure 6-1. Water Levels, San Mateo Bridge, Alt A, Year 50, Summer
 Figure 6-2. Water Levels, Dumbarton Bridge, Alt A, Year 50, Summer
 Figure 6-3. Water Levels, Channel Marker 17, Alt A, Year 50, Summer

Figure 6-4. Changes in MLLW, Alt A, Year 50, Summer
Figure 6-5. Changes in MHHW, Alt A, Year 50, Summer
Figure 6-6. Changes in Tidal Propagation, Alt A, Year 50, Summer
Figure 6-7. Water Levels, ACFCC Downstream, Alt A, Year 50, Summer
Figure 6-8. Water Levels, ACFCC Upstream, Alt A, Year 50, Summer
Figure 6-9. Water Levels, Old Alameda Creek Downstream, Alt A, Year 50, Summer
Figure 6-10. Water Levels, Old Alameda Creek Upstream, Alt A, Year 50, Summer
Figure 6-11. Water Levels, Coyote Creek Power Tower, Alt A, Year 50, Summer
Figure 6-12. Water Levels, Coyote Creek Railroad Bridge, Alt A, Year 50, Summer
Figure 6-13. Water Levels, Coyote Creek/Island Ponds, Year 50, Summer
Figure 6-14. Water Levels, Coyote Creek Upstream, Year 50, Summer
Figure 6-15. Water Levels, Mud Slough Downstream, Alt A, Year 50, Summer
Figure 6-16. Water Levels, Mud Slough Upstream, Alt A, Year 50, Summer
Figure 6-17. Water Levels, Alviso Slough Downstream, Alt A, Year 50, Summer
Figure 6-18. Water Levels, Alviso Slough Upstream, Alt A, Year 50, Summer
Figure 6-19. Water Levels, Guadalupe Slough Downstream, Alt A, Year 50, Summer
Figure 6-20. Water Levels, Guadalupe Slough Upstream, Alt A, Year 50, Summer
Figure 6-21. Water Levels, Moffett Channel, Alt A, Year 50, Summer
Figure 6-22. Water Levels, Steven Creek Downstream, Alt A, Year 50, Summer
Figure 6-23. Water Levels, Stevens Creek Upstream, Alt A, Year 50, Summer
Figure 6-24. Water Levels, Mountain View Slough Downstream, Alt A, Year 50, Summer
Figure 6-25. Water Levels, Mountain View Slough Upstream, Alt A, Year 50, Summer
Figure 6-26. Water Levels, Charleston Slough Downstream, Alt A, Year 50, Summer
Figure 6-27. Water Levels, Charleston Slough Upstream, Alt A, Year 50, Summer
Figure 6-28. Water Levels, Ravenswood Slough Downstream, Alt A, Year 50, Summer
Figure 6-29. Water Levels, Ravenswood Slough Upstream, Alt A, Year 50, Summer
Figure 6-30. Tidal Prism, San Mateo and Dumbarton Bridges, Alt A, Year 50, Summer
Figure 6-31. Tidal Prism, Channel Marker 17 and Calaveras Point, Alt A, Year 50, Summer
Figure 6-32. Tidal Prism, ACFCC and Old Alameda Creek, Alt C, Year A, Summer
Figure 6-33. Tidal Prism, Coyote Creek, Alt A, Year 50, Summer
Figure 6-34. Tidal Prism, Alviso and Guadalupe Sloughs, Alt A, Year 50, Summer
Figure 6-35. Tidal Prism, Stevens Creek and, Mountain View Sloughs, Alt A, Year 50, Summer
Figure 6-36. Tidal Prism, Charleston and Ravenswood Sloughs, Alt A, Year 50, Summer
Figure 6-37. Salinity, San Mateo Bridge, Alt A, Year 50, Summer
Figure 6-38. Salinity, Dumbarton Bridge, Alt A, Year 50, Summer
Figure 6-39. Salinity, Channel Marker 17, Alt A, Year 50, Summer
Figure 6-40. Salinity at Spring HHW, Alt A, Year 50, Summer
Figure 6-41. Salinity at Spring LLW, Alt A, Year 50, Summer
Figure 6-42. Salinity, ACFCC Downstream, Alt A, Year 50, Summer
Figure 6-43. Salinity, ACFCC Upstream, Alt A, Year 50, Summer
Figure 6-44. Salinity, Old Alameda Creek Downstream, Alt A, Year 50, Summer
Figure 6-45. Salinity, Old Alameda Creek Upstream, Alt A, Year 50, Summer
Figure 6-46. Salinity at Spring HHW, Eden Landing, Alt A, Year 50, Summer

Figure 6-47. Salinity at Spring LLW, Eden Landing, Alt A, Year 50, Summer
Figure 6-48. Salinity, Coyote Creek Power Tower, Alt A, Year 50, Summer
Figure 6-49. Salinity, Coyote Creek Railroad Bridge, Alt A, Year 50, Summer
Figure 6-50. Salinity, Coyote Creek/Island Ponds, Year 50, Summer
Figure 6-51. Salinity, Coyote Creek Upstream, Year 50, Summer
Figure 6-52. Salinity, Mud Slough Downstream, Alt A, Year 50, Summer
Figure 6-53. Salinity, Mud Slough Upstream, Alt A, Year 50, Summer
Figure 6-54. Salinity, Alviso Slough Downstream, Alt A, Year 50, Summer
Figure 6-55. Salinity, Alviso Slough Upstream, Alt A, Year 50, Summer
Figure 6-56. Salinity, Guadalupe Slough Downstream, Alt A, Year 50, Summer
Figure 6-57. Salinity, Guadalupe Slough Upstream, Alt A, Year 50, Summer
Figure 6-58. Salinity, Moffett Channel, Alt A, Year 50, Summer
Figure 6-59. Salinity, Steven Creek Downstream, Alt A, Year 50, Summer
Figure 6-60. Salinity, Stevens Creek Upstream, Alt A, Year 50, Summer
Figure 6-61. Salinity, Mountain View Slough Downstream, Alt A, Year 50, Summer
Figure 6-62. Salinity, Mountain View Slough Upstream, Alt A, Year 50, Summer
Figure 6-63. Salinity, Charleston Slough Downstream, Alt A, Year 50, Summer
Figure 6-64. Salinity, Charleston Slough Upstream, Alt A, Year 50, Summer
Figure 6-65. Salinity at Spring HHW, Alt A, Alviso, Year 50, Summer
Figure 6-66. Salinity at Spring LLW, Alt A, Alviso, Year 50, Summer
Figure 6-67. Salinity, Ravenswood Slough Downstream, Ravenswood, Alt A, Year 50, Summer
Figure 6-68. Salinity, Ravenswood Slough Upstream, Ravenswood, Alt A, Year 50, Summer
Figure 6-69. Salinity at Spring HHW, Ravenswood, Alt A, Year 50, Summer
Figure 6-70. Salinity at Spring LLW, Ravenswood, Alt A, Year 50, Summer
Figure 6-71. Velocity, San Mateo Bridge, Alt A, Year 50, Summer
Figure 6-72. Velocity, Dumbarton Bridge, Alt A, Year 50, Summer
Figure 6-73. Velocity, Channel Marker 17, Alt A, Year 50, Summer
Figure 6-74. Velocity at Spring Flood, Alt A, Year 50, Summer
Figure 6-75. Velocity at Spring Ebb, Alt A, Year 50, Summer
Figure 6-76. Velocity, ACFCC Downstream, Alt A, Year 50, Summer
Figure 6-77. Velocity, Old Alameda Creek Downstream, Alt A, Year 50, Summer
Figure 6-78. Velocity at Spring Flood, Eden Landing, Alt A, Year 50, Summer
Figure 6-79. Velocity at Spring Ebb, Eden Landing, Alt A, Year 50, Summer
Figure 6-80. Velocity, Coyote Creek Power Tower, Alt A, Year 50, Summer
Figure 6-81. Velocity, Coyote Creek Railroad Bridge, Alt A, Year 50, Summer
Figure 6-82. Velocity, Coyote Creek/Island Ponds, Year 50, Summer
Figure 6-83. Velocity, Mud Slough Downstream, Alt A, Year 50, Summer
Figure 6-84. Velocity, Alviso Slough Downstream, Alt A, Year 50, Summer
Figure 6-85. Velocity, Guadalupe Slough Downstream, Alt A, Year 50, Summer
Figure 6-86. Velocity, Moffett Channel, Alt A, Year 50, Summer
Figure 6-87. Velocity, Steven Creek Downstream, Alt A, Year 50, Summer
Figure 6-88. Velocity, Mountain View Slough Downstream, Alt A, Year 50, Summer
Figure 6-89. Velocity, Charleston Slough Downstream, Alt A, Year 50, Summer

Figure 6-90. Velocity at Spring Flood, Alviso, Alt A, Year 50, Summer
Figure 6-91. Velocity at Spring Ebb, Alviso, Alt A, Year 50, Summer
Figure 6-92. Velocity, Ravenswood Slough Downstream, Alt A, Year 50, Summer
Figure 6-93. Velocity at Spring Flood, Ravenswood, Alt A, Year 50, Summer
Figure 6-94. Velocity at Spring Ebb, Ravenswood, Alt A, Year 50, Summer
Figure 6-95. South Bay Residual Circulation, Baseline, Summer
Figure 6-96. South Bay Residual Circulation, Alt A, Year 50, Summer
Figure 6-97. South Bay Residual Circulation, Difference, Year 50, Summer
Figure 6-98. Far South Bay Residual Circulation, Baseline, Summer
Figure 6-99. Far South Bay Residual Circulation, Alt A, Year 50, Summer
Figure 6-100. Far South Bay Residual Circulation, Difference, Year 50, Summer
Figure 6-101. Tidal Bed Shear Stress, South Bay, Alt A, Year 50, Summer
Figure 6-102. Tidal Bed Shear Stress, Eden Landing, Alt A, Year 50, Summer
Figure 6-103. Tidal Bed Shear Stress, Alviso, Alt A, Year 50, Summer
Figure 6-104. Tidal Bed Shear Stress, Ravenswood, Alt A, Year 50, Summer
Figure 6-105. Total Bed Shear Stress, South Bay, Alt A, Year 50, Summer
Figure 6-106. Total Bed Shear Stress, Eden Landing, Alt A, Year 50, Summer
Figure 6-107. Total Bed Shear Stress, Alviso, Alt A, Year 50, Summer
Figure 6-108. Total Bed Shear Stress, Ravenswood, Alt A, Year 50, Summer
Figure 7-1. Water Levels, San Mateo Bridge, Alt C, Year 50, Summer
Figure 7-2. Water Levels, Dumbarton Bridge, Alt C, Year 50, Summer
Figure 7-3. Water Levels, Channel Marker 17, Alt C, Year 50, Summer
Figure 7-4. Changes in MLLW, Alt C, Year 50, Summer
Figure 7-5. Changes in MHHW, Alt C, Year 50, Summer
Figure 7-6. Changes in Tidal Propagation, Alt C, Year 50, Summer
Figure 7-7. Water Levels, ACFCC Downstream, Alt C, Year 50, Summer
Figure 7-8. Water Levels, ACFCC Upstream, Alt C, Year 50, Summer
Figure 7-9. Water Levels, Old Alameda Creek Downstream, Alt C, Year 50, Summer
Figure 7-10. Water Levels, Old Alameda Creek Upstream, Alt C, Year 50, Summer
Figure 7-11. Water Levels, Coyote Creek Power Tower, Alt C, Year 50, Summer
Figure 7-12. Water Levels, Coyote Creek Railroad Bridge, Alt C, Year 50, Summer
Figure 7-13. Water Levels, Coyote Creek/Island Ponds, Year 50, Summer
Figure 7-14. Water Levels, Coyote Creek Upstream, Year 50, Summer
Figure 7-15. Water Levels, Mud Slough Downstream, Alt C, Year 50, Summer
Figure 7-16. Water Levels, Mud Slough Upstream, Alt C, Year 50, Summer
Figure 7-17. Water Levels, Alviso Slough Downstream, Alt C, Year 50, Summer
Figure 7-18. Water Levels, Alviso Slough Upstream, Alt C, Year 50, Summer
Figure 7-19. Water Levels, Guadalupe Slough Downstream, Alt C, Year 50, Summer
Figure 7-20. Water Levels, Guadalupe Slough Upstream, Alt C, Year 50, Summer
Figure 7-21. Water Levels, Moffett Channel, Alt C, Year 50, Summer
Figure 7-22. Water Levels, Steven Creek Downstream, Alt C, Year 50, Summer
Figure 7-23. Water Levels, Stevens Creek Upstream, Alt C, Year 50, Summer
Figure 7-24. Water Levels, Mountain View Slough Downstream, Alt C, Year 50, Summer

Figure 7-25. Water Levels, Mountain View Slough Upstream, Alt C, Year 50, Summer
Figure 7-26. Water Levels, Charleston Slough Downstream, Alt C, Year 50, Summer
Figure 7-27. Water Levels, Charleston Slough Upstream, Alt C, Year 50, Summer
Figure 7-28. Water Levels, Ravenswood Slough Downstream, Alt C, Year 50, Summer
Figure 7-29. Water Levels, Ravenswood Slough Upstream, Alt C, Year 50, Summer
Figure 7-30. Tidal Prism, San Mateo and Dumbarton Bridges, Alt C, Year 50, Summer
Figure 7-31. Tidal Prism, Channel Marker 17 and Calaveras Point, Alt C, Year 50, Summer
Figure 7-32. Tidal Prism, ACFCC and Old Alameda Creek, Alt C, Year 50, Summer
Figure 7-33. Tidal Prism, Coyote Creek, Alt C, Year 50, Summer
Figure 7-34. Tidal Prism, Alviso and Guadalupe Sloughs, Alt C, Year 50, Summer
Figure 7-35. Tidal Prism, Stevens Creek and, Mountain View Sloughs, Alt C, Year50, Summer
Figure 7-36. Tidal Prism, Charleston and Ravenswood Sloughs, Alt C, Year 50, Summer
Figure 7-37. Salinity, San Mateo Bridge, Alt C, Year 50, Summer
Figure 7-38. Salinity, Dumbarton Bridge, Alt C, Year 50, Summer
Figure 7-39. Salinity, Channel Marker 17, Alt C, Year 50, Summer
Figure 7-40. Salinity at Spring HHW, Alt C, Year 50, Summer
Figure 7-41. Salinity at Spring LLW, Alt C, Year 50, Summer
Figure 7-42. Salinity, ACFCC Downstream, Alt C, Year 50, Summer
Figure 7-43. Salinity, ACFCC Upstream, Alt C, Year 50, Summer
Figure 7-44. Salinity, Old Alameda Creek Downstream, Alt C, Year 50, Summer
Figure 7-45. Salinity, Old Alameda Creek Upstream, Alt C, Year 50, Summer
Figure 7-46. Salinity at Spring HHW, Eden Landing, Alt C, Year 50, Summer
Figure 7-47. Salinity at Spring LLW, Eden Landing, Alt C, Year 50, Summer
Figure 7-48. Salinity, Coyote Creek Power Tower, Alt C, Year 50, Summer
Figure 7-49. Salinity, Coyote Creek Railroad Bridge, Alt C, Year 50, Summer
Figure 7-50. Salinity, Coyote Creek/Island Ponds, Year 50, Summer
Figure 7-51. Salinity, Coyote Creek Upstream, Year 50, Summer
Figure 7-52. Salinity, Mud Slough Downstream, Alt C, Year 50, Summer
Figure 7-53. Salinity, Mud Slough Upstream, Alt C, Year 50, Summer
Figure 7-54. Salinity, Alviso Slough Downstream, Alt C, Year 50, Summer
Figure 7-55. Salinity, Alviso Slough Upstream, Alt C, Year 50, Summer
Figure 7-56. Salinity, Guadalupe Slough Downstream, Alt C, Year 50, Summer
Figure 7-57. Salinity, Guadalupe Slough Upstream, Alt C, Year 50, Summer
Figure 7-58. Salinity, Moffett Channel, Alt C, Year 50, Summer
Figure 7-59. Salinity, Steven Creek Downstream, Alt C, Year 50, Summer
Figure 7-60. Salinity, Stevens Creek Upstream, Alt C, Year 50, Summer
Figure 7-61. Salinity, Mountain View Slough Downstream, Alt C, Year 50, Summer
Figure 7-62. Salinity, Mountain View Slough Upstream, Alt C, Year 50, Summer
Figure 7-63. Salinity, Charleston Slough Downstream, Alt C, Year 50, Summer
Figure 7-64. Salinity, Charleston Slough Upstream, Alt C, Year 50, Summer
Figure 7-65. Salinity at Spring HHW, Alt C, Alviso, Year 50, Summer
Figure 7-66. Salinity at Spring LLW, Alt C, Alviso, Year 50, Summer
Figure 7-67. Salinity, Ravenswood Slough Downstream, Ravenswood, Alt C, Year 50, Summer

Figure 7-68. Salinity, Ravenswood Slough Upstream, Ravenswood, Alt C, Year 50, Summer
Figure 7-69. Salinity at Spring HHW, Ravenswood, Alt C, Year 50, Summer
Figure 7-70. Salinity at Spring LLW, Ravenswood, Alt C, Year 50, Summer
Figure 7-71. Velocity, San Mateo Bridge, Alt C, Year 50, Summer
Figure 7-72. Velocity, Dumbarton Bridge, Alt C, Year 50, Summer
Figure 7-73. Velocity, Channel Marker 17, Alt C, Year 50, Summer
Figure 7-74. Velocity at Spring Flood, Alt C, Year 50, Summer
Figure 7-75. Velocity at Spring Ebb, Alt C, Year 50, Summer
Figure 7-76. Velocity, ACFCC Downstream, Alt C, Year 50, Summer
Figure 7-77. Velocity, Old Alameda Creek Downstream, Alt C, Year 50, Summer
Figure 7-78. Velocity at Spring Flood, Eden Landing, Alt C, Year 50, Summer
Figure 7-79. Velocity at Spring Ebb, Eden Landing, Alt C, Year 50, Summer
Figure 7-80. Velocity, Coyote Creek Power Tower, Alt C, Year 50, Summer
Figure 7-81. Velocity, Coyote Creek Railroad Bridge, Alt C, Year 50, Summer
Figure 7-82. Velocity, Coyote Creek/Island Ponds, Year 50, Summer
Figure 7-83. Velocity, Mud Slough Downstream, Alt C, Year 50, Summer
Figure 7-84. Velocity, Alviso Slough Downstream, Alt C, Year 50, Summer
Figure 7-85. Velocity, Guadalupe Slough Downstream, Alt C, Year 50, Summer
Figure 7-86. Velocity, Moffett Channel, Alt C, Year 50, Summer
Figure 7-87. Velocity, Steven Creek Downstream, Alt C, Year 50, Summer
Figure 7-88. Velocity, Mountain View Slough Downstream, Alt C, Year 50, Summer
Figure 7-89. Velocity, Charleston Slough Downstream, Alt C, Year 50, Summer
Figure 7-90. Velocity at Spring Flood, Alviso, Alt C, Year 50, Summer
Figure 7-91. Velocity at Spring Ebb, Alviso, Alt C, Year 50, Summer
Figure 7-92. Velocity, Ravenswood Slough Downstream, Alt C, Year 50, Summer
Figure 7-93. Velocity at Spring Flood, Ravenswood, Alt C, Year 50, Summer
Figure 7-94. Velocity at Spring Ebb, Ravenswood, Alt C, Year 50, Summer
Figure 7-95. South Bay Residual Circulation, Baseline, Summer
Figure 7-96. South Bay Residual Circulation, Alt C, Year 50, Summer
Figure 7-97. South Bay Residual Circulation, Difference, Year 50, Summer
Figure 7-98. Far South Bay Residual Circulation, Baseline, Summer
Figure 7-99. Far South Bay Residual Circulation, Alt C, Year 50, Summer
Figure 7-100. Far South Bay Residual Circulation, Difference, Summer
Figure 7-101. Tidal Bed Shear Stress, South Bay, Alt C, Year 50, Summer
Figure 7-102. Tidal Bed Shear Stress, Eden Landing, Alt C, Year 50, Summer
Figure 7-103. Tidal Bed Shear Stress, Alviso, Alt C, Year 50, Summer
Figure 7-104. Tidal Bed Shear Stress, Ravenswood, Alt C, Year 50, Summer
Figure 7-105. Total Bed Shear Stress, South Bay, Alt C, Year 50, Summer
Figure 7-106. Total Bed Shear Stress, Eden Landing, Alt C, Year 50, Summer
Figure 7-107. Total Bed Shear Stress, Alviso, Alt C, Year 50, Summer
Figure 7-108. Total Bed Shear Stress, Ravenswood, Alt C, Year 50, Summer
Figure 10-1. GSFBR Summer 2001 Salinity, Pier 24/Bay Bridge
Figure 10-2. GSFBR Summer 2001 Salinity, San Mateo Bridge

Figure 10-3. GSFb Summer 2001 Salinity Transect
Figure 10-4. GSFb Summer 2001 Salinity Transect
Figure 10-5. GSFb Summer 2001 Salinity Transect
Figure 10-6. GSFb Summer 2000 Salinity, Pier 24/Bay Bridge
Figure 10-7. GSFb Summer 2000 Salinity, San Mateo Bridge
Figure 10-8. GSFb Summer 2000 Salinity Transect
Figure 10-9. GSFb Summer 2000 Salinity Transect
Figure 10-10. GSFb Winter 2004 Salinity, San Mateo Bridge
Figure 10-11. GSFb Winter 2004 Salinity, Dumbarton Bridge
Figure 10-12. GSFb Winter 2004 Salinity, Channel Marker 17
Figure 10-13. GSFb Winter 2004 Salinity Transect
Figure 10-14. GSFb Winter 2004 Salinity Transect
Figure 10-15. South Bay Winter 2004 Salinity, San Mateo Bridge
Figure 10-16. South Bay Winter 2004 Salinity, Dumbarton
Figure 10-17. South Bay Winter 2004 Salinity, Channel Marker 17
Figure 10-18. South Bay Winter 2004 Salinity, Power Tower
Figure 10-19. South Bay Winter 2004 Salinity, Railroad Bridge
Figure 10-20. South Bay Winter 2004 Salinity, Alviso Slough
Figure 10-21. South Bay Winter 2004 Salinity, ACFCC
Figure 10-22. South Bay Winter 2004 Salinity Transect

ABBREVIATIONS AND ACRONYMS

1D	One-dimensional
2D	Two-dimensional
3D	Three-dimensional
ACFCWCD	Alameda County Flood Control and Water Conservation District
ACFCC	Alameda Creek Flood Control Channel
ADF	Alternatives Development Framework
aka	also known as
BAAQMD	Bay Area Air Quality Management District
Bay	San Francisco Bay
CO-OPS	Center for Operational Oceanographic Products and Services
CEM	Coastal Engineering Manual
Central Bay	Central San Francisco Bay
CEQA	California Environmental Quality Act
Corps	U.S. Army Corps of Engineers
CIMIS	California Irrigation Management Information System
Delta	San Francisco Bay Delta
EBRPD	East Bay Regional Park District
EIR	Environmental Impact Record
EIS	Environmental Impact Statement
far South Bay	portion of the South Bay south of Dumbarton Bridge
GSFB	Greater San Francisco Bay DELFT3D Model
HEC-RAS	Hydrologic Engineering System – River Analysis System
HHW	high high water
HLW	high low water
ISP	Initial Stewardship Plan
LiDAR	Light Detection and Ranging
LLW	low low water
NCDC	National Climate Data Center
NEPA	National Environmental Policy Act
NHC	Northwest Hydraulic Consultants
NOAA	National Oceanic and Atmospheric Administration
NOS	National Ocean Service
North Bay	North San Francisco Bay
MHHW	mean higher high water
MLLW	mean lower low water
PMT	Project Management Team
ppt	parts per thousand
PWA	Philip Williams & Associates, Ltd.
RMP	Regional Monitoring Program
RWQCB	Regional Water Quality Control Board
SBSP	South Bay Salt Pond

SCVWD	Santa Clara Valley Water District
SFO Study	San Francisco International Airport Runway Reconfiguration Study
SFPORTS	San Francisco Physical Oceanographic Real-Time System
Shoreline Study	South San Francisco Bay Shoreline Study
South Bay	South San Francisco Bay
SPM	Shore Protection Manual
SWAN	Simulating Waves Nearshore
USGS	U.S. Geological Survey
WSE	water surface elevation
WWTP	Waste Water Treatment Plant

INTRODUCTION

This document presents the results of the programmatic hydrodynamic modeling for the South Bay Salt Pond (Sbsp) Restoration Project. Restoring ponds to tidal inundation has the potential to significantly alter the dynamics of the South Bay through changes in hydrodynamic and geomorphic processes. In order to evaluate these potential changes, a two-dimensional (2D) DELFT3D hydrodynamic model of the South Bay has been calibrated and validated for use in evaluating alternatives and National Environmental Policy Act / California Environmental Quality Act (NEPA/CEQA) impact analysis. A detailed description of the model set-up, calibration and validation process, and input and boundary condition data can be found in PWA (2006a).

1.1 Modeling Objectives

The programmatic modeling for the Sbsp Restoration Project is designed to support project planning and NEPA/CEQA environmental impact analyses. The objective of the modeling is to assess ecosystem-scale response to large-scale tidal restoration, and to bound the range of potential impacts and habitat conditions. The modeling focuses on understanding system-wide responses to restoring 90-percent of the 15,000-acre planning area to tidal action (Alternative C). The No Action Alternative (Alternative A) is also modeled, and both alternatives are compared to fall 2006 baseline conditions. Alternative B, which restores 50-percent of the planning area to tidal action, was not explicitly modeled as it represents an intermediate point between Alternatives A and C; therefore, the impacts associated with Alternative B can be qualitatively assessed based on the results of the Alternative A and C simulations. The modeled alternatives incorporate conceptual design features such as approximate levee breach locations and sizes in order to mobilize the potential tidal prism within the tidally-restored ponds, and, therefore exert the maximum impact on South Bay hydrodynamics.

The planning and modeling of the Phase 1 actions will be used to evaluate specific operations and management regimes as well as the layout of pond-specific design features such as breach locations and islands. The objective of this modeling will be to more clearly define both local and system-wide impacts associated with the restoration of individual ponds and small pond clusters prior to implementation. This document addresses only the programmatic modeling efforts. Phase 1 modeling and analyses, as appropriate, will be addressed separately.

1.2 Restoration Alternatives

The modeled scenarios are based on the alternatives presented in the Final Alternatives Report (PWA and others 2006). The alternatives represent potential “end states” at year 50, meaning they represent a best guess at the eventual landscape based on the desired habitat mix. It is fully anticipated that the landscape that will evolve over time through the implementation of phased project actions will not be exactly what is depicted by any of the end-state alternatives. Instead, the future landscape will be the result of modifications to the restoration plan over time within the context of the programmatic decision process and adaptive management to best achieve the Project Objectives. Thus the evaluation of the alternatives

for the Project by its very nature will not be as precise as if this were a project aimed at constructing one particular facility such as a building.

In summary, the alternatives are defined as:

- **Alternative A: No Action.** This is the most likely outcome in the absence of implementing a long-term restoration plan. Alternative A assumes that, over time, pond operations and management would become more limited. With continued levee subsidence, wave erosion and sea-level rise, the levees would be increasingly prone to failure. Measures would be used to slow deterioration of key flood protection levees as funding allows, and other levees would be allowed to erode, restoring tidal action to some ponds through uncontrolled breaching.
- **Alternative B: Managed Pond Emphasis (50:50 Tidal Habitat : Managed Ponds by area).** Alternative B emphasizes managed pond habitat and provides approximately 7,500 acres each of tidal marsh and managed pond habitat. Approximately 20 percent of the managed ponds (approximately 1,600 acres) would be reconfigured to significantly enhance foraging, roosting, and nesting opportunities for shorebirds, waterfowl, and other waterbirds. The remaining ponds would be managed for target bird species with minimal reconstruction and grading. A system of shoreline levees would be designed to provide coastal flood protection and minimize fluvial flood risks, and new recreation, education, and interpretive opportunities would be provided.
- **Alternative C: Tidal Habitat Emphasis (90:10 Tidal Habitat : Managed Ponds by area).** Alternative C emphasizes tidal restoration and provides approximately 13,400 acres of tidal marsh habitat and 1,600 acres of managed pond habitat. All managed ponds under Alternative C would be reconfigured to significantly enhance foraging, roosting, and nesting opportunities for shorebirds, waterfowl, and other waterbirds. As with Alternative B, a system of shoreline levees would be designed to provide coastal flood protection and minimize fluvial flood risks, and new recreation, education, and interpretive opportunities would be provided.

1.3 NEPA/CEQA Baseline

For the EIS/R, the baseline for evaluating the alternatives is assumed to be set at fall 2006 to allow consideration of recent Initial Stewardship Plan (ISP) actions and their effects on the ponds for certain topics (e.g., water quality and biological resources). In addition to the ISP, the Eden Landing Ecological Reserve will be considered part of the baseline. However, this baseline is set in the future (at the time of this writing), and ISP operations have continued to change since the first actions were implemented in 2004 (see California Department of Fish and Game 2005; U.S. Fish and Wildlife Service 2005; U.S. Fish and Wildlife Service 2006) in order to meet pond discharge requirements. Fall 2006 pond operations are likely to differ from both previous and current operations, and the exact management scheme is unknown. Based on this and other considerations, the modeling calibration and validation focused on the 2000 to 2004 period, or pre-ISP conditions. For restoration scenario simulations, summer 2001 and winter 2004 boundary and initial condition data (e.g., tides, winds, etc.) will be utilized. A complete description of the boundary and initial condition data is presented in PWA (2006a).

1.4 Report Organization

This report is divided into six major sections, describing the important aspects of the hydrodynamic modeling for NEPA/CEQA impact analysis for the SBSP Restoration Project:

- **Section 2. Modeling Context.** This section provides a brief review of the major assumptions in the programmatic modeling and provides a brief description of the modeling simulations under consideration.
- **Section 3. Restoration Scenario Model Set-up.** This section describes additional model set-up required for scenario modeling simulations.
- **Section 4. Alternative C, Year 0, Summer Conditions.** This section presents the results of the hydrodynamic modeling for Alternative C at year 0 under summer conditions, and provides a comparison with baseline conditions. The year 0 simulations provide a hypothetical “maximum impact” scenario assuming all tidally-restored ponds are restored at once.
- **Section 5. Alternative C, Year 0, Winter Conditions.** This section presents the results of the hydrodynamic modeling for Alternative C at year 0 under winter conditions, and provides a comparison with baseline conditions. The year 0 simulations provide a hypothetical “maximum impact” scenario assuming all tidally-restored ponds are restored at once.
- **Section 6. Alternative A, Year 50, Summer Conditions.** This section presents the results of the hydrodynamic modeling for Alternative A, the No Action Alternative, at year 50 under summer conditions, and provides a comparison with baseline conditions.
- **Section 7. Alternative C, Year 50, Summer Conditions.** This section presents the results of the hydrodynamic modeling for Alternative C at year 50 under summer conditions, and provides a comparison with baseline conditions.

<This page intentionally left blank>

2. MODELING CONTEXT

A challenge facing the SBSP Restoration Project is the overall timing of the project schedule. A major goal of the project is to select Phase 1 actions and usher them through final design so implementation can begin in 2008. In order to meet this schedule in a timely fashion, and stay within the Project budget, the analysis approach throughout the planning process is designed to match the level of analysis with the planning needs at each stage. The analyses presented herein were designed to evaluate the programmatic alternatives for the long-term restoration plan and guide the assessment of impacts in the EIS/R. The analyses presented herein were not designed to evaluate the Phase 1 actions; the analysis and modeling of the Phase 1 actions is presented in separate technical appendices to the EIS/R.

2.1 Model Development

DELFT3D was chosen as the primary hydrodynamic modeling tool for the SBSP Restoration Project. DELFT3D, developed by WL | Delft Hydraulics in coordination with Delft University, consists of an integrated set of modules that simulate hydrodynamic flow, scalar transport (e.g., salinity and temperature), and wave generation and propagation through integration with the SWAN wave model (Booij and others 1999; WL | Delft Hydraulics 2003). DELFT3D simulates a large number of physical processes, including wind shear, wave forces, tidal forces, density-driven flows, atmospheric pressure, evaporation, precipitation, flow through hydraulic structures, and drying and flooding of intertidal mudflats (WL | Delft Hydraulics 2003). A curvilinear flexible-mesh grid system is utilized, which allows some capacity to vary the grid resolution over the domain.

The modeling effort for the SBSP Restoration Project aims to capture the full hydrodynamic effects of the Sacramento-San Joaquin Delta-San Francisco Bay-Pacific Ocean system, while focusing on the impacts within the South Bay, defined as the region south of the San Bruno Shoal (from Coyote Point on the western shore to San Leandro Marina on the eastern shore). These two goals are not realistic through the use of a single DELFT3D model, since the grid resolution required to resolve features within the restoration area cannot practically be applied to the larger system. Consequently, a nested two model approach was developed; a larger, low-resolution model (the Greater San Francisco Bay Model, or GSFB Model) covers the entire system while a higher-resolution model covers the South Bay (the South Bay Model).

The primary purpose of the GSFB Model is to provide boundary condition data for the South Bay Model near the Oakland-Bay Bridge. The GSFB Model was originally developed by the U. S. Geological Survey (USGS) (Barnard and others in press) for examining flows through the Golden Gate, and was refined to complete the NEPA/CEQA impact analyses. The model includes much of the Bay-Delta system, extending as far upstream as Big Break on the San Joaquin branch and as far as Rio Vista on the Sacramento branch (Figure 2-1). The model also extends past the Golden Gate approximately 50 km into the Pacific Ocean, extending as far north as Point Reyes and as far south as Half Moon Bay. The grid cell resolutions vary throughout the domain, with higher resolutions used for areas of interest and areas with significant spatial information, and lower resolutions applied where such requirements are lessened. Near

the mouth of the Golden Gate and throughout much of the North Bay and Delta, characteristic grid cell sizes are 200 m (Figure 2-2). In the South Bay, and along the direct approach to the Golden Gate, characteristic sizes are 500 m.

The South Bay Model includes the portions of San Francisco Bay south of the Oakland-Bay Bridge and includes the entire South Bay and the three pond complexes: the Alviso pond complex located at the southernmost end of the far South Bay (south of Dumbarton Bridge), the Ravenswood pond complex located on the western side of the Dumbarton Bridge, and the Eden Landing pond complex located on the eastern shore just south of the San Mateo Bridge (Figure 2-3). The model grid also includes tidal sloughs in the South Bay including downstream portions of Coyote Creek, Alviso Slough, Mud Slough, Guadalupe Slough, and the Alameda Creek Flood Control Channel. The computational grid was developed using DELFT3D's curvilinear flexible mesh grid system in order to allow for a gradual increase in resolution with increasing distance from the Bay Bridge. The grid was constructed using a resolution on the order 100 to 150 m at the Bay Bridge, and 15 to 20 m south of Calaveras Point (Figure 2-4). Details with respect to both the GSFB and the South Bay Models are documented in the Hydrodynamic Model Calibration Report (PWA 2006a), and a summary of the model calibration is presented in Appendix A.

2.2 Programmatic Modeling Simulations

The modeling strategy is based on performing six primary simulations, as presented in Table 2-1, focused on evaluating Alternatives A and C. These alternatives represent the “bookends” with respect to tidal restoration. At year 0, Alternative A represents baseline conditions with no tidal restoration occurring within the project area other than the Island Ponds (A19, A20 and A21) and the Eden Landing Ecological Reserve. In order to account for seasonal variations, baseline conditions were simulated under summer conditions (run 1) and winter conditions (run 2). These simulations will be used as the basis for evaluating potential impacts, as they approximate existing conditions and the NEPA/CEQA baseline (Section 1.3).

Alternative C, year 0, was simulated in order to assess the potential impacts to the South Bay of restoring 90 percent of the project area to tidal action. As with the baseline conditions simulations, Alternative C, year 0, was simulated under summer (run 3) and winter (run 4) conditions, and comparisons were made with the corresponding baseline simulation.

Alternative A and Alternative C were also simulated at year 50 (runs 5 and 6, respectively), representing potential future conditions. Under Alternative A, levee failures are assumed to have occurred over the 50-year horizon, resulting in approximately 35 percent of the project area reverting to tidal action in an unplanned manner (PWA and others 2006). This assumption is based on the professional judgment of landowners and project planners with respect to future levels of funding for land-management, the expected lifetime of existing levees and hydraulic structures, and other factors that are inherently difficult to estimate. Under both alternatives, the tidally-restored ponds are assumed to have accumulated sufficient sediment to raise pond bottom elevations to vegetation colonization elevations (PWA 2006b), and the tidal sloughs are assumed to have scoured and deepened as a result of the increased tidal prism.

Section 3 provides additional details relating to these assumptions. The year 50 simulations were performed under summer conditions only, and the model predictions are compared with the summer baseline simulation (run 1).

Alternative B, which restores 50 percent of the project area to tidal action, was not modeled. The short-term (year 0) impacts associated with Alternative B will be qualitatively assessed in the EIS/R as a mid-point between Alternatives A and C. The long-term (year 50) impacts to the South Bay associated with Alternative B may more closely resemble the long-term impacts of Alternative A, as Alternative A at year 50 assumes levee failures occur resulting in approximately 35 percent of the project area reverting to tidal action in an unplanned manner (PWA and others 2006).

Table 2-1. Hydrodynamic Model Runs

Run	Alternative	Year	Season	Description of Modeling Simulation	Compared with Run
1	Baseline	0	Summer	Existing conditions – no restoration	
2	Baseline	0	Winter	Existing conditions – no restoration	
3	Alt C – Tidal Habitat Emphasis	0	Summer	Conditions immediately after restoring 90 percent of the ponds to tidal action	1
4	Alt C – Tidal Habitat Emphasis	0	Winter	Conditions immediately after restoring 90 percent of the ponds to tidal action	2
5	Alt A – No Action	50	Summer	Future conditions – no planned restoration, levee failures and unplanned tidal conversions occur	1
6	Alt C – Tidal Habitat Emphasis	50	Summer	Future conditions after restoring 90 percent of the ponds to tidal action	1

2.3 Major Assumptions and Uncertainties

There are several assumptions and uncertainties associated with the programmatic-level modeling, including:

- No project phasing, all ponds restored at year 0
- Programmatic level of detail with respect to design features
- Managed ponds discharges not simulated
- No direct modeling of sediment transport and/or morphologic change
- Limited grid resolution in some areas
- Year 50 bathymetric change estimates from separate geomorphic assessment
- Two-dimensional modeling approach

2.3.1 Phasing

The simulations assume that all ponds specified for tidal restoration under a given alternative are restored at the same time (year 0). This is considered a conservative, or “hypothetical”, assumption since it provides the maximum system-wide response and the largest hydrodynamic changes. In reality, restoration will be phased over many years, thereby reducing the magnitude of the project’s impacts. Since the selection and phasing of future actions for implementation will be driven largely by the Monitoring and Adaptive Management Plan and other considerations that are not known at this time, a modeling approach based around the eventual phasing plan and timeline is not possible.

2.3.2 Level of Detail

An additional programmatic-level assumption concerns the level of detail included in the model simulations. As the alternatives will be not specified at a project level of detail, assumptions regarding levee breach locations and sizes will be made throughout the project area so that restored ponds can be hydraulically connected to the South Bay. For most ponds, levee breaches will be located near historic channel networks in order to reconnect historic drainage paths. For ponds without historic channel networks, or with channel networks that cannot logically be reconnected due to extensive physical changes in the nearby systems (e.g., some ponds in the Eden Landing Complex), levee breaches will be located based on professional judgment and the locations may be refined based on modeling results. Breaches will likely be oversized in order to mobilize the potential tidal prism within the restored ponds. Future project-level modeling may be used to assess the importance of design features (e.g., starter channels, ditch blocks, wave breaks) within a particular pond in order to evaluate pond circulation, sedimentation and residence times. These features will not be considered at the programmatic level.

2.3.3 Managed Pond Discharges

The managed ponds are not included in the programmatic-level tidal restoration simulations. The intent of the programmatic modeling is to bracket the range of potential impacts, focusing on characterizing impacts on the South Bay ecosystem scale. Based on a review of the modeling completed for the ISP (Gross and Schaaf & Wheeler 2003b), full implementation of the ISP resulted in salinity differences on the order of 1 – 4 ppt in tidal sloughs, with little to no impact on Bay-wide salinity. Partial implementation (ensuing from 50 and 90 percent of the ponds being restored to tidal action), will likely result in smaller salinity differences.

Although the impact to tidal slough salinity from managed pond discharges is measurable, the addition of pond discharges is expected to make less of a difference in slough response than other processes not included in the analyses. For example, phasing is not included because it is an unknown – future phasing for implementation will likely be defined through planning and adaptive management decisions throughout the life of the project. The system response to the broad assumption that all ponds are restored at year 0 will likely dwarf the slough response to managed pond operations. Additional modeling in future phases for implementation may require the inclusion of managed ponds to appropriately characterize slough response at the project-level.

2.3.4 Sediment Transport and Geomorphic Modeling

Sediment transport and geomorphic modeling was not performed at the programmatic level for NEPA/CEQA impact analyses. The development of a sediment transport and geomorphic model of the South Bay system would be an extensive effort requiring additional data collection efforts and a significant amount of resources and time. The effort involved in setting up such a model is not practical for impact analyses at the programmatic level, particularly with respect to the gross assumptions for this level of analysis. However, such a model would be useful for informing future restoration phases and adaptive management decisions, therefore it is assumed that the development of a sediment transport and geomorphic model will be undertaken as part of the longer-term modeling efforts. The Project's National Science Panel recommended that the Project initiate an RFP-based effort for the development of such a suite of models.

Although sediment transport and geomorphic modeling will not be performed, potential impacts to sediment erosion and deposition patterns will be inferred based on comparisons of the changes in total bed shear stress as result of tidal restoration. Potential changes to the tidal sloughs in response to the increased tidal prism will be estimated based on hydraulic geometry relationships (Williams and others 2002), as discussed in PWA (2005). These methods have been used successfully for previous restoration project EIS/R documents (Jones & Stokes 2004a; Jones & Stokes 2004b; U.S. Fish and Wildlife Service and others 2004).

2.3.5 Grid Resolution

One of the largest uncertainties affecting the model results is the accuracy and resolution of the available bathymetry and the grid resolution used to resolve this bathymetry. To the extent possible, the models have made use of the most recent and best available bathymetric data which minimizes the uncertainty introduced by bathymetry. However, when the bathymetric data is sampled onto the model grids, additional filtering of bathymetric data occurs which limits the capacity of the model to resolve small-scale bathymetric features. To help reduce this effect in the South Bay channels, sounding data collected by Sea Surveyor in 2005 was used to develop the grid bathymetry in areas where it was available.

The grid resolution of the South Bay Model was selected to be as fine as possible, subject to the computational resources currently available. The grid resolution varies over the domain and in the primary areas of interest, as shown on Figure 2-4 and discussed in Section 2.1. The Eden Landing and Ravenswood pond complexes are modeled with a grid resolution on the order of 40 to 80 m. This grid resolution does not allow for adequate resolution of the tidal sloughs, which for the most part have channel widths narrower than 40 m. Ravenswood Slough in the Ravenswood pond complex is approximately 25 m wide and is represented in the model with a channel width on the order of 80 m. This overestimation of the channel width will affect the accuracy of the modeled water levels and salinity in Ravenswood Slough, and will lead to a large overestimate of the modeled slough tidal prism. Old Alameda Creek in the Eden Landing pond complex, which consists of two narrow channels separated by a mud bar, is also represented in the model as a single channel approximately 80 m wide and therefore the model results will contain similar inaccuracies in this creek.

The Alviso pond complex is modeled with a grid resolution on the order of 15 to 25 m; therefore the tidal sloughs within this complex are represented more accurately than those in the Eden Landing and Ravenswood pond complexes. However, due to the alignment of the tidal sloughs with the model grid, some sloughs are still modeled with widths that are nearly double their actual, physical widths (e.g., Charleston Slough, Mountain View Slough and Stevens Creek). The model results associated with these tidal sloughs will therefore contain greater inaccuracies than those sloughs which are better represented in the model (e.g., Coyote Creek, Alviso Slough, and Guadalupe Slough). However, even the use of 15- to 20-m grid resolution limits the capacity of the model to accurately resolve the bathymetry in the subtidal channel and tidal sloughs; therefore, considerable uncertainty exists in these areas. The use of finer grid resolution for project-level modeling would allow for more grid resolution across slough channels and could help reduce these uncertainties, but the capacity of the model would still be limited by the resolution of the available bathymetric data.

The Alviso pond complex was modeled at a greater level of detail because it represents approximately 80 percent of the total potential tidal prism added to the Bay by the tidally-restored ponds under Alternative C due to the larger pond area and the more subsided nature of the ponds. In addition, the surface area of the Alviso pond complex is similar to that of the far South Bay; therefore, restoration in the Alviso pond complex has the potential to appreciably alter the near-field hydrodynamics. Although the Eden Landing and Ravenswood pond complexes are modeled at a lesser level of detail, the effect of tidal restoration within these complexes on Bay hydrodynamics is still well represented.

2.3.6 Two-dimensional Model Approach

Both the GSFB and South Bay Model simulations utilize a 2D depth-averaged approximation. The use of 2D simulations significantly reduces the computational time required for the model simulations but also introduces additional model uncertainty both in the hydrodynamic and the salinity predictions. Under summer conditions in the South Bay, little stratification is present in the main channel (Cheng and others 1993). However, in the far South Bay tidal sloughs stratification exists and flows have a highly three-dimensional structure even during low freshwater inflows. The effects of stratification on hydrodynamics and salinity transport, and therefore important tidal circulation mechanisms, are not represented in the 2D simulations. Near-field salinity mixing which occurs near pond breaches can not be resolved in the model because the model can't resolve processes that occur on a scale smaller than a single grid cell. Instead, pond discharges will be mixed uniformly into a model cell over both the cell area and the total water depth, which can lead to a significant over estimation of dilution of near-field salinity gradients. Additionally, 2D modeling requires calibration of 2D dispersion coefficients to approximate transport due to 3D mechanisms. While these coefficients can be calibrated for existing conditions, they are not necessarily valid for restored conditions. Thus, the use of 2D simulations introduces significant uncertainty to model predictions in areas where 3D processes are important.

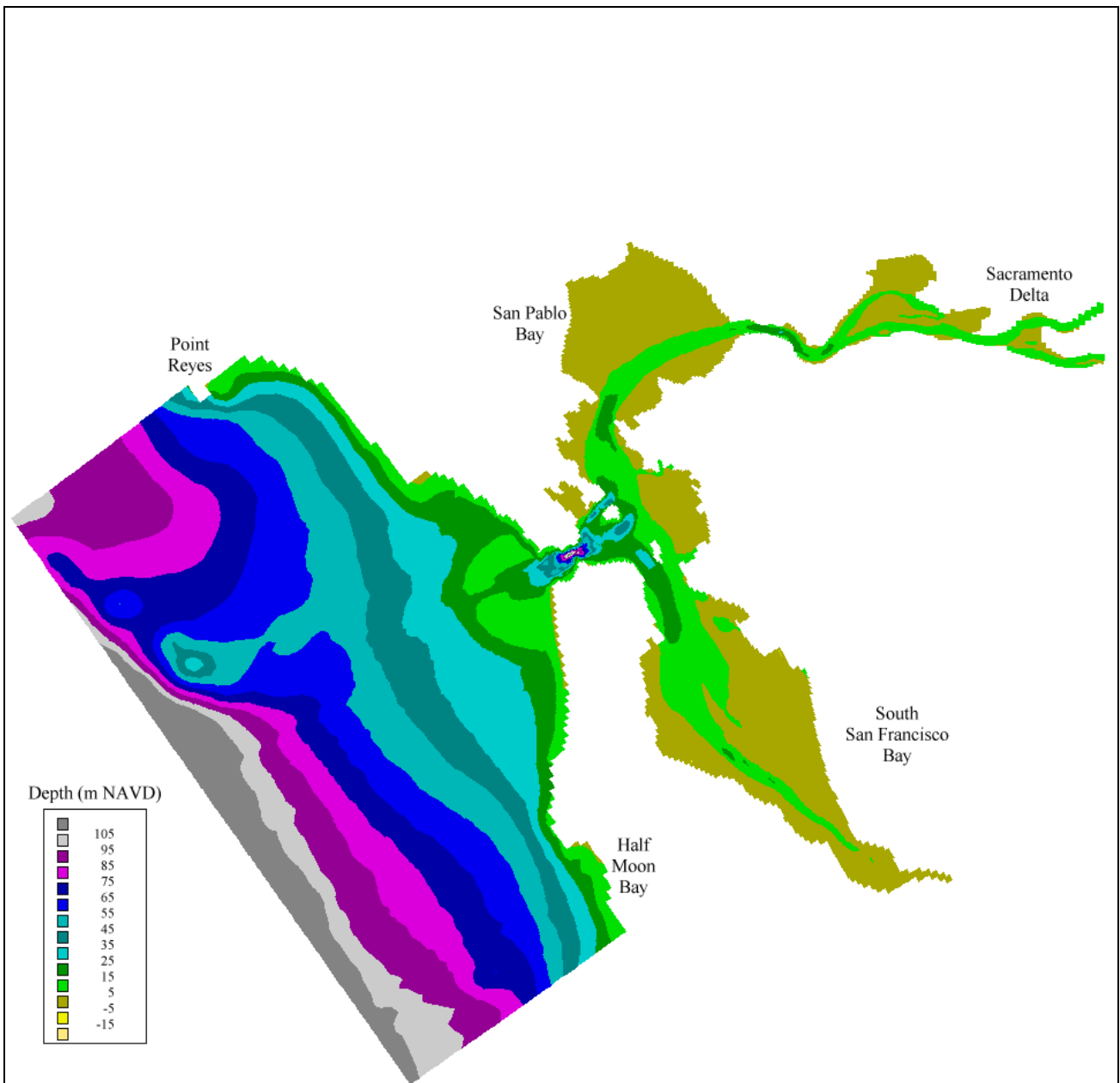
2.3.7 Long-term Bathymetric Change

The model simulations of long-term, year 50, conditions rely on bathymetric change estimates documented in the South Bay Geomorphic Assessment (SBGA, PWA 2006b). The SBGA provides an overview of the potential magnitude of regional geomorphic changes in the South Bay 50 years into the

future for the three alternatives, including gains and losses in mudflat and fringing marsh. In essence, the SBGA is a first approximation of potential habitat change at a very coarse, regional scale. The SBGA includes analyses of historical bathymetric change, and draws on data and analyses by the USGS (Foxgrover and others 2004; Jaffe and Foxgrover 2006a; Jaffe and Foxgrover 2006b; Jaffe and Fregoso in progress), and sediment budget calculations. There are considerable uncertainties in this assessment relating to: the sediment budget components, sediment dynamics and the major sediment transport pathways, the morphologic response to sediment surpluses and deficits, and future rates of sea-level rise. There is, therefore, considerable uncertainty inherent in the predictions of long-term geomorphic change in response to the alternatives.

Although it is acknowledged that considerable uncertainty is associated with the long-term bathymetric change estimates, it is also recognized that developing long-term morphologic predictions is a relatively new applied science (Wilcock and Iverson 2003), and based on the available information, a more complex approach may not necessarily yield more certain results as it is inherently difficult to predict the future. However, since the year 50 modeling simulations are based on an analysis which contains considerable uncertainty, it should be noted that the same considerable uncertainty, if not greater uncertainty, is therefore attached to the year 50 modeling results. The year 50 modeling results represent an estimate of potential future conditions, based on the best available information, in order to evaluate the potential long-term changes in Bay hydrodynamics as a result of the SBSP Restoration Project.

<This page intentionally left blank>



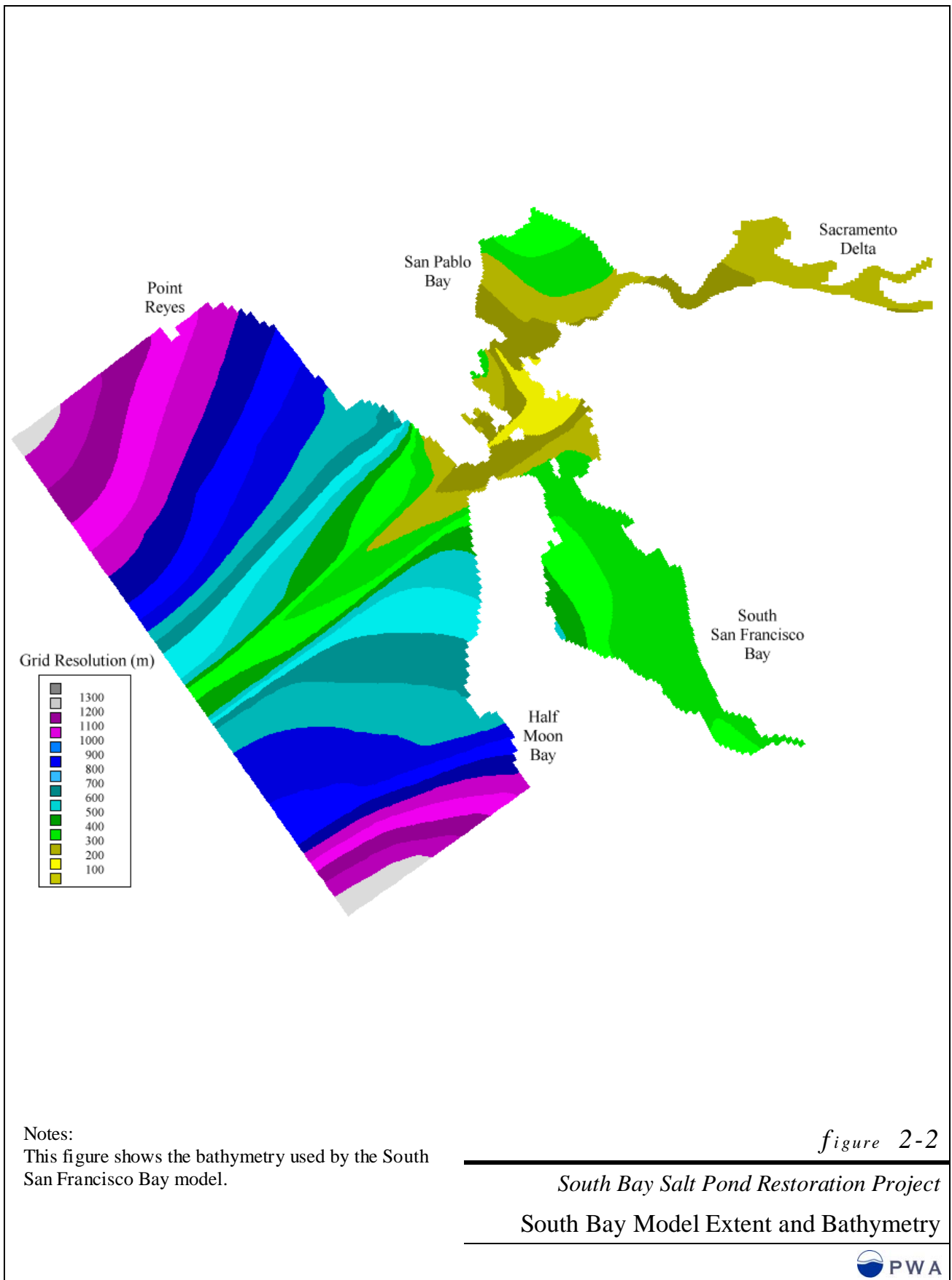
Notes:
 This figure shows the bathymetry used by the Greater San Francisco Bay Model

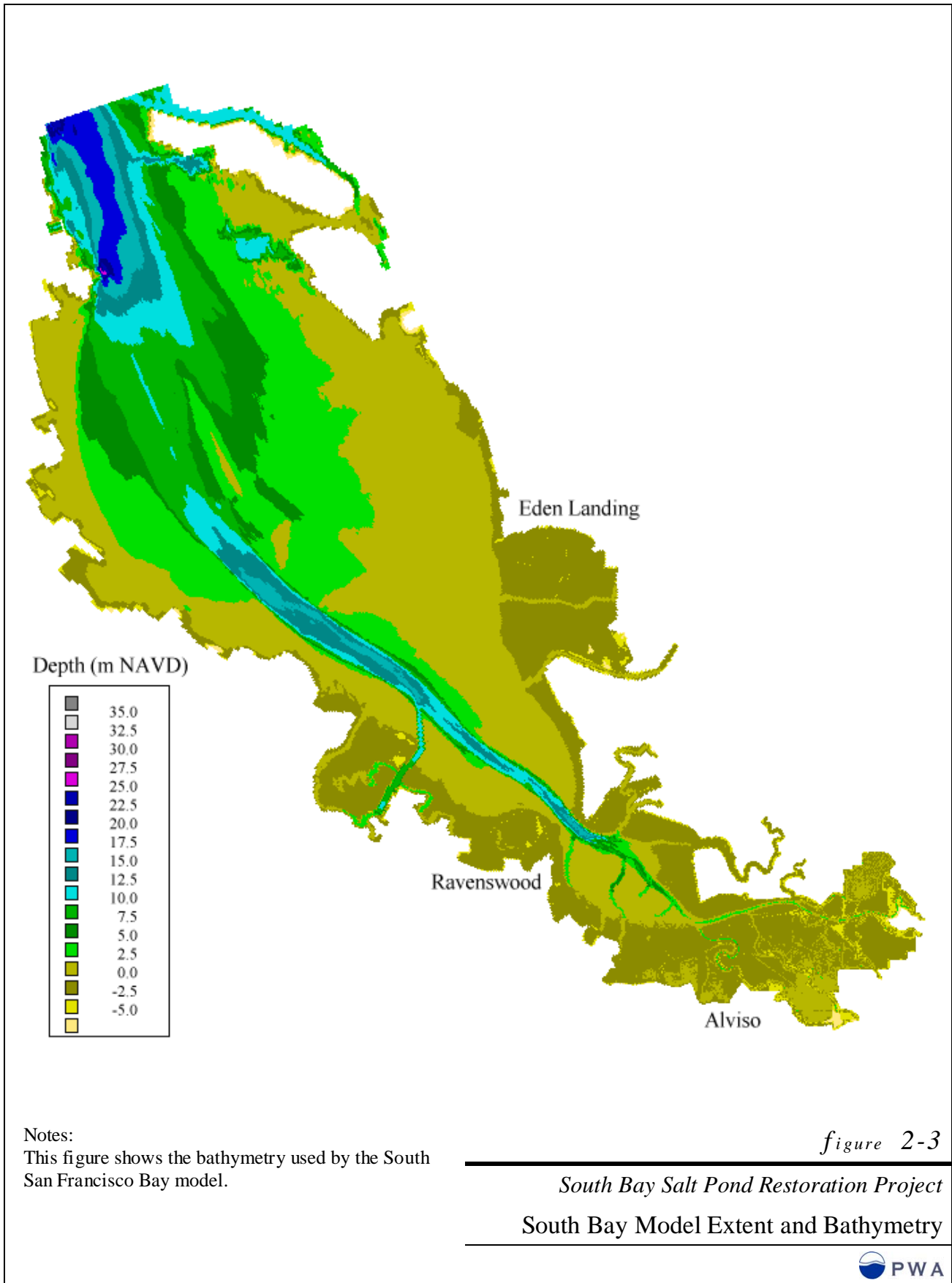
figure 2-1

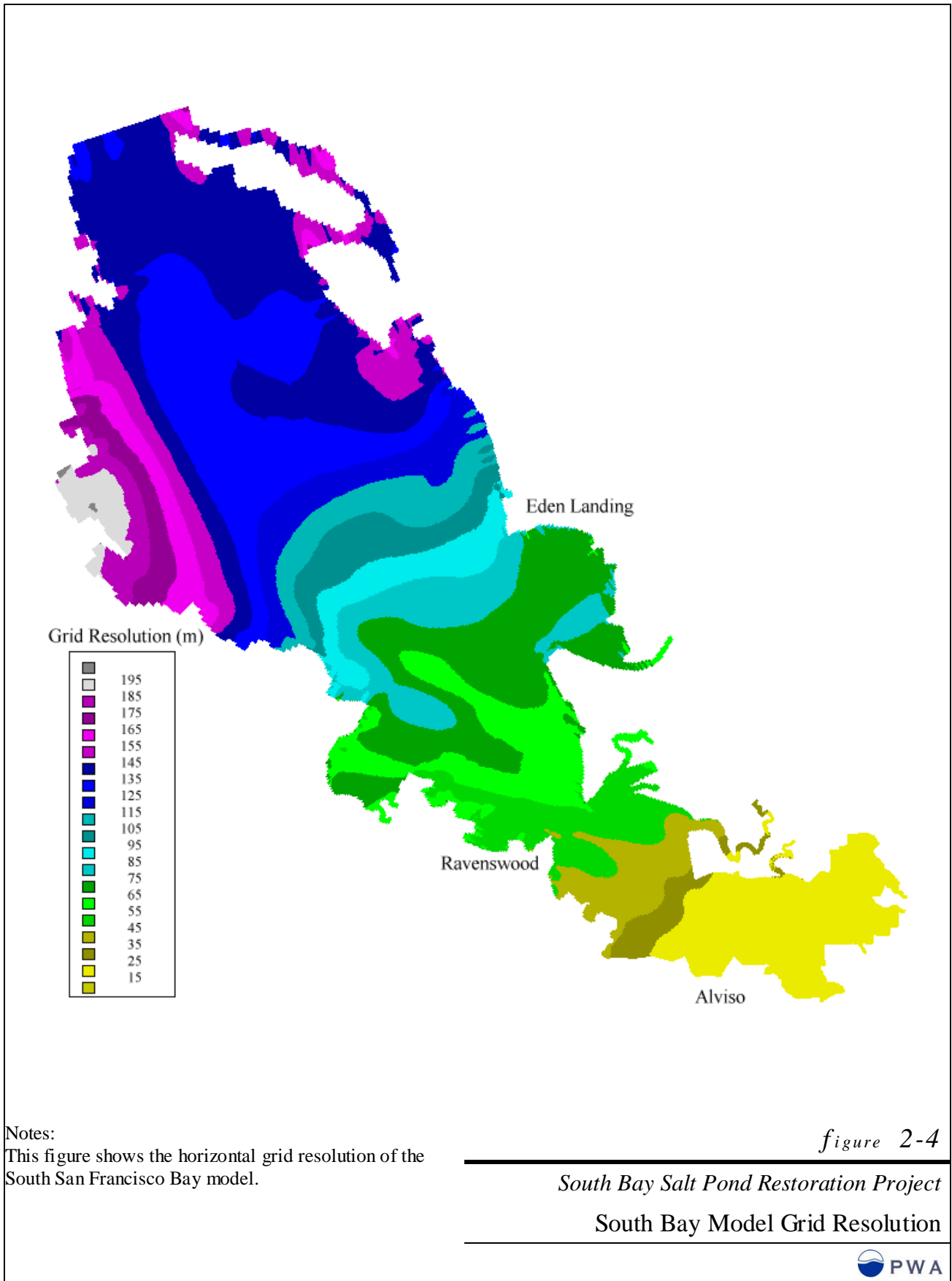
South Bay Salt Pond Restoration Project

Greater San Francisco Bay Model Extent and Bathymetry









3. RESTORATION SCENARIO MODEL SET-UP

This section describes the model-set up and boundary and initial condition data required for the restoration scenario simulations. The model set-up described is in addition to the model set-up presented in the Modeling Methods and Strategy Report (PWA 2005) and the Hydrodynamic Modeling Calibration Report (PWA 2006a).

3.1 Baseline Conditions

Baseline conditions in the model are assumed to represent planned ISP operations as of fall 2006 in accordance with the NEPA/CEQA baseline (Section 1.3). The Island Ponds (A19, 20 and 21) in the Alviso pond complex and the Eden Landing Ecological Reserve in the Eden Landing pond complex represent the only ponds within the SBSP Restoration Project Area experiencing tidal inundation; the remaining ponds are assumed to continue to operate as managed ponds and are not included in the model simulation. Figure 3-1 through Figure 3-3 depict baseline conditions at each pond complex, including the intended management of the managed ponds. The management of the ponds may change prior to fall 2006 under the direction of the landowners in order to meet habitat goals and Regional Water Quality Control Board (RWQCB) discharge requirements; however, any management changes will be confined to managed pond operations and are not expected to affect the extent of tidal restoration. A full discussion of baseline South Bay hydrodynamics is presented in the Hydrodynamics and Sediment Dynamics Existing Conditions Report (PWA and others 2005).

3.1.1 Island Ponds

The Island Ponds (Ponds A19, A20 and A21) in the Alviso pond complex were breached in March 2006. The restoration design was completed by the Santa Clara Valley Water District (U.S. Fish and Wildlife Service and Santa Clara Valley Water District 2006) and includes two breaches to Pond A19, one breach to Pond A20, and two breaches to Pond A21. All breaches are located on the south side of the ponds and connect to Coyote Creek with a new channel through the outboard marsh. The actual breaches are 12-14 m wide. The sills of the breaches and the connector channels were graded to an elevation of 0.82 m NAVD88, approximately one meter above MLLW.

The Island Ponds restoration was included in the baseline simulations by connecting the ponds to Coyote Creek with a small channel one grid cell wide at approximately the actual breach locations (Figure 3-4). The model bathymetry was altered at the breach and along the connector channel to reflect the specified grading in the restoration design of 0.82 m NAVD88. Grid resolution in this region is approximately 20 m; therefore the modeled breach widths are larger than the actual breach dimensions, therefore the modeled exchange into the ponds should represent an upper bound on the actual exchange.

3.1.2 Eden Landing Ecological Reserve

The Eden Landing Ecological Reserve in the Eden Landing pond complex is located in the northeast corner of the complex, as shown on Figure 3-1. The design of this project was completed by Kamman

Hydrology and Engineering under the oversight of the East Bay Regional Park District (EBRPD). The project area originally consisted of fifteen salt ponds, and the restoration plan involved breaching several of the internal levees and excavating historic channels, thereby creating two distinct wetlands (Kamman Hydrology and Engineering 2004). These wetlands, referred to as the North and South wetlands, connect to the South Bay via Mount Eden Creek and North Creek, a spur off of Old Alameda Creek. These connector creeks were both dredged, and the levees on Mount Eden Creek were set back to enhance conveyance between the South Bay and the restored wetlands.

The model bathymetry was altered to reflect this restoration project, as shown in Figure 3-5. The dredged creeks and excavated historic channels were represented in the model as a series of contiguous cells. The bottom elevations within the restored wetlands and the channels match the design drawings for the restoration plan (Kamman Hydrology and Engineering 2004). The elevations range from 0.52 m NAVD88 at the mouth of Mount Eden Creek to 0.82 m NAVD88 within the North wetlands and from 0.21 m NAVD88 at the mouth of North Creek to 0.82 m NAVD88 within the South wetlands. As with the Island Pond breaches, the breach and channel widths within the Eden Landing Ecological Reserve are limited by the grid cell resolution in this region, therefore they are larger than actual dimensions.

3.1.3 Boundary and Initial Conditions

Boundary conditions for the baseline simulations utilized observations from the time period of May-June 2001 for summer conditions, as described for the 2001 model calibration period (PWA 2006a) and February-March 2004 for winter conditions, as described for the 2004 model validation period (PWA 2006a). Freshwater inflows are specified for the tidal sloughs, creeks and the waste-water treatment plants (WWTP). Temporally-varying but spatially-uniform wind stresses and evaporation rates were also applied to the water surface. Table 3-1 lists the data sources for the input and boundary condition data, with “GSFB” noted for data required only for the GSFB Model simulations, and “Both” noted for data required for the GSFB and South Bay Model simulations. Additional details with respect to the input and boundary condition data are described in the PWA (2006a).

At the open boundary of the South Bay Model, spatially- and temporally-varying water surface elevations and salinity introduced tidal action into the model domain. These boundary conditions were derived from the GSFB Model, as described by PWA (2006a), and are presented in Figure 3-6 for the summer period. Initial conditions were derived from the GSFB Model simulations (PWA 2006a). Water level, velocity, and salinity conditions from the GSFB Model simulations were extrapolated over the South Bay model domain to provide initial conditions for the baseline simulations.

The baseline simulations assume the majority of the ponds within the SBSP Restoration Project Area are operated as managed ponds, and are therefore not included in the model, as discussed in Section 2.3.3. The existing restoration areas, the Island Ponds (A19, A20 and A21) in the Alviso pond complex, and the Eden Landing Ecological Reserve in the Eden Landing pond complex are included in the simulations. However, the restorations areas are not included in the GSFB Model; therefore the initial conditions required specification. The model spin-up period was chosen to begin at HHW, therefore initial velocities within the restorations areas were set to zero. Initial water levels and salinities were specified based on the

water levels and salinities in the outboard slough channels at the start of the simulations. The model was spun up for two weeks, removing any initial effects associated with the hydrodynamics. Salinities typically require longer spin-up periods; however, due to the small volume of the restoration areas, the simulation appears to represent equilibrium conditions by the end of the spin-up period. Although equilibrium is approached within the tidal sloughs due to their relatively short residence times, the South Bay could require significantly longer spin-up times (on the order of several months to one year) to remove the affect of the initial salinity conditions. Due to the relatively long run times required, a spin-up time of this length was not included in the model simulations. However, under baseline simulations, the initial salinity condition within the ponds does not contribute to a significant freshening of the South Bay due to the relatively limited volume of water contained within the two restoration areas.

The initial salinity condition within the ponds is based on the assumption that ponds would be operated as muted tidal systems prior to breaching, and the restoration areas would be breached in the spring when pond salinities are at their lowest, thereby limiting the adverse affects associated with high salinity releases in the tidal sloughs and the South Bay. The muted tidal assumption is consistent with current ISP pond operations. In the spring, salinities within the tidal sloughs and ponds would be at their lowest due to the influence of winter and spring freshwater tributary inflows, and the influence of high summer evaporation rates on salinity could be neglected. However, this assumption could underestimate the initial salinity conditions if breaching were to occur in summer or fall when the effect of evaporation cannot be neglected, and it does not account for the potential increase in slough and pond salinities due to muted tidal operations of the ponds.

Table 3-1. Input and Boundary Condition Data Sources

Model	Location	Dates	Agency or Organization	Source
Tidal Boundary Conditions				
GSFB	Point Reyes (9415020)	1/1/1996 – present	NOAA/NOS	http://tidesandcurrents.noaa.gov/
GSFB	San Francisco (9414290)	1/1/1901 – present	NOAA/NOS	http://tidesandcurrents.noaa.gov/
Salinity Boundary Conditions				
GSFB	Oceanic Salinity	Various	PRBO	http://shorestation.ucsd.edu/
Salinity Initial Conditions				
GSFB	San Francisco Bay Salinity Transects	4/1969 – 5/2005	USGS	http://sfbay.wr.usgs.gov/access/wqdata Cruise data collected approximately monthly at discrete points along the main channel
Fluvial Flows				
GSFB	Delta Outflow	10/1/1955 – 9/30/2004	IEP	http://www.iep.ca.gov/dayflow/
Both	Coyote Creek @ Highway 237	1/1/1999 – 9/30/2004	USGS	http://waterdata.usgs.gov/
Both	Guadalupe River @ San Jose	10/1/1929 – 4/30/2000	USGS	http://waterdata.usgs.gov/
Both	Alameda Creek near Niles	1/4/1891 – 9/30/2004	USGS	http://waterdata.usgs.gov/
Both	Alameda Creek Flood Control Channel @ Union City	10/1/1958 – 9/30/2004	USGS	http://waterdata.usgs.gov/
Both	San Francisquito Creek @ Stanford Univ.	10/1/1930 – 9/30/2004	USGS	http://waterdata.usgs.gov/
Both	Matadero Creek @ Palo Alto	10/1/1952 – 9/30/2004	USGS	http://waterdata.usgs.gov/
Both	Saratoga Creek @ Saratoga	10/1/1933 – 9/30/2004	USGS	http://waterdata.usgs.gov/
Both	Upper Penitencia Creek @ Piedmont Rd	10/1/1942 – present	SCVWD	http://www.valleywater.org/
Both	Calabazas Creek @ Wilcox School	10/1/1945 – present	SCVWD	http://www.valleywater.org/
Both	Permanente Creek @ Berry Ave	10/1/1944 – present	SCVWD	http://www.valleywater.org/
Both	Hale Creek @ Magdalena Road	10/1/1945 – present	SCVWD	http://www.valleywater.org/
Both	Stevens Creek @ Highway 85	10/1/1942 – present	SCVWD	http://www.valleywater.org/
Both	Los Gatos @ Lincoln Ave	11/2/1955 – present	SCVWD	http://www.valleywater.org/
Both	Coyote Creek @ Edenvale	10/1/1963 – present	SCVWD	http://www.valleywater.org/

Table 3-1. Input and Boundary Condition Data Sources (cont.)

Model	Location	Dates	Agency or Organization	Source
Both	Thompson Creek @ Quimby Rd	10/1/1980 – present	SCVWD	http://www.valleywater.org/
Both	San Jose Waste Water Treatment Plant Outfall	1/1/1999 – 6/30/2005	City of San Jose	City of San Jose
Both	Sunnyvale Waste Water Treatment Plant Outfall	1/1/1999 – 6/30/2005	City of Sunnyvale	City of Sunnyvale
Both	Palo Alto Waste Water Treatment Plant Outfall	1/1/1999 – 5/31/2005	City of Palo Alto	City of Palo Alto
Wind				
Both	Alviso, Bethel Island, Chevron Refinery, Concord, Concord STP, NUMMI, Port of Oakland, Oakland STP, Pacific Refinery, Phillips Carbon, Phillips Hillcrest, Phillips Rodeo, Rio Vista, San Carlos, San Mateo, Santa Rosa, Shell Refinery East, Shell Refinery West, Sonoma, Tesoro Refinery, Richmond, Valero Warehouse, Valley Ford	1/1/1999 – 12/31/2003	BAAQMD	http://gate1.baaqmd.gov/aqmet/met.aspx
Both	Redwood City (9414523)	1/1/2004 – 12/31/2004	NOAA	http://tidesandcurrents.noaa.gov/
Evaporation and Precipitation				
Both	Fremont	8/29/1991 – 6/19/2000	CIMIS	http://www.cimis.water.ca.gov/
Both	Union City	2/5/2001 – present	CIMIS	http://www.cimis.water.ca.gov/

3.1.4 Potential Tidal Prism

As part of the ISP, the Island Ponds in the Alviso pond complex and the Eden Landing Ecological Reserve in the Eden Landing pond complex were opened to tidal action and have been included in the baseline simulations. The potential tidal prism within these regions – the volume of water than can be mobilized by the tides – can be estimated as the surface area of the project area multiplied by the difference in elevation between the pond bottoms and MHHW. Table 3-2 presents the estimated potential tidal prism for these two project areas. Each region adds just over one million cubic meters of potential tidal prism to the South Bay, which is approximately two orders of magnitude less than the tidal prism at the San Mateo Bridge.

Table 3-2. Potential Tidal Prism of ISP Project Areas

S BSP ISP project areas	Potential tidal prism (m³, millions)
Island Ponds	1.3
EBRPD wetlands	1.4

3.2 Alternative C – Tidal Habitat Emphasis, Year 0

Alternative C emphasizes tidal restoration and provides an approximately 90:10 ratio by area of tidal habitat to managed ponds (Figure 3-7 through Figure 3-9). At year 0, all of the ponds designated as tidal habitat will be hydraulically connected to the South Bay via over-sized breaches to the tidal sloughs in order to mobilize the potential tidal prism. Based on this assumption, the ponds will drain and fill with the tides, and dependent on their pond bottom elevations will either resemble open water areas (deep ponds) or intertidal mudflats (shallow ponds).

At year 0, no pond sedimentation or vegetation establishment is assumed to have occurred. In addition, the connecting slough channels (Old Alameda Creek, the Alameda Creek Flood Control Channel, Coyote Creek, Alviso Slough, Guadalupe Slough, Stevens Creek and Mountain View Slough) are assumed to maintain their existing channel geometry – no widening or deepening has occurred in response to the increased tidal prism. As with the baseline simulations, the managed ponds are not included in the model simulation.

3.2.1 Breach Sizes and Locations

In order to include the tidally-restored ponds in the model simulation, breach locations were selected and sized. This included selecting external breaches between the ponds and tidal sloughs, as well as internal breaches to facilitate pond drainage. Breach locations were selected by reviewing the historic channel networks and drainage areas, aerial photos of existing remnant antecedent channels, and the final alternatives as shown in PWA and others (2006). Wherever possible, breaches were located near the antecedent channels in order to promote reoccupation of the historic drainage paths. Particular care was taken to locate breaches as far upstream as possible on the tidal sloughs in order to facilitate channel scour and provide maximum flood protection benefits. A few breaches were located on the bayward side of the ponds in order to increase tidal exchange within the ponds and minimize tidal damping. Figure 3-15 through Figure 3-17 display the modeled breach locations for each pond complex. It is assumed that the

outboard levees will largely remain intact in order to provide wind-wave protection to the ponds until sufficient sediment accretes so that vegetation can establish. No levee lowering or levee removal was included in the model.

The minimum breach sizes were determined two ways: by relating hydraulic geometry to drainage area and by relating hydraulic geometry to the potential tidal prism. As a rule of thumb, external breaches were assumed to be at least 40 m wide, and internal breaches were assumed to be at least 20 m wide.

Implementing breaches of this size in the model was constrained by the grid resolution because breaches must span a minimum of one grid cell. In the Alviso pond complex, where the grid resolution is 15 to 20 m square, internal breaches one cell wide and external breaches two cells wide closely approximate the assumed breach sizes of 20 m and 40 m, respectively. In the Eden Landing and Ravenswood pond complexes, where the grid resolution is coarser, the modeled breaches are larger than the assumed breach sizes. The actual modeled dimensions depend upon the specific cell dimensions of a particular pond and the orientation of the grid cells. Generally, the maximum internal breach size in the Ravenswood and Eden Landing pond complexes is 40 m and the maximum external size is 80 m. The model bathymetry was also modified to include a pilot channel the same width as the breach. For external breaches, the pilot channel extends from the breach to the nearest slough channel and the depth is equal to the slough channel depth. For internal breaches, the channel is only a few cells long and the depth is set based on the pond bed elevation of the deeper pond.

Over sizing breaches is consistent with the principle that the breach width should not limit the exchange of tidal prism. Rather, from the programmatic perspective, the modeling should capture the impact of the breaches on mobilizing a conservatively large amount of tidal prism. Regardless of breach size, at year 0, the full mobilized tidal prism is potentially limited more by the conveyance capacity in the tidal sloughs. The sloughs' hydraulic geometry at year 0 has been set by the existing, much lower, tidal exchange and channel scour in response to the increased tidal prism has not been included. The slough channels will likely scour over time; however, the timing of the slough scour is unknown.

3.2.2 Boundary and Initial Conditions

Boundary and initial conditions for Alternative C are largely identical to those for the baseline simulations, as described in Section 3.1.3 and shown in Figure 3-6; however, under Alternative C, the area of tidally-restored ponds is significantly greater. Consequently, the impact from the initial salinity condition within the ponds on the South Bay is more apparent, and salinity conditions within the South Bay do not reach equilibrium within the analysis period. For this simulation, the hydrodynamic model was run for an additional two months in order to more quantitatively discuss the long-term equilibrium conditions within the tidal sloughs and the South Bay.

Ideally, the GSFb Model would be updated accordingly for each simulation in Table 2 1 in order to derive an appropriate boundary condition for the South Bay Model. For example, the simulation of Alternative C at year 0 with 90 percent of the ponds opened to tidal action would require modifying both the GSFb and South Bay Models to include the tidally-restored ponds. The boundary condition for the

South Bay Model simulation would then be derived from the GSFb Model simulation of Alternative C year 0 conditions. Simulations of Alternative A and C under year 50 conditions would also require modifications to both models. However, the grid resolution of the GSFb Model is on the order of 300 – 500 m in the South Bay, which is not adequate for performing the necessary model modifications for the alternative simulations.

In order to simplify the analysis, the GSFb Model was not modified to match the bathymetric changes included in the South Bay Model simulations. Instead, the same open boundary condition was applied for all South Bay Model summer simulations, and the open boundary condition for the winter South Bay Model simulation was derived from an unaltered GSFb Model simulation of winter conditions. In order to test the sensitivity of the model results to this simplification, the GSFb Model was modified to crudely represent the tidally-restored ponds in the Alternative C year 0 simulation by adding cells to the model domain in the vicinity of the three pond complexes to roughly approximate the amount of restored tidal prism contained within the tidally-restored ponds. The South Bay Model was then run for both the original GSFb Model boundary and the modified “GSFb Model Alternative C” boundary condition and the results compared. Figure 3-10 displays the station locations used in the open boundary condition sensitivity analysis.

Figure 3-11 displays the South Bay Model’s water level open boundary condition near the Oakland-Bay Bridge extracted from the GSFb Model under baseline and Alternative C conditions. In general, the water levels are similar under both scenarios. With the GSFb Model Alternative C implementation, tidal damping is observed at the Oakland-Bay Bridge, with the most marked difference observed at higher low water, and a negligible difference observed at both daily high water marks. Figure 3-12 displays water levels at two stations in the Bay from the GSFb Model under baseline and Alternative C conditions, one station is located just north of the Oakland-Bay Bridge and one station is located at Channel Marker 17 in the far South Bay. At the northern station, tidal damping is similar to that observed at the Oakland-Bay Bridge (Figure 3-12a). At the southern station, the tidal damping increases, with lower water levels observed at both high water marks, and high water levels observed at both low water marks, with the largest differences at observed at low water (Figure 3-12b). Therefore, implementation of Alternative C in the GSFb Model, albeit in a simplified manner, results in tidal damping in the Bay, with increasing tidal damping southwards into the South Bay.

Figure 3-13a compares the modeled flux of water at the Oakland-Bay Bridge boundary from GSFb Model under baseline and Alternative C conditions. Under Alternative C conditions, the modeled flux decreases. This result is somewhat counter-intuitive. Under Alternative C, approximately 13,400 acres of salt ponds are restored to tidal action, and thus the volume of the South Bay increases. However, this increase in volume is not accompanied by a corresponding increase in tidal prism. Rather, the restoration’s effect on the tidal range roughly cancels out the increase in volume. Figure 3-13b compares the modeled flux of water at the Oakland-Bay Bridge boundary from the South Bay Model under baseline conditions and Alternative C conditions – modeled using both the baseline and Alternative C water levels from the GSFb Model. The modeled flux is similar for all three simulations, with the greatest differences observed at higher low water.

Figure 3-14 compares the modeled water levels at the San Mateo Bridge, the Dumbarton Bridge, and Channel Marker 17 in the far South Bay from the South Bay Model under baseline and Alternative C conditions, with Alternative C conditions represented using both the baseline and Alternative C water level boundary condition derived from the GSFB Model. The comparisons show that the tidal propagation in the South Bay under both Alternative C simulations is similar, with increasing tidal damping in the far South Bay. The largest differences observed between the two Alternative C simulations are at higher low water at both bridge stations, and the differences at LLW and both high water marks are negligible.

Based on this sensitivity analysis of the water level open boundary condition derived from the GSFB Model, the water levels from the baseline GSFB Model simulation were applied to all South Bay Model simulations for alternatives analysis. However, it should be noted that use of the baseline boundary condition may lead to an underestimation of the tidal damping in the South Bay as a result of tidal restoration, as is seen on Figure 3-14. It should also be noted that the differences observed in this analysis for Alternative C at year 0 (assuming all ponds are opened and restored at once) are larger than would be expected under the year 50 simulations. By year 50, pond sedimentation and salt marsh establishment within the ponds is assumed to occur, reducing the added volume of the ponds to approximately 20 of the year 0 volume.

3.2.3 Potential Tidal Prism

Alternative C represents a significant change to the existing tidal prism within the South Bay, as shown in Table 3-3. The total potential tidal prism, as estimated from the pond volumes as described in Section 3.1.4, will add twenty times more potential tidal prism than added under baseline conditions. Nearly 80 percent of the potential tidal prism is contained within the Alviso pond complex, as is expected due to this pond complex's larger area, more subsided pond bottom elevations, and greater tidal range when compared with the Eden Landing and Ravenswood pond complexes. The total potential tidal prism assumes full hydraulic connectivity between the ponds and the Bay. The actual modeled tidal prism will likely be less as the ponds will be connected to the Bay through a series of external and internal breaches which will limit the hydraulic connectivity.

Table 3-3. Potential Tidal Prism of SBSP Alternative C Project Areas

SBSP Alternative C project areas	Potential tidal prism (m³, millions)
Eden Landing complex	7.1
Ravenswood complex	3.5
Alviso complex	41
Total	52

3.3 Alternative A – No Action, Year 50

Alternative A, the No Action Alternative is the most likely outcome in the absence of a long-term restoration plan. The long-term, year 50 conditions associated with Alternative A are based on the professional judgment of the landowners and project planners with respect to future levels of funding for land-management, the expected lifetime of existing levees and hydraulic structures, and other factors that

are inherently difficult to estimate. Alternative A may change somewhat in the future as specific assumptions are refined; however, for modeling and impact analysis purposes, Alternative A at year 50 was modeled as described in Appendix C of the Final Alternatives Report (PWA and others 2006) and presented in Figure 3-18 through Figure 3-20. Over the 50-year horizon, levees that do not provide key flood protection were assumed to have failed and eroded, restoring approximately 35 percent of the SBSR Restoration Project Area to tidal action in an unplanned manner. The bathymetry of the South Bay and the tidal sloughs was modified in response to the unplanned tidal restoration, sea-level rise, and the continuation of current morphologic trends.

3.3.1 Ponds

Over the 50-year horizon, the tidally-restored ponds are assumed to develop into mature salt marsh (PWA 2006b). Sedimentation is assumed to have raised pond-bottom elevations above vegetation-colonization elevations, vegetation is assumed to have established and marsh channels are assumed to have developed within the restored marsh. These changes were incorporated into the Alternative A, year 50 bathymetry. Mature salt marsh exists within the South Bay at an elevation near MHHW; therefore, the bathymetry within tidally-restored ponds was raised to MHHW. Sea-level rise is expected to increase water levels by approximately 15 cm (IPCC 2001); therefore, the year 50 MHHW is assumed to be 15 cm higher than baseline MHHW.

While the establishment of salt marsh effectively raises the bottom bathymetry to MHHW, the restored marsh areas still represent an increase in tidal prism when compared to baseline conditions. Much of this tidal prism is from the establishment of a mature marsh channel network. However, the marsh channels are too small to represent in the model bathymetry because of grid resolution limitations. The additional tidal prism supplied by the marsh channels was therefore approximated using a single channel within each pond extending from the breach location to the interior of the pond. For each breach, the expected tidal prism volume was calculated using hydraulic geometry relationships (see Section 3.3.2). A one-cell wide channel was then added to the marsh, linearly sloping from the breach depth to MHHW. The length of this channel was adjusted until its tidal prism approximated the predicted tidal prism.

3.3.2 Tidal Sloughs

The long-term slough channel cross-sectional areas for Alternative A were estimated using hydraulic-geometry relationships developed by Williams and others (2002) for San Francisco Bay. These empirical relationships are based on data from historic and existing mature San Francisco Bay salt marshes ranging in size from 2 to 5,700 ha (Williams and others 2002). The relationships equate channel depth, width and cross-sectional area to both marsh drainage area and tidal prism, and they can be used to predict potential long-term slough dimensions in response to changes in marsh drainage area and tidal prism.

Historically, the sloughs within the SBSR Restoration Project Area drained expansive areas of tidal marsh. Following the construction of levees to create the ponds, the tidal sloughs were isolated from the contributing tidal marsh area, thus reducing the tidal prism in the sloughs. Over time, the slough channels adjusted to the reduced tidal prism through sediment deposition and shoaling within the channels, which lead to the development of fringe marsh banks along the sloughs. Restoring the ponds to tidal action by

breaching the levees will increase the drainage area and tidal prism in the adjacent sloughs, inducing tidal scour as the channels adjust towards a new equilibrium in balance with the restored tidal prism.

The hydraulic-geometry relationships were used to estimate both the long-term tidal prism in the sloughs after levee failures and unplanned tidal conversions occur and mature salt marsh develops within the ponds, and the associated long-term equilibrium slough cross-sectional area. The assumption that mature marsh would develop over the 50-year horizon (i.e., marsh bed elevations would be close to MHHW and tidal channel networks would be fully developed) is based on the results of the SBGA (PWA 2006b).

The long-term equilibrium slough dimensions depend in part on the baseline tidal prism in the slough and whether the slough is currently in equilibrium with respect to the baseline tidal prism. It is likely that some of the sloughs are still accreting sediment and are therefore oversized with respect to the baseline tidal prism. Based on current available information and observed trends, Coyote Creek and Alviso Slough appear oversized. This was accounted for in the hydraulic-geometry estimates by using the existing modeled tidal prism in Coyote Creek and the tidal prism modeled by Schaaf & Wheeler (2004) for Alviso Slough. The remaining sloughs within the SBSP Restoration Project Area were assumed to be in equilibrium, therefore any increase in tidal prism in response to unplanned tidal conversion would result in scour and channel enlargement. This assumption may not be valid for all sloughs as some sloughs may be oversized and accreting sediment. However, the equilibrium assumption provides a conservative (high-end) estimate of tidal prism, tidal scour and long-term channel dimensions.

The long-term slough cross-sectional areas were calculated by estimating the combined baseline tidal prism and the tidal prism associated with the tidally-restored marsh drainage area. The marsh drainage areas were estimated using GIS for each assumed unplanned levee breach. The cumulative total upstream tidal prism was then estimated at specified slough cross sections for application within the model. Table 3-4 presents the estimated baseline and year 50 tidal prism at the slough mouths.

Although this analysis provided long-term estimates of slough depths and widths associated with the predicted increase in cross-sectional area, grid-resolution constraints prevented utilizing this information in the model simulations. Instead, a change in depth was calculated from the predicted cross-sectional area based on the assumption that the channel width remained constant. Table 3-5 presents the estimated increase in slough depth for each slough within the SBSP Restoration Project Area.

Table 3-4. Long-term Increase in Tidal Prism, Alternative A

Slough	Baseline Tidal Prism (m³, millions)¹	Alternative A Tidal Prism (m³, millions)	Increase (%)
Mt. Eden Creek ²	0.21	1.18	460%
North Creek ²	0.17	0.22	30%
Old Alameda Creek ²	0.32	2.10	560%
ACFCC	0.07	0.81	1,010%
Ravenswood Slough	0.02	--	--
Mud Slough	0.62	--	--
Artesian Slough	1.40	--	--
Alviso Slough	0.83	1.71	110%
Guadalupe Slough ³	14.38	15.36	10%
Stevens Creek	0.01	--	--
Mountain View Slough	0.02	--	--
Charleston Slough	0.03	--	--
Coyote Creek, d/s of Alviso Slough	6.70	7.84	20%

¹ Baseline tidal prism for Alviso Slough is from Schaaf & Wheeler (2004); baseline tidal prism for Coyote Creek is based on the DELFT3D baseline modeling results; baseline tidal prism for all other sloughs is estimated from hydraulic geometry relationships (Williams and others 2002).

² Baseline tidal prism for Mt. Eden Creek, North Creek, and Old Alameda Creek include tidal prism associated with the Eden Landing Ecological Reserve

³ Baseline tidal prism for Guadalupe Slough was estimated at the deepest point in the slough which is just upstream of the slough mouth.

Table 3-5. Long-term Increase in Channel Depth, Alternative A

Slough Name	Location	Depth Increase (meters)
Mt. Eden Creek	Up-slough	2.8
	Mouth	2.9
North Creek	Up-slough	--
	Mouth	1.5
Old Alameda Creek	Up-slough	0.2
	Mid-slough	1.1
	Mouth	1.1
ACFCC	Up-slough	--
	Mid-slough	1.2
	Mouth	1.4
Ravenswood Slough	Up-slough	--
	Mid-slough	--
	Mouth	--
Mud Slough	Mid-slough	--
Artesian Slough	Mouth	--
Alviso Slough	Up-slough	--
	Mid-slough	0.6
	Mouth	0.7
Guadalupe Slough	Up-slough	0.2
	Mid-slough	0.4
	Mouth	0.1
Stevens Creek	Up-slough	--
Mountain View Slough	Mid-slough	--
	Mouth	--
Charleston Slough	Up-slough	--
	Mouth	--
Coyote Creek	Up-slough	--
	Mid-slough	--
	Mouth	--

3.3.3 South Bay Bathymetry

The South Bay is expected to change significantly over the 50 year horizon both with and without the SBSP Restoration Project (PWA 2006b). The Alternative A, year 50 model bathymetry was modified in order to account for the potential changes in the absence of the SBSP Restoration Project by applying the predictions of intertidal mudflat loss and gain documented in the SBGA (PWA 2006b) and discussed briefly in Section 2.3.7. The SBGA’s long-term predictions for Alternative A include the following changes: North of San Bruno Shoal, no bathymetric change is predicted; between the San Bruno Shoal and the Dumbarton Bridge, approximately 25 cm of erosion is estimated to occur on the intertidal

mudflats; South of Dumbarton Bridge in the far South Bay, approximately 34 cm of sedimentation is estimated to occur on the mudflats; and no bathymetric changes are assumed to occur within the main South Bay channel or the subtidal areas (PWA 2006b). The baseline bathymetry was modified using these estimates of bathymetric change. Only the bottom elevations of the intertidal mudflat areas were raised or lowered depending on the assumption of deposition or erosion. This area extended from MHHW to the bottom of wave-induced sweep zone, defined as 1.8 m (6 ft) below MLLW. In order to avoid a step at the transition between the raised or lowered regions and the existing bathymetry, a smoothing routine was applied at the transition. However, the grid resolution of the Bay (see Figure 2-4) is large relative to the estimated bathymetric change, therefore any discontinuity between the modified and existing bathymetry is negligible.

The depths of the tidal sloughs were also modified to account for the increase in tidal prism associated with the breached ponds. Hydraulic geometry calculations were used to determine the depth of the channel thalwegs, as discussed in section 3.3.2. No bathymetric changes were applied to the channels and sloughs outside of the SBSP Restoration Project Area.

3.3.4 Boundary and Initial Conditions

Boundary conditions for Alternative A at year 50 were based on those for baseline conditions as presented in Section 3.1.3. The only change involved included projected sea-level rise based on IPCC (2001) mid-range estimates, consistent with other SBSP Restoration Project reports (PWA 2006b). The projected sea-level rise rate of 0.3 cm/year results in a water level increase of approximately 15 cm over 50 years. To account for sea-level rise within the model, the water levels at the boundary (near the Oakland-Bay Bridge) were increased by 15 cm. Surface winds and tributary inflows were unchanged from baseline conditions.

Initial conditions were also modified to account for sea-level rise. The initial water level condition was uniformly raised 15 cm. The initial velocity field and initial salinity condition are unchanged from baseline conditions. The initial salinity condition within the tidally-restored ponds (35 percent of the project area assuming unplanned levee failure and erosion) was developed using the same method described for the baseline simulation in Section 3.1.3.

3.4 Alternative C – Tidal Habitat Emphasis, Year 50

Over the 50-year horizon, the tidally-restored ponds in Alternative C were assumed to develop into mature salt marsh (PWA 2006b). Sedimentation is assumed to raise pond-bottom elevations above vegetation-colonization elevations, vegetation is assumed to establish and marsh channels are assumed to develop within the restored marsh. Correspondingly, the bathymetry of the South Bay and the tidal sloughs were modified in response to the tidal restoration, sea-level rise, and the continuation of current morphologic trends.

3.4.1 Ponds

Under Alternative C, all of the tidally-restored ponds were assumed to develop into mature salt marsh over the 50-year horizon. These changes were incorporated into the Alternative C, year 50 bathymetry, following the same approach outlined in Section 3.3.1.

3.4.2 Tidal Sloughs

The long-term slough dimensions and tidal prism for Alternative C were estimated using the same method described for Alternative A in Section 3.3.2. Table 3-6 presents the estimated baseline and year 50 tidal prism at the slough mouths in response to restoring 90 percent of the ponds within the SBSP Restoration Project Area to tidal action. As with Alternative A, all ponds restored to tidal action were assumed to develop into mature salt marsh over the 50-year horizon. Table 3-7 presents the estimated increase in slough depth.

Table 3-6. Long-term Increase in Tidal Prism, Alternative C

Slough	Baseline Tidal Prism (m ³ , millions) ¹	Alternative C Tidal Prism (m ³ , millions)	Increase (%)
Mt. Eden Creek ²	0.21	0.57	170%
North Creek ²	0.17	0.81	380%
Old Alameda Creek ²	0.32	3.56	1,030%
ACFCC	0.07	1.26	1,630%
Ravenswood Slough	0.02	1.28	6,530%
Mud Slough	0.62	1.49	140%
Artesian Slough	1.40	1.57	10%
Alviso Slough	0.83	3.28	300%
Guadalupe Slough ³	14.38	15.83	10%
Stevens Creek	0.01	0.34	6,050%
Mountain View Slough	0.02	0.62	2,960%
Charleston Slough	0.03	0.11	270%
Coyote Creek, d/s of Alviso Slough	6.70	12.73	90%

¹ Baseline tidal prism for Alviso Slough is from Schaaf & Wheeler (2004); baseline tidal prism for Coyote Creek is based on the DELFT3D baseline modeling results; baseline tidal prism for all other sloughs is estimated from hydraulic geometry relationships (Williams and others 2002).

² Baseline tidal prism for Mt. Eden Creek, North Creek, and Old Alameda Creek include tidal prism associated with the Eden Landing Ecological Reserve

³ Baseline tidal prism for Guadalupe Slough was estimated at the deepest point in the slough which is just upstream of the slough mouth

Table 3-7. Long-term Increase in Channel Depth, Alternative C

Slough Name	Location	Depth Increase (meters)
Mt. Eden Creek	Up-slough	1.9
	Mouth	2.4
North Creek	Up-slough	2.2
	Mouth	2.3
Old Alameda Creek	Up-slough	0.4
	Mid-slough	1.4
	Mouth	1.4
ACFCC	Up-slough	0.2
	Mid-slough	1.6
	Mouth	1.8
Ravenswood Slough	Up-slough	0.6
	Mid-slough	2.0
	Mouth	2.3
Mud Slough	Mid-slough	0.7
Artesian Slough	Mouth	0.1
Alviso Slough	Up-slough	0.3
	Mid-slough	0.9
	Mouth	1.1
Guadalupe Slough	Up-slough	1.1
	Mid-slough	0.2
	Mouth	0.1
Stevens Creek	Up-slough	1.8
Mountain View Slough	Mid-slough	1.6
	Mouth	1.8
Charleston Slough	Up-slough	0.3
	Mouth	0.6
Coyote Creek	Up-slough	0.3
	Mid-slough	0.9
	Mouth	0.4

3.4.3 South Bay Bathymetry

The Alternative C, year 50 bathymetry was developed using the same approach outlined for Alternative A, year 50 as described in Section 3.3.3. The SBGA’s long-term predictions for Alternative C include the following changes: North of San Bruno Shoal, no bathymetric change is predicted; between the San Bruno Shoal and the Dumbarton Bridge, approximately 25 cm of erosion is estimated to occur on the intertidal mudflats; South of Dumbarton Bridge, 22 cm of mudflat erosion is estimated to occur; and no bathymetric change is assumed to occur in the main South Bay channel, the subtidal areas, or within

channels and sloughs outside of the SBSP Restoration Project Area (PWA 2006b). The channel depths were also updated based on hydraulic geometry calculations as described in Section 3.4.2.

3.4.4 Boundary and Initial Conditions

Boundary conditions for Alternative C at year 50 were based on those for Alternative C at year 0 (Section 3.2.2). The only change involved included projected sea-level rise, as described for Alternative A, year 50 in Section 3.3.4. Surface winds and tributary inflows were unchanged from baseline conditions.

Initial conditions were also modified using the same approach as Alternative A at year 50. The initial water level condition was raised to account for sea-level rise and the initial velocity and salinity conditions are unchanged from baseline conditions. The initial salinity condition within the tidally-restored ponds is the same as described for Alternative C, year 0, summer conditions (Section 3.2.2).

<This page intentionally left blank>

4. ALTERNATIVE C, YEAR 0, SUMMER CONDITIONS

This section presents the results of the Alternative C, year 0, simulation under summer conditions, including a comparison with baseline summer conditions. The model predictions are analyzed using time series at stations throughout the South Bay. Figure 4-1 through Figure 4-4 show the station locations for the South Bay and three pond complexes. The model predictions are also analyzed at specific snapshots in time for the entire South Bay and the pond complexes. Figure 4-5 shows where in the analysis period the snapshots were taken with respect to the spring-neap tidal cycle.

The model predictions are compared to baseline summer predictions in order to assess the short-term impacts of opening 90 percent of the ponds to tidal action. As discussed in Section 2.3.1, phasing is not considered and all tidally-restored ponds are opened at year 0. This assumption is considered conservative – and hypothetical – and would result in the maximum system-wide response and the largest potential hydrodynamic changes. Therefore, the results presented in this section are likely an overstatement of the potential impacts. In reality, the restoration will be phased over many years, thereby reducing the magnitude of the project’s impacts. In addition, the simulations presented in this section do not account for the potential scour that would occur as a result of the increased tidal prism in the sloughs and in the main South Bay channel. The sloughs will eventually adjust to the tidal prism, although the timing for this adjustment is unknown – it could be weeks in some sloughs and years in others. The year 50 simulations include estimates of long-term potential channel scour. Modeling with and without scour provides a conservative range of potential hydrodynamic changes.

The sections below present the results with respect to water levels, tidal prism, salinity, circulation, and bed shear stress.

4.1 Water Levels

This section presents the model results with respect to water levels in the South Bay, the tidal sloughs, and the ponds under Alternative C, year 0, summer conditions. The water levels within the South Bay are primarily driven by the tides. The tides in the South Bay are mixed semidiurnal, with two high and two low tides of unequal heights each day. In addition, the tides exhibit strong spring-neap variability, with the spring tides (larger average tidal range) occurring approximately every two weeks during the full and new moon. Spring tides exhibit the greatest difference between successive high and low tides. Neap tides (smaller average tidal range) occur approximately every two weeks during the moon’s quarters, and exhibit the smallest difference between successive high and low tides. Alternative C has the potential to alter the water levels within the South Bay and the tidal sloughs, as presented in the sections below.

4.1.1 South Bay

In the South Bay, the modeled water levels at the San Mateo and Dumbarton Bridges under Alternative C exhibit minimal change when compared with the baseline. Table 4-1 shows the water surface elevation and phase difference for the South Bay under Alternative C summer conditions. Positive values in Table 4-1 represent an increase in water surface elevation when compared with baseline conditions, and

negative values represent a decrease in water surface elevation. Positive phase values correspond to a slower arrival time under Alternative C, or a phase lag when compared with baseline conditions, whereas negative values represent that modeled water levels under Alternative C are leading baseline conditions.

At the San Mateo Bridge (Figure 4-6), lower low water (LLW) increases by approximately 1 cm under both neap and spring conditions (see Table 4-1), and higher high water (HHW) decreases by approximately 1 cm. At the Dumbarton Bridge (Figure 4-7), LLW increases by approximately 2 cm under neap tide and 1 cm under spring tide, and HHW decreases by approximately 1 cm under neap tide and 4 cm under spring tide. The water level changes are relatively negligible north of the Dumbarton Bridge, and the differences are similar to the level of accuracy of the model calibration with respect to tidal amplitudes. The model predicts no noticeable change in phase relative to baseline conditions at either bridge station.

Within the far South Bay, water level and phase changes under Alternative C become more pronounced. At Channel Marker 17 (Figure 4-8), located near the mouth of Coyote Creek, LLW increases by approximately 16 cm under neap tide and 62 cm under spring tide, and HHW decreases by approximately 4 cm under neap tide and 9 cm under spring tide. In general, there is a reduction of the tidal amplitude on three phases of the tidal day (a decrease in high water levels and an increase in low water levels), with the largest change observed at LLW under spring tide conditions. The larger change observed at LLW reflect the influence of the Bay's bathymetry on the water-level dynamics. At LLW, the wetted cross-sectional area conveying water is small, particularly in the far South Bay. The main channel in the far South Bay and through the Dumbarton Narrows is draining a larger surface area than under baseline conditions (e.g., the far South Bay plus the tidally-restored ponds). The baseline wetted cross-sectional area (the area below baseline LLW) does not provide adequate conveyance to drain this larger area, therefore LLW increases. The percent difference in wetted cross-sectional area at HHW between baseline and Alternative C, year 0 conditions is not as great; therefore, the change observed at HHW is smaller than that observed at LLW. It is likely the differences observed at LLW and the asymmetry between the differences observed at LLW and HHW would decrease once the tidal channels and the main South Bay channel have scoured and the conveyance potential is increased.

The long-term trend in reduced tidal amplitude would lead to an increase in the MLLW tidal datum, and a decrease in the MHHW tidal datum. Figure 4-9 depicts the change in MLLW in response to the tidal restoration. The increase in MLLW is most evident in the far South Bay, with the change trending toward zero just north of the San Mateo Bridge. Similar changes are seen with respect to MHHW (Figure 4-10), with the largest reduction occurring in the far South Bay, and the reduction trending toward zero just north of the San Mateo Bridge.

Harmonic analysis was performed on water levels at several stations along the main South Bay channel, and the computed phase and amplitudes of the M_2 and K_1 tidal constituents for baseline and Alternative C, year 0 conditions are compared (Figure 4-11). By comparing the phase and amplitude of the two primary harmonic constituents along the centerline of the South Bay, it is possible to assess how the tidal restoration is affecting the tidal propagation within the South Bay. Figure 4-11a presents the computed phase of the M_2 and K_1 tidal constituents. Little difference is observed in the South Bay as a result of the

restoration project, which is consistent with Table 4-1. Figure 4-11b presents the computed amplitude of the M_2 and K_1 tidal constituents. As the tides propagate into the South Bay, the amplitude of both tidal constituents is decreased, with a more marked difference observed in the M_2 tidal constituent in the far South Bay.

Table 4-1. South Bay Tidal Water Surface Elevation and Phase Differences under Alt C, Year 0, Summer (Water surface elevation differences in cm, phase differences in minutes. June 13 = neap tide, June 22 = spring tide.)

Station Name	June 13 LLW		June 13 HHW		June 22 LLW		June 22 HHW	
	WSE	Phase	WSE	Phase	WSE	Phase	WSE	Phase
San Mateo Bridge, Figure 4-6	1	0	-1	0	1	0	-1	0
Dumbarton Bridge, Figure 4-7	2	0	-1	0	1	0	-4	0
Channel Marker 17, Figure 4-8	16	10	-4	10	62	20	-9	10

4.1.2 Tidal Sloughs

Alternative C has a significant effect on modeled tidal slough water levels within all the three pond complexes. This is expected as the tidally-restored ponds are breached directly to the tidal sloughs, and the volume of water exchanged through the breach represents an increase over the existing, or baseline, tidal prism in the slough. The overall magnitude of the effect on water levels within each slough is therefore dependent on the baseline tidal prism and the tidal prism added to the slough by the restored ponds. The bathymetry and model resolution of the sloughs also plays an important role in determining the change in water levels. As described in Section 3.2, potential slough scour was not included in the simulation; therefore many of the sloughs are undersized relative to the newly restored flow conditions. Tidal damping, or a reduction in tidal amplitude, occurs in undersized sloughs. Over time, the sloughs would widen and deepen, eventually reaching equilibrium conditions and removing the effects of tidal damping. However, this morphological response is not included in the year 0 simulation. As discussed in Section 2.3.5, some of the sloughs, particularly those in the Eden Landing and Ravenswood pond complex, are modeled with larger than actual channel widths due to limitations with respect to the grid resolution; therefore, the model results for these sloughs may underestimate the potential short-term changes in water levels.

Table 4-2 shows the water surface elevation and phase difference for the water levels under Alternative C at both upstream (landward) and downstream (near the mouth) stations in each tidal slough. Positive values in Table 4-2 represent an increase in water surface elevation when compared with baseline conditions and negative values represent a decrease in water surface elevation. Positive phase values correspond to a slower arrival time under Alternative C, or a phase lag when compared with baseline conditions, whereas negative values represent that modeled water levels under Alternative C are leading baseline conditions.

Near the mouths of sloughs (downstream stations), the water level trends are similar to that seen at Channel Marker 17 in the South Bay. For most sloughs, there is a moderate reduction of tidal amplitude on three phases of the tidal day (a moderate decrease in high water levels and an increase in low water

levels), with the largest change observed at LLW when compared to baseline conditions. The larger increase in water levels at LLW reflects the influence of the channel geometry on the water level dynamics. At low water levels, the wetted cross-section area of the channel is small, yet it is draining a large surface area (e.g., the tidally-restored ponds). Therefore, in order to convey the larger volume of water, LLW is increased relative to baseline conditions. The relative difference between the wetted cross-sectional area under baseline and Alternative C, year 0 conditions is not as great at HHW, therefore a smaller water level difference is observed. Water levels downstream in Alviso Slough (Figure 4-22) provide an example of this response pattern. At both high water marks and higher low water (HLW), Alternative C predicts damping on the order of 20 – 60 cm during spring tides and by 10 – 40 cm during neap tides. In contrast, the tidal range of LLW is predicted to dampen by more than 100 cm during spring tides and by 60 cm during neap tides. The sloughs located in the far South Bay in the Alviso pond complex experience the largest reductions in tidal amplitude owing to the larger baseline tidal range and the subsided nature of the ponds in the Alviso pond complex which provide for greater increases in tidal prism.

Phasing changes are relatively small at the downstream stations in the Eden Landing pond complex, with Alternative C lagging behind baseline conditions by approximately 20 minutes during neap tides and 30 minutes during spring tides. In the Ravenswood pond complex, Alternative C lags behind baseline conditions on the order of 10 – 30 minutes during neap tide and 40 – 90 minutes during spring tide. In the Alviso pond complex, phase changes are on the order of 60 minutes during neap tide and 90 minutes during spring tide in Alviso Slough (Figure 4-22) and Guadalupe Slough (Figure 4-24) and slightly less in Coyote Creek (Figure 4-16).

Water level changes are more pronounced upstream in the tidal sloughs, owing both to friction and the undersized nature of the sloughs. The asymmetry between the increase in LLW and the reductions in tidal amplitude on the other phases of the tide is also less pronounced than at the downstream stations. The greater frictional effects coupled with the undersized nature of the sloughs relative to the tidal prism they supply also leads to greater phase differences, with Alternative C lagging approximately 2 hours behind baseline conditions upstream in Alviso Slough (Figure 4-23) and Guadalupe Slough (Figure 4-25).

Table 4-2. Tidal Slough Water Surface Elevation and Phase Differences under Alt C, Year 0, Summer (Water surface elevation differences in cm, phase differences in minutes. June 13 = neap tide, June 22 = spring tide.)

Station Name	June 13 LLW		June 13 HHW		June 22 LLW		June 22 HHW	
	WSE	Phase	WSE	Phase	WSE	Phase	WSE	Phase
<i>Eden Landing pond complex</i>								
ACFCC Downstream, Figure 4-12	16	20	-8	20	31	20	-32	30
ACFCC Upstream, Figure 4-13	0	60	-5	20	5	-30	-33	50
Old Alameda Creek Downstream, Figure 4-14	8	0	-4	0	37	10	-18	0
Old Alameda Creek Upstream, Figure 4-15	10	10	-6	20	49	30	-41	80
<i>Alviso pond complex</i>								
Coyote Creek Power Tower, Figure 4-16	25	30	-12	0	69	100	-26	0
Coyote Creek Railroad Bridge, Figure 4-17	20	40	-23	30	73	80	-46	50
Coyote Creek/Island Ponds, Figure 4-18	19	20	-23	30	71	70	-49	60
Coyote Creek Upstream, Figure 4-19	19	30	-25	30	71	60	-52	70
Mud Slough Downstream, Figure 4-20	19	30	-25	10	72	80	-52	20
Mud Slough Upstream, Figure 4-21	17	20	-28	70	67	60	-57	100
Alviso Slough Downstream, Figure 4-22	60	50	-27	20	110	80	-46	30
Alviso Slough Upstream, Figure 4-23	79	100	-45	130	103	110	-65	110
Guadalupe Slough Downstream, Figure 4-24	52	50	-11	10	119	90	-17	0
Guadalupe Slough Upstream, Figure 4-25	75	110	-41	130	100	110	-56	90
Moffett Channel, Figure 4-26	75	110	-41	130	100	110	-56	90
Stevens Creek Downstream, Figure 4-27	12	0	-17	20	26	-10	-23	30
Stevens Creek Upstream, Figure 4-28	11	0	-29	130	28	0	-27	70
Mountain View Slough Downstream, Figure 4-29	51	60	-29	110	71	30	-20	60
Mountain View Slough Upstream, Figure 4-30	50	30	-28	110	69	20	-20	60
Charleston Slough Downstream, Figure 4-31	41	50	-21	60	55	30	-21	70
Charleston Slough Upstream, Figure 4-32	32	60	-21	50	49	20	-21	70
<i>Ravenswood pond complex</i>								
Ravenswood Slough Downstream, Figure 4-33	15	10	-14	30	71	40	-46	90
Ravenswood Slough Upstream, Figure 4-34	49	30	-11	10	65	10	-13	10

4.1.3 Ponds

Under baseline conditions, only the Island Ponds in the Alviso pond complex and the Eden Landing Ecological Reserve in the Eden Landing pond complex are open to tidal inundation. Restoring additional ponds to tidal action would therefore impact water levels within these existing restoration sites. Figure 4-35 displays the water level in the center of Pond A20 (one of the Island Ponds). Under Alternative C, Pond A20 experiences a reduction in high water levels. Low water levels remain unchanged as Pond A20 sits relatively high in the tide frame and the pond is effectively drained under low water conditions.

In the Eden Landing Ecological Reserve, water levels in the north wetlands remain largely unaffected (Figure 4-36). These wetlands are hydraulically connected to the South Bay via Mount Eden Creek, which experiences only a nominal increase in tidal prism under Alternative C. The southern wetlands are hydraulically connected to the South Bay via North Creek. The tidal prism in North Creek is expected to increase by approximately 380 percent due to the tidal breaches under Alternative C (Figure 3-15); therefore the water levels in the southern wetlands experience reductions in tidal amplitude (a decrease in high water levels and an increase in low water levels), with the largest changes occurring on spring tides (Figure 4-37).

Ponds that are not hydraulically connected to the South Bay under baseline conditions (except by culverts and flap gates) would be connected under Alternative C through tidal breaches to the sloughs. The water levels in the ponds are therefore similar to that of the tidal sloughs. In the Eden Landing and Ravenswood ponds complexes, the pond bottom elevations are relatively high in the tide frame; therefore, the ponds are only inundated during high tides. Figure 4-38 shows the water level variability in Pond E6B in the Eden Landing pond complex. This pond only experiences diurnal tidal variability during spring tides, and during neap tides, most of the pond area would be effectively drained. However, marsh channels inside the pond would likely exhibit more tidal variability.

In the Alviso pond complex, pond bottom elevations sit lower in the tide frame and the ponds are therefore exposed to diurnal tidal action throughout the spring-neap tide cycle. Ponds A7 and A8 (Figure 4-39 and Figure 4-40, respectively) provide an example of the tide range expected within the subsided ponds. Unlike Pond E6B and similar ponds with higher bottom elevations, Ponds A7 and A8 do not experience cycles of wetting and drying during the diurnal tidal cycle. Instead, the ponds contain water at all times. The tide range within any specific pond will depend on the location of its hydraulic connection to the Bay and the pond's elevation relative to the tides.

4.2 Tidal Prism

Tidal prism – the volume of water exchanged over a complete tidal cycle – is a useful quantity for examining the changes in water mass movement as a result of the different restoration alternatives. Estimates of tidal prism provide a first order indicator of several potential responses to the restoration. For example, the tidal prism controls the evolving geomorphology of the system by determining the scour potential from tidal currents. Additionally, tidal prism delivers suspended sediment into the restored regions, thereby promoting the infill of subsided salt ponds. Tidal prism also comprises the denominator in the estimate of flushing time. Flushing time indicates the rate of water turnover in a region, which often influences water quality (Monsen and others 2002; Sheldon and Alber 2006).

For the basis of comparing tidal prism estimates with previous studies, tidal prism has been estimated as the volume of water crossing a cross-section during a flood tide. Tidal prism was estimated from the DELFT3D model by first calculating the instantaneous discharge as the product of velocity and water depth across the cross-sections shown in Figure 4-41 through Figure 4-44. These instantaneous discharges were then integrated for each flood tide to estimate the total volume of water entering through

that cross-section during each tide. The reported tidal prism is the average of all the flood tide volumes which occurred during the analysis period.

Estimates of tidal prism based on the DELFT3D model results for the baseline conditions exhibit fair to good agreement with previous estimates of tidal prism, as shown in Table 4-3. The DELFT3D baseline estimate of tidal prism exceeds Schemel’s (1995) estimate at the San Mateo Bridge by approximately 15 percent, and at the Dumbarton Bridge, the model and Schemel (1995) agree within approximately 10 percent. The agreement with the results of Gross and Schaaf & Wheeler (2003a) are within 40 percent at Calaveras Point and Coyote Creek at the Railroad Bridge. On Coyote Creek east of the Island Ponds, the two estimates differ by just over a factor of two. Some of these discrepancies may be attributed to different methods for estimating tidal prism, consideration of different tidal periods, and, in the case of Gross and Schaaf & Wheeler (2003a), different landward extents of the model domains.

Table 4-3. Comparison of Previous Estimates of Tidal Prism with DELFT3D Baseline Estimates

Transect location	Tidal prism (millions of cubic meters)		
	Schemel (1995)	Gross and Schaaf & Wheeler (2003a)	DELFT3D baseline Alternative A, year 0, summer
San Mateo Bridge	220	-	270
Dumbarton Bridge	62		70
Calaveras Point	-	9.9	14
Coyote Creek at RR Bridge	-	1.6	2.2
Coyote Creek east of Island Ponds	-	0.25	0.53

The tidal prism estimates for Alternative C, year 0, summer conditions are compared against baseline conditions in Table 4-4. For cross-sections outside of the project area, such as the San Mateo Bridge, the Dumbarton Bridge, and non-project sloughs, the difference between baseline and Alternative C, year 0, summer conditions is less than five percent. Figure 4-45 displays the instantaneous modeled flux through San Mateo and Dumbarton Bridge cross-sections under baseline and Alternative C, year 0, summer conditions. At the San Mateo Bridge cross-section, little difference is evident. However, at the Dumbarton Bridge cross-section, the modeled flux decreases slightly under Alternative C conditions. This is consistent with the tidal prism estimates presented in Table 4-4.

At a cross-section through Channel Marker 17, the modeled flux is slightly larger under Alternative C conditions when compared to baseline conditions (Figure 4-46). Further south at Calaveras Point, the modeled flux under Alternative C is noticeably larger than under baseline conditions, which is consistent with the 21 percent increase in tidal prism predicted in Table 4-4.

The tidal prism associated with the sloughs in the three pond complexes is predicted to increase. The increase is dependent on the volume of the tidally-restored ponds breached to particular slough and how accurately a slough is represented in the model. For example, the tidal prism in the ACFCC is predicted to increase by approximately 63 percent, which is consistent with the pond volume draining to the flood control channel. In contrast, the tidal prism in Old Alameda Creek is predicted to increase by less than 15

percent. Although this volume increase is consistent with the volume of ponds breached to this slough, this is likely an underestimate of the actual percentage increase in tidal prism as a result of the SBSP Restoration Project. Old Alameda Creek, and the associated channels of Mt. Eden Creek and North Creek, are oversized in the model grid, as discussed in Section 2.3.5. The baseline tidal prism in Old Alameda Creek from estimated from GIS is 0.32 million cubic meters (Table 3-6), which is an order or magnitude less than the baseline estimate from the model of 1.4 million cubic meters (Table 4-4). However, the increase in tidal prism of 0.2 million cubic meters is likely representative of the added pond volume due to the restoration; therefore the tidal prism in Old Alameda Creek could increase approximately 67 percent (from 0.32 to 0.52 million cubic meters). Figure 4-47 presents the modeled flux through the ACFCC and Old Alameda Creek transects under both baseline and Alternative C, year 0, summer conditions. The modeled flux is predicted to increase in both sloughs, with a larger increase associated with the ACFCC.

A range of tidal prism response is predicted within the Alviso pond complex. Most of the slough transects exhibit an increase in tidal prism as more water flows through the sloughs and into the breached ponds. Along Coyote Creek, there is a progression of tidal prism changes (Figure 4-48). Near the mouth, at the Power Tower, the predicted change is several million cubic meters. Since Coyote Creek is a large channel, this change represents an increase of only 36 percent over baseline even though several large ponds would breach to this channel. Further up Coyote Creek, at the Railroad Bridge and east of the Island Ponds, the tidal prism decreases as a result of restoration. This decrease occurs because flows which reach these transects under baseline conditions are deflected into the newly breached ponds under Alternative C.

Alviso Slough and Guadalupe Slough are represented fairly well in the model, and the modeled flux at the downstream transects does increase measurably in both sloughs (Figure 4-49), with an increase in tidal prism of approximately 160 percent predicted by the model (Table 4-4). The predicted increases are largest for those cross-sections across small sloughs which access large pond areas. For instance, a tidal prism increase of approximately 280 percent is predicted for Mountain View Slough, a small slough that would connect two large ponds to the Bay. In addition, the large increase associated with Mountain View Slough is caused in part by a portion of Charleston Slough's existing and potential tidal prism being routed through the upstream breach to Pond A1 on Charleston Slough, through Pond A1, and into Mountain View Slough. Mountain View Slough is among those sloughs that are oversized in the model; therefore the actual percent increase in tidal prism may be larger. The same can be said for Charleston Slough and Stevens Creek. These sloughs have relatively little flow under baseline summer conditions, and the modeled flux at the downstream transects increases markedly under Alternative C, year 0, summer conditions (Figure 4-50 and Figure 4-51).

The model predicts an increase of approximately 180 percent in tidal prism for Ravenswood Slough, the main tidal channel in the Ravenswood pond complex (Figure 4-51). Under baseline conditions, Ravenswood Slough's tidal prism is among the smallest of all the cross-section presented in Table 4-4. Hence, with the addition of nearly the entire complex's pond area to the slough's drainage area, the large increase is expected. Ravenswood Slough is also among those sloughs that are oversized in the model, as discussed in Section 2.3.5; therefore, the actual percent increase in tidal prism may be larger.

The tidal prism within each slough may be larger than presented in Table 4-4 after sloughs scour and deepen and before pond sedimentation raises pond bottom elevations. Due to the subsided nature of the ponds within the Alviso pond complex, this potential increase in tidal prism would be greatest in the Alviso pond complex sloughs.

Table 4-4. Comparison of Tidal Prism between Baseline and Alternative C, year 0, Summer

Transect Location	Tidal Prism (millions of cubic meters)		
	Baseline summer	Alternative C year 0, summer	% change baseline to Alt. C
<i>South Bay</i>			
San Mateo Bridge	270	260	-2.6%
Dumbarton Bridge	71	68	-3.7%
<i>Eden Landing pond complex</i>			
ACFCC	1.4	2.3	63%
Old Alameda Creek	1.4	1.6	14%
Mount Eden Creek	0.58	0.74	27%
<i>Ravenswood pond complex</i>			
Ravenswood Slough	0.53	1.5	180%
<i>Alviso pond complex</i>			
Calaveras Point	14	17	21%
Coyote Creek at Power Tower	6.8	9.2	36%
Coyote Creek at RR Bridge	2.2	1.6	-28%
Coyote Creek east of Island Ponds	0.53	0.36	-31%
Charleston Slough	0.55	0.94	72%
Mountain View Slough	0.21	0.82	280%
Stevens Creek	0.11	0.23	110%
Guadalupe Slough	1.1	2.9	160%
Alviso Slough	1.1	2.9	160%
Artesian Slough	0.48	0.60	25%
<i>Non-project Sloughs</i>			
Corkscrew Slough	3.4	3.4	-1.0%
Redwood Creek	16	15	-3.3%
Westpoint Slough	2.9	2.9	-1.2%
Mowry Slough	0.41	0.39	-4.4%
Plummer Slough	0.32	0.31	-2.4%
Newark Slough	0.86	0.84	-2.3%

4.3 Salinity

This section presents the model results with respect to salinity in the South Bay and the tidal sloughs under Alternative C, year 0, summer conditions. The model predictions are compared to baseline summer predictions in order to assess the impact of opening 90 percent of the ponds to tidal action.

Salinity in the South Bay is governed by the salinity in the Central Bay and exchange between South and Central Bays, freshwater inflows to South Bay, and evaporation. Generally, the South Bay is vertically well mixed (i.e. there is little tidally-averaged vertical salinity variation) with near oceanic salinities due to low freshwater inputs to the far South Bay in the summer and fall, and year round during dry years. The SBSP Restoration Project has the potential to alter the salinity regimes within the South Bay, as presented in the sections below.

Modeled salinity within the South Bay is highly dependent on the initial salinity condition, particularly due to the relatively long residence times within the South Bay under summer conditions. As discussed in Section 3.2.2, the initial salinity prescribed within the ponds was set by the salinity in the neighboring tidal sloughs, which approximates breaching the ponds in the spring when freshwater tributary inflows would have lowered salinities within the tidal sloughs and ponds, and the influence of high summer evaporation rates on salinity could be neglected. However, if breaching were to occur later in the summer or fall, salinity levels within the ponds would likely be higher at the time of breaching due to evaporation.

Upon initially opening the ponds to tidal action, the mass of lower salinity water in the Alviso ponds begins to exchange with the South Bay, introducing a significant source of freshwater and resulting in an apparent “freshening” of the far South Bay. This is expected to be a transient effect, and as the mass of freshwater works its way out of the South Bay, salinities in the South Bay would increase above baseline levels. However, quantification of this salinity increase would require running the hydrodynamic model for several months to a year, which is impractical due to the long run times required. The South Bay Model currently runs approximately three to four times faster than real time, therefore a one-year simulation would require three months of run time at a minimum.

The hydrodynamic model was run for an additional two months beyond the analysis period (July and August), and the increase in salinities in the far South Bay is evident as the system approaches equilibrium (Figure 4-52). The salinity results presented in this section, therefore, focus on the modeling results from August rather than the June analysis period.

4.3.1 South Bay

Under Alternative C, immediately after restoring 90-percent of the SBSP Restoration Project Area to tidal action, the far South Bay experiences a freshening effect based on the initial salinity conditions within the ponds, therefore the analysis in this section focuses on August conditions when the South Bay has approached equilibrium conditions. (Table 4-5) presents modeled salinity differences in the South Bay under both spring and neap conditions at LLW and HHW. Positive values in Table 4-5 represent an increase in salinities relative to the baseline, and negative values represent a decrease in salinities relative

to baseline conditions. At the San Mateo and Dumbarton Bridges, there are no significant differences in salinity when compared with baseline conditions (Figure 4-53 and Figure 4-54, respectively). This trend is expected to continue, and the SBSP Restoration Project is not expected to impact South Bay salinities north of the San Mateo Bridge.

At Channel Marker 17, salinity is initially depressed in response to the initial pond conditions. Due to the shorter residence times near Coyote Creek, equilibrium conditions are reached by August and salinities are slightly higher than baseline conditions at HHW and approximately 6 ppt higher at LLW (Figure 4-55). The salinity changes are highly correlated with the changes in water levels observed in the South Bay, with the largest changes occurring at LLW.

Figure 4-56 displays the salinities in the South Bay during spring conditions at HHW, representing peak salinity conditions during the August analysis period. As can be seen, little difference in peak South Bay salinities occurs under summer conditions with respect to Alternative C, year 0 conditions. The largest changes in salinity are confined to the tidal sloughs. Figure 4-57 displays South Bay salinities at LLW during spring tide conditions. At low water, the observed differences are higher downstream of the tidal sloughs and in the subtidal channels in the far South Bay.

Table 4-5. South Bay Salinity Differences under Alt C, Year 0, Summer
(Salinity differences in ppt. Aug 27 = neap tide, Aug 19 = spring tide.)

Station Name	Aug 27 LLW	Aug 27 HHW	Aug 19 LLW	Aug 19 HHW
San Mateo Bridge, Figure 4-53	-0.1	-0.1	-0.1	-0.1
Dumbarton Bridge, Figure 4-54	-0.1	-0.1	0.0	-0.1
Channel Marker 17, Figure 4-55	6.4	0.1	6.5	0.3

4.3.2 Tidal Sloughs

As with the salinities in the South Bay, the initial conditions specified in the tidally-restored ponds have a transient affect on salinities. Salinities are initially depressed and then slowly trend towards equilibrium conditions. Table 4-6 shows the salinity difference under Alternative C for neap and spring tide conditions. Positive values represent an increase in salinities relative to the baseline, and negative values represent a decrease in salinities relative to baseline conditions.

In the Eden Landing pond complex, salinities in Old Alameda Creek (Figure 4-60 and Figure 4-61) and the upstream portion of the ACFCC (Figure 4-59) exhibit little change relative to baseline conditions. Downstream in ACFCC (Figure 4-58) exhibits a greater change in salinities which are highly correlated with the modeled changes in water levels (Figure 4-12). Peak salinities at HHW increase slightly relative to the baseline, while salinities at LLW show a marked increase greater than 13 ppt relative to baseline conditions in response to the increased tidal prism and greater mixing between the slough and the Bay.

Figure 4-62 and Figure 4-63 present the peak salinities in the Eden Landing pond complex during spring HHW and LLW conditions, respectively. As can be seen, the largest salinity changes are observed in the ACFCC and the South Bay directly downstream.

Within the tidal sloughs in the Alviso pond complex, the short-term freshening response is more evident. Salinities are initially depressed in response to the mass of freshwater entering the system from the breached ponds, and salinities steadily increase over the three-month simulation as equilibrium conditions are obtained. In the downstream reaches of Coyote Creek (Figure 4-64 and Figure 4-65), salinities increase 1 – 3 ppt on high water levels, with larger increases on the order of 5 – 9 ppt at low water. In the upstream reaches of Coyote Creek (Figure 4-66 and Figure 4-67) salinities increase with respect to baseline conditions on all phases of tide.

Both Alviso Slough and Guadalupe Slough experience a significant damping of the diurnal salinity range near the slough mouths (Figure 4-70 and Figure 4-72, respectively), with salinities at high water slightly above baseline conditions, while salinities at LLW are more than 10 ppt higher than baseline conditions. Upstream, salinities increase on all phases of the tide, with increases greater than 15 ppt occurring on spring tides (Figure 4-71 and Figure 4-73). These increases in salinity levels are correlated with the modeled changes in water levels. The salinities in the sloughs increase due to the increased mixing between the sloughs and the Bay.

Stevens Creek, Mountain View and Charleston Sloughs exhibit very little diurnal salinity variation under both baseline and Alternative C conditions due to the low summer tributary freshwater inflow contributions. These sloughs are also represented in the model at approximately twice their actual width; therefore, they are more hydraulically connected to the Bay in the model than they are in reality. The salinities are therefore highly correlated with Bay salinities and increase approximately 0 – 2 ppt above baseline conditions downstream (Figure 4-75, Figure 4-77 and Figure 4-79, respectively) and upstream (Figure 4-76, Figure 4-78 and Figure 4-80, respectively). Figure 4-81 and Figure 4-82 present the peak salinities in the Alviso pond complex during spring HHW and LLW conditions, respectively. In general, salinity increases are observed throughout the Alviso pond complex, with larger increases observed at LLW.

Salinities in Ravenswood Slough in the Ravenswood pond complex (Figure 4-83 and Figure 4-84) are similar to those seen at the Dumbarton Bridge (Figure 4-54) due to the close proximity of this station, and the minimal tributary freshwater contribution from Ravenswood Slough during the dry summer season. Figure 4-85 and Figure 4-86 present the peak salinities in the Ravenswood pond complex during spring HHW and LLW conditions, respectively. As can be seen, little difference is observed between baseline and Alternative C, year 0 conditions.

Table 4-6. Tidal Slough Salinity Differences under Alt C, Year 0, Summer
(Salinity differences in ppt. Aug 27 = neap tide, Aug 19 = spring tide)

Station Name	Aug 27 LLW	Aug 27 HHW	Aug 19 LLW	Aug 19 HHW
<i>Eden Landing pond complex</i>				
ACFCC Downstream, Figure 4-58	13.6	1.4	13.5	0.2
ACFCC Upstream, Figure 4-59	0.0	0.0	0.1	-0.3
Old Alameda Creek Downstream, Figure 4-60	-0.1	-0.1	-0.4	0.2
Old Alameda Creek Upstream, Figure 4-61	-0.4	-0.4	-0.1	0.1
<i>Alviso pond complex</i>				
Coyote Creek Power Tower, Figure 4-64	8.9	0.5	7.7	0.6
Coyote Creek Railroad Bridge, Figure 4-65	4.3	2.1	5.7	1.2
Coyote Creek/Island Ponds , Figure 4-66	5.0	4.2	5.3	6.9
Coyote Creek Upstream, Figure 4-67	3.8	3.9	4.1	4.1
Mud Slough Downstream, Figure 4-68	7.6	6.9	9.3	3.6
Mud Slough Upstream, Figure 4-69	5.1	5.4	4.9	4.4
Alviso Slough Downstream, Figure 4-70	10.3	1.0	11.7	0.9
Alviso Slough Upstream, Figure 4-71	13.6	13.6	13.2	13.2
Guadalupe Slough Downstream, Figure 4-72	7.9	1.1	8.4	1.4
Guadalupe Slough Upstream, Figure 4-73	15.1	13.9	16.4	13.9
Moffett Channel, Figure 4-74	13.1	12.3	15.4	14.1
Stevens Creek Downstream, Figure 4-75	1.4	0.7	1.8	1.1
Stevens Creek Upstream, Figure 4-76	0.7	0.6	1.5	1.5
Mountain View Slough Downstream, Figure 4-77	0.3	0.2	0.6	0.8
Mountain View Slough Upstream, Figure 4-78	0.2	0.1	0.5	0.5
Charleston Slough Downstream, Figure 4-79	0.2	0.2	0.5	0.5
Charleston Slough Upstream, Figure 4-80	1.0	0.2	0.8	0.5
<i>Ravenswood pond complex</i>				
Ravenswood Slough Downstream, Figure 4-83	0.2	0.3	0.1	0.2
Ravenswood Slough Upstream, Figure 4-84	0.3	0.3	0.6	0.6

4.4 Circulation

Potential changes to South Bay circulation can be evaluated by examining current velocities at specific locations within the Bay and tidal sloughs, and by examining general changes to South Bay residual circulation. The most important factor influencing circulation patterns in South Bay is bathymetry (Cheng and Gartner 1985). At year 0, the only bathymetric change associated with the simulation is hydraulically connecting the ponds to the Bay and re-introducing tidal action. This, in itself, represents a large-scale bathymetric change.

4.4.1 Current Velocity

South Bay

In the South Bay, modeled velocities at the San Mateo and Dumbarton Bridges exhibit little change relative to baseline conditions. Table 4-7 shows the peak velocity magnitudes at the bridge and Channel Marker 17 stations under baseline and Alternative C conditions. Positive values indicate a higher modeled velocity under Alternative C, and negative values indicate a decrease in current velocity under Alternative C.

At the San Mateo Bridge (Figure 4-87), velocity magnitudes are slightly higher under Alternative C relative to baseline conditions, although the difference is relatively minor. At the Dumbarton Bridge (Figure 4-88), velocity magnitude differences are becoming more noticeable. This is expected as the tidally-restored areas are located on both sides of the bridge, with approximately 20 percent of the added potential tidal prism to the north of the Dumbarton Bridge, and 80 percent located to the south in the Alviso pond complex. Velocity magnitudes decrease slightly relative to baseline conditions. This decrease is due in part to the undersized nature of the tidal sloughs which restrict tidal exchange between the ponds and the Bay.

In the far South Bay at Channel Marker 17 (Figure 4-89), velocity magnitude increases are more pronounced relative to baseline conditions due to the close proximity of the Alviso pond complex and the location of the station in the main South Bay channel. Velocity magnitude increases of greater than 50 cm/s are predicted. The velocity magnitude increases are highest under strong ebb conditions; however, this dynamic is also a function of the undersized nature of the tidal sloughs connecting the ponds and the Bay. As the sloughs widen and deepen, the flood-ebb asymmetry in the velocity magnitude increase relative to baseline conditions is diminished, as is shown in the year 50 simulation presented in Section 7 when bathymetric change is included in the model simulations. The velocity increase at Channel Marker 17 is larger than observed at the Dumbarton Bridge due to the relative wetted cross-sectional area at LLW when velocities are highest. The main South Bay channel in the vicinity of the Channel Marker 17 is currently oversized, as is evident by its recent rate of infilling (Jaffe and Foxgrover 2006b). It is possible that the channel would be subject to scour post restoration, rather than continued deposition.

Figure 4-90 and Figure 4-91 depict velocity magnitudes within the South Bay under peak flood and peak ebb conditions under baseline and Alternative C conditions, as well as the difference between the two model predictions. The difference is strongest under spring ebb conditions near the mouths of the tidal sloughs and in the main South Bay channel. The differences under spring flood conditions are primarily seen near the mouths of the tidal sloughs.

Table 4-7. South Bay Peak Velocity Magnitude Comparisons: Alt C, Year 0, Summer vs. Baseline, Summer

(All velocities in cm/s)

Station Name	Baseline	Alt C	Difference
San Mateo Bridge, Figure 4-87	102	103	1
Dumbarton Bridge, Figure 4-88	34	31	-3
Channel Marker 17, Figure 4-89	67	119	52

Tidal Sloughs

In the South Bay, modeled velocities within the tidal sloughs experience significant changes in response to the restoration. The majority of the tidal sloughs exhibit a strong flood-ebb asymmetry in the velocity magnitude increases due to the undersized nature of the sloughs, with a larger increase in velocity magnitudes on ebb tide. This asymmetry is expected to dissipate as the sloughs widen and deepen in response to the increased tidal prism. Table 4-8 shows the peak velocity magnitudes at the downstream stations in the tidal sloughs under baseline and Alternative C conditions. Positive values indicate a higher modeled velocity under Alternative C, and negative values indicate a decrease in current velocity under Alternative C.

In the Eden Landing pond complex, velocity magnitudes in the ACFCC increase significantly in response to the increased tidal prism, with velocity magnitudes increasing by a factor of two on ebb and flood tides (Figure 4-92). This increase is due to the relatively large increase in tidal prism associated with the restored ponds. In Old Alameda Creek, velocity magnitudes increase on the order of 5 – 20 cm/s (Figure 4-93). This increase may be an underestimate due to the oversized representation of Old Alameda Creek in the model, as discussed in Section 2.3.5. Figure 4-94 and Figure 4-95 depict the tidal slough velocity magnitudes within the Eden Landing pond complex at both strong flood and strong ebb, respectively. At strong ebb, the largest differences are seen in the South Bay just beyond the slough mouth. At strong flood, the largest velocity magnitude differences relative to baseline conditions are seen in the downstream reaches of the sloughs.

In the Alviso pond complex, velocity magnitudes at the downstream stations increase relative to baseline conditions. The magnitude of the increase is correlated with the associated increase in upstream tidal prism. This can be seen in Coyote Creek at the Power Tower station which is downstream of breaches along Coyote Creek and Alviso Slough (Figure 4-96). Farther upstream in Coyote Creek, stations at the Railroad Bridge (Figure 4-97) and at the upstream edge of the Island Ponds (Figure 4-98) are located upstream of the majority of the pond breaches. At these stations, velocity magnitudes decrease relative to baseline conditions due to the large percentage of the flow captured by the ponds.

Velocity magnitudes are also predicted to decrease in Charleston Slough (Figure 4-105) because the model predicts that a portion of Charleston Slough’s existing and potential tidal prism is routed through the upstream breach to Pond A1 on Charleston Slough, through Pond A1, and into Mountain View Slough. This flow path could be prevented during the detailed design phase for Pond A1. As with Old

Alameda Creek, the velocity changes may be underestimated in Stevens Creek, Charleston Slough and Mountain View Slough due to the oversized representation of these sloughs in the model.

Figure 4-106 and Figure 4-107 depict the tidal slough velocity magnitudes within the Alviso pond complex at both strong flood and strong ebb, respectively. As with the Eden Landing pond complex, the largest differences under strong ebb conditions are seen in the far South Bay just beyond the slough mouth. At strong flood, the largest velocity magnitude differences relative to baseline conditions are seen in the downstream reaches of the tidal sloughs.

In the Ravenswood pond complex, peak velocity magnitudes increase by a factor of two with respect to baseline conditions under both flood and ebb conditions (Figure 4-108). Figure 4-109 and Figure 4-110 depict the tidal slough velocities within the Ravenswood pond complex at both strong flood and strong ebb, respectively. As with the other pond complexes, the largest differences under strong ebb conditions are seen in the far South Bay just beyond the slough mouth. At strong flood, the largest velocity magnitude differences relative to baseline conditions are seen in the downstream reach of the slough.

Table 4-8. Tidal Slough Peak Velocity Comparisons: Alt C, Year 0, Summer vs. Baseline, Summer
(All velocities in cm/s)

Station Name	Baseline	Alt C	Difference
ACFCC Downstream, Figure 4-92	45	105	60
Old Alameda Creek Downstream, Figure 4-93	53	72	19
Coyote Creek Power Tower, Figure 4-96	76	104	28
Coyote Creek Railroad Bridge, Figure 4-97	82	59	-23
Coyote Creek/Island Ponds, Figure 4-98	39	23	-16
Mud Slough Downstream, Figure 4-99	46	49	4
Alviso Slough Downstream, Figure 4-100	49	135	86
Guadalupe Slough Downstream, Figure 4-101	46	110	64
Moffett Channel, Figure 4-102	5	1	-3
Stevens Creek Downstream, Figure 4-103	51	101	49
Mountain View Slough Downstream, Figure 4-104	49	75	26
Charleston Slough Downstream, Figure 4-105	77	64	-13
Ravenswood Slough Downstream, Figure 4-108	38	83	45

4.4.2 Residual Circulation

The total residual current observed in the South Bay is a product of tidally-driven residual currents, as well as wind-driven and density-driven circulation patterns. Density-driven currents are generally insignificant in the South Bay due to isohaline conditions (Walters and others 1985), and are not well-represented by the 2D depth-averaged model formulation. Wind-driven circulation in the main South Bay channel is also not well-represented in a 2D model, as the wind can drive a surface flow in the direction of the wind, and a return flow in the deep channel. In the South Bay, the wind-driven surface current is typically towards the south in the summer and fall, with a northward return flow deep in the main South Bay channel.

The residual currents presented here are a product of tidally-driven and wind-driven circulation. Residual circulation is the net advective transport of water and its constituents, which can be obtained by averaging the velocities at each point over one tidal cycle (Fischer and others 1979). Since no tidal cycle is identical to the next, the residual circulation will vary spatially and temporally. In order to compare the potential impact to residual circulation within the South Bay, the velocities at each point in the model were averaged at two hour intervals over two spring-neap tidal cycles, or approximately 29 days (from June 1, 2001 to June 29, 2001).

Figure 4-111 displays the 29-day residual circulation under summer baseline conditions. The residual currents observed in the model simulation agree with previous modeling exercises and field studies (Cheng and Casulli 1982; Gross 1997; Lucas 1997; Walters and others 1985). In general, there is a northward tidally-driven residual current along the eastern shoal, with a counter-clockwise gyre directly north of the San Mateo Bridge, and a clockwise gyre directly south of the San Bruno Shoal (Cheng and Casulli 1982; Lucas 1997; Walters and others 1985). The strongest residual current south of the San Mateo Bridge is in the main South Bay channel, with a southerly flow running from the San Mateo Bridge past the Dumbarton Bridge and into the far South Bay. A strong northerly residual current is also seen in Coyote Creek.

Figure 4-112 displays the 29-day residual circulation for Alternative C, with 90 percent of the ponds restored to tidal action, and Figure 4-113 displays the difference between the predicted residual circulation under baseline and Alternative C conditions (Alternative C minus baseline). Little to no change in residual circulation is observed north of the San Mateo Bridge, and little change is observed near the Eden Landing pond complex. The increased tidal prism from the Ravenswood pond complex is observed in the residual currents from Ravenswood Slough.

Figure 4-114 displays the 29-day residual circulation under summer baseline conditions for the far South Bay, and

Figure 4-115 displays the same under Alternative C conditions, while Figure 4-116 displays the difference. The increased tidal prism associated with each tidal slough in the Alviso pond complex is evident. In general, the largest changes in residual circulation are seen in the far South Bay, as is expected by the comparatively large area of the Alviso pond complex and the number of deeply subsided ponds which contribute to the increase in tidal prism. The net-northward residual current is stronger under Alternative C than under baseline conditions.

4.5 Bed Shear Stress

Potential impacts to sediment erosion and deposition patterns are inferred based on comparisons of total bed shear stress both before and after tidal restoration, where total bed shear stress is a function of both tidal currents and locally-generated wind-waves. Cloern and others (1989) found that suspended sediment in the South Bay is weakly correlated with the advective flux, highlighting the importance of local resuspension. In the shallow regions of the South Bay where significant erosion has been shown to occur (Foxgrover and others 2004; Jaffe and Foxgrover 2006b), tidal forcing is generally weak and insufficient

to resuspend sediment, therefore locally-generated wind-waves are hypothesized to be the dominant factor affecting mudflat erosion. This hypothesis is further supported by Schoellhamer (1996), who found that suspended sediment concentrations in the South Bay are well correlated with wind and local wind-wave induced shear stress.

Tidal restoration has the potential to alter both tidally-driven bed shear stress by impacting current velocities, and wind-driven bed shear stress through alterations in water levels, as wind-driven bed shear stress is a function of water depth, wind speed and fetch (U.S. Army Corps of Engineers 1984). The DELFT3D model calculates the tidally-driven bed shear stress directly; however, the wind-wave-driven bed shear stress is not a specified model output. Instead, the model outputs the maximum wind-wave induced orbital velocity, which can be used to approximate the wind-wave-driven bed shear stress (Grant and Madsen 1979). The total bed shear stress can then be defined as the linear sum of the tidally-driven and wind-wave-driven bed shear stress (Grant and Madsen 1979; van Rijn 1993). This approximation is presented below and is for impact assessment purposes only. This approximation is not part of the DELFT3D model formulation.

$$\tau_b = \tau_{bw} + \tau_{bc} \quad (\text{Grant and Madsen 1979; van Rijn 1993})$$

where τ_b = total bed shear stress, τ_{bw} = wind-driven bed shear stress, and τ_{bc} = tidally-driven bed shear stress.

$$\tau_{bw} = 1/2 \rho f_w u_b^2 \quad (\text{Madsen and Wikramanayake 1991})$$

where ρ = density of water, f_w = wave friction factor, u_b = maximum near-bottom wave-induced orbital velocity.

Assuming $f_w = 0.05$ (Madsen and Wikramanayake 1991), and u_b and τ_{bc} are given by output from the DELFT3D model at each grid cell and time step, the total bed shear stress can be estimated over the model domain.

Figure 4-5 displays the time period used to calculate the peak tidally-induced bed shear stress and the period used to calculate the peak combined wind-wave- and tidally-induced bed shear stress. The first period was chosen because the largest tidal velocities on both ebb and flood occur. The second period was chosen as strong summer winds (7 – 10 m/s) occur coincidentally with strong tides, and therefore the combined bed shear stress is at a maximum. These periods therefore coincide with maximum bed shear stresses and an increased potential for sediment erosion.

4.5.1 South Bay

Within the South Bay, the largest changes to the tidally-induced bed shear stress are seen in the subtidal channels and in the regions downstream of the tidal sloughs (Figure 4-117). The difference map shown on Figure 4-117 depicts red regions where the erosive potential increases (bed shear stresses are higher under Alternative C relative to baseline conditions), and the areas depicted in blue correspond to regions with a

potential for increased deposition. As the critical shear stresses for erosion are not well known within the South Bay, and they vary spatially depending on the sediment characteristics and level of compaction of the substrate, the red and blue areas are for illustrative purposes only and do not predict erosion or deposition under Alternative C.

When the combined wind-wave- and tidally-induced shear stress is considered in the South Bay, additional changes become apparent. MLLW is higher and MHHW is lower under Alternative C (Figure 4-9 and Figure 4-10, respectively). Because wind-wave-driven bed shear stress is a function of water depth, and the erosive potential decreases with increasing water depth, the reduction in tidal amplitude leads to a reduction in the total bed shear stresses in the shallow areas of the South Bay, including the shallows in the far South Bay (Figure 4-123) and the eastern and western shoals north of the Dumbarton Bridge (Figure 4-122 and Figure 4-124, respectively).

4.5.2 Tidal Sloughs

Within and adjacent to the Eden Landing pond complex (Figure 4-118), the maximum tidally-induced bed shear stress is increased downstream of tidal breaches, corresponding to the increased tidal prism, and decreased upstream of the tidal breaches because a portion of the flow upstream in the tidal slough under baseline conditions is captured within the tidally-restored ponds under restored conditions. Within and adjacent to the Alviso pond complex (Figure 4-119) and the Ravenswood pond complex (Figure 4-120), the dynamic is similar to that observed in the Eden Landing pond complex. Tidally-induced bed shear stresses increase downstream of tidal breaches and decrease upstream of tidal breaches.

The primary effect of the combined wind-wave- and tidally-induced shear stress is evident in the South Bay, rather than in the tidal sloughs, as wind-induced waves require sufficient fetch to develop.

Figure 4-1. South Bay Stations

Figure 4-2. Eden Landing Stations

Figure 4-3. Ravenswood Stations

Figure 4-4. Alviso Stations

Figure 4-5. Time Series Snapshot Points

Figure 4-6. Water Levels, San Mateo Bridge, Alt C, Year 0, Summer

Figure 4-7. Water Levels, Dumbarton Bridge, Alt C, Year 0, Summer

Figure 4-8. Water Levels, Channel Marker 17, Alt C, Year 0, Summer

Figure 4-9. Changes in MLLW, Alt C, Year 0, Summer

Figure 4-10. Changes in MHHW, Alt C, Year 0, Summer

Figure 4-11. Changes in Tidal Propagation, Alt C, Year 0, Summer

Figure 4-12. Water Levels, ACFCC Downstream, Alt C, Year 0, Summer

Figure 4-13. Water Levels, ACFCC Upstream, Alt C, Year 0, Summer

Figure 4-14. Water Levels, Old Alameda Creek Downstream, Alt C, Year 0, Summer

Figure 4-15. Water Levels, Old Alameda Creek Upstream, Alt C, Year 0, Summer

Figure 4-16. Water Levels, Coyote Creek Power Tower, Alt C, Year 0, Summer

Figure 4-17. Water Levels, Coyote Creek Railroad Bridge, Alt C, Year 0, Summer

Figure 4-18. Water Levels, Coyote Creek/Island Ponds, Year 0, Summer

Figure 4-19. Water Levels, Coyote Creek Upstream, Year 0, Summer

Figure 4-20. Water Levels, Mud Slough Downstream, Alt C, Year 0, Summer

Figure 4-21. Water Levels, Mud Slough Upstream, Alt C, Year 0, Summer

Figure 4-22. Water Levels, Alviso Slough Downstream, Alt C, Year 0, Summer

Figure 4-23. Water Levels, Alviso Slough Upstream, Alt C, Year 0, Summer

Figure 4-24. Water Levels, Guadalupe Slough Downstream, Alt C, Year 0, Summer

Figure 4-25. Water Levels, Guadalupe Slough Upstream, Alt C, Year 0, Summer

Figure 4-26. Water Levels, Moffett Channel, Alt C, Year 0, Summer

Figure 4-27. Water Levels, Steven Creek Downstream, Alt C, Year 0, Summer

Figure 4-28. Water Levels, Stevens Creek Upstream, Alt C, Year 0, Summer

Figure 4-29. Water Levels, Mountain View Slough Downstream, Alt C, Year 0, Summer

Figure 4-30. Water Levels, Mountain View Slough Upstream, Alt C, Year 0, Summer

Figure 4-31. Water Levels, Charleston Slough Downstream, Alt C, Year 0, Summer

Figure 4-32. Water Levels, Charleston Slough Upstream, Alt C, Year 0, Summer

Figure 4-33. Water Levels, Ravenswood Slough Downstream, Alt C, Year 0, Summer

Figure 4-34. Water Levels, Ravenswood Slough Upstream, Alt C, Year 0, Summer

Figure 4-35. Water Levels, Pond A20, Alt C, Year 0, Summer

Figure 4-36. Water Levels, ELER North, Alt C, Year 0, Summer

Figure 4-37. Water Levels, ELER South, Alt C, Year 0, Summer

Figure 4-38. Water Levels, Pond E6B, Alt C, Year 0, Summer

Figure 4-39. Water Levels, Pond A7, Alt C, Year 0, Summer

Figure 4-40. Water Levels, Pond A8, Alt C, Year 0, Summer

Figure 4-41. South Bay Tidal Prism Cross-Section Locations

Figure 4-42. Eden Landing Tidal Prism Cross-Section Locations

Figure 4-43. Alviso Tidal Prism Cross-Section Locations

Figure 4-44. Ravenswood Tidal Prism Cross-Section Locations

Figure 4-45. Tidal Prism, San Mateo and Dumbarton Bridges, Alt C, Year 0, Summer

Figure 4-46. Tidal Prism, Channel Marker 17 and Calaveras Point, Alt C, Year 0, Summer

Figure 4-47. Tidal Prism, ACFCC and Old Alameda Creek, Alt C, Year 0, Summer

Figure 4-48. Tidal Prism, Coyote Creek, Alt C, Year 0, Summer

Figure 4-49. Tidal Prism, Alviso and Guadalupe Sloughs, Alt C, Year 0, Summer

Figure 4-50. Tidal Prism, Stevens Creek and, Mountain View Sloughs, Alt C, Year 0, Summer

Figure 4-51. Tidal Prism, Charleston and Ravenswood Sloughs, Alt C, Year 0, Summer

Figure 4-52. Salinity at Spring HHW Jun – Aug, Alt C, Year 0, Summer

Figure 4-53. Salinity, San Mateo Bridge, Alt C, Year 0, Summer

Figure 4-54. Salinity, Dumbarton Bridge, Alt C, Year 0, Summer

Figure 4-55. Salinity, Channel Marker 17, Alt C, Year 0, Summer

Figure 4-56. Salinity at Spring HHW, Alt C, Year 0, Summer

Figure 4-57. Salinity at Spring LLW, Alt C, Year 0, Summer

Figure 4-58. Salinity, ACFCC Downstream, Alt C, Year 0, Summer

Figure 4-59. Salinity, ACFCC Upstream, Alt C, Year 0, Summer

Figure 4-60. Salinity, Old Alameda Creek Downstream, Alt C, Year 0, Summer

Figure 4-61. Salinity, Old Alameda Creek Upstream, Alt C, Year 0, Summer

Figure 4-62. Salinity at Spring HHW, Eden Landing, Alt C, Year 0, Summer

Figure 4-63. Salinity at Spring LLW, Eden Landing, Alt C, Year 0, Summer

Figure 4-64. Salinity, Coyote Creek Power Tower, Alt C, Year 0, Summer

Figure 4-65. Salinity, Coyote Creek Railroad Bridge, Alt C, Year 0, Summer

Figure 4-66. Salinity, Coyote Creek/Island Ponds, Year 0, Summer

Figure 4-67. Salinity, Coyote Creek Upstream, Year 0, Summer

Figure 4-68. Salinity, Mud Slough Downstream, Alt C, Year 0, Summer

Figure 4-69. Salinity, Mud Slough Upstream, Alt C, Year 0, Summer

Figure 4-70. Salinity, Alviso Slough Downstream, Alt C, Year 0, Summer Summer

Figure 4-71. Salinity, Alviso Slough Upstream, Alt C, Year 0, Summer Summer

Figure 4-72. Salinity, Guadalupe Slough Downstream, Alt C, Year 0, Summer Summer

Figure 4-73. Salinity, Guadalupe Slough Upstream, Alt C, Year 0, Summer Summer

Figure 4-74. Salinity, Moffett Channel, Alt C, Year 0, Summer Summer

Figure 4-75. Salinity, Steven Creek Downstream, Alt C, Year 0, Summer Summer

Figure 4-76. Salinity, Stevens Creek Upstream, Alt C, Year 0, Summer Summer

Figure 4-77. Salinity, Mountain View Slough Downstream, Alt C, Year 0, Summer Summer

Figure 4-78. Salinity, Mountain View Slough Upstream, Alt C, Year 0, Summer Summer

Figure 4-79. Salinity, Charleston Slough Downstream, Alt C, Year 0, Summer Summer

Figure 4-80. Salinity, Charleston Slough Upstream, Alt C, Year 0, Summer Summer

Figure 4-81. Salinity at Spring HHW, Alt C, Alviso, Year 0, Summer Summer

Figure 4-82. Salinity at Spring LLW, Alt C, Alviso, Year 0, Summer Summer

Figure 4-83. Salinity, Ravenswood Slough Downstream, Ravenswood, Alt C, Year 0, Summer Summer

Figure 4-84. Salinity, Ravenswood Slough Upstream, Ravenswood, Alt C, Year 0, Summer Summer

Figure 4-85. Salinity at Spring HHW, Ravenswood, Alt C, Year 0, Summer

Figure 4-86. Salinity at Spring LLW, Ravenswood, Alt C, Year 0, Summer

Figure 4-87. Velocity, San Mateo Bridge, Alt C, Year 0, Summer

Figure 4-88. Velocity, Dumbarton Bridge, Alt C, Year 0, Summer

Figure 4-89. Velocity, Channel Marker 17, Alt C, Year 0, Summer

Figure 4-90. Velocity at Spring Flood, Alt C, Year 0, Summer

Figure 4-91. Velocity at Spring Ebb, Alt C, Year 0, Summer

Figure 4-92. Velocity, ACFCC Downstream, Alt C, Year 0, Summer

Figure 4-93. Velocity, Old Alameda Creek Downstream, Alt C, Year 0, Summer

Figure 4-94. Velocity at Spring Flood, Eden Landing, Alt C, Year 0, Summer

Figure 4-95. Velocity at Spring Ebb, Eden Landing, Alt C, Year 0, Summer

Figure 4-96. Velocity, Coyote Creek Power Tower, Alt C, Year 0, Summer

Figure 4-97. Velocity, Coyote Creek Railroad Bridge, Alt C, Year 0, Summer

Figure 4-98. Velocity, Coyote Creek/Island Ponds, Year 0, Summer

Figure 4-99. Velocity, Mud Slough Downstream, Alt C, Year 0, Summer

Figure 4-100. Velocity, Alviso Slough Downstream, Alt C, Year 0, Summer

Figure 4-101. Velocity, Guadalupe Slough Downstream, Alt C, Year 0, Summer

Figure 4-102. Velocity, Moffett Channel, Alt C, Year 0, Summer

Figure 4-103. Velocity, Steven Creek Downstream, Alt C, Year 0, Summer

Figure 4-104. Velocity, Mountain View Slough Downstream, Alt C, Year 0, Summer

Figure 4-105. Velocity, Charleston Slough Downstream, Alt C, Year 0, Summer

Figure 4-106. Velocity at Spring Flood, Alviso, Alt C, Year 0, Summer

Figure 4-107. Velocity at Spring Ebb, Alviso, Alt C, Year 0, Summer

Figure 4-108. Velocity, Ravenswood Slough Downstream, Alt C, Year 0, Summer

Figure 4-109. Velocity at Spring Flood, Ravenswood, Alt C, Year 0, Summer

Figure 4-110. Velocity at Spring Ebb, Ravenswood, Alt C, Year 0, Summer

Figure 4-111. South Bay Residual Circulation, Baseline, Summer

Figure 4-112. South Bay Residual Circulation, Alt C, Year 0, Summer

Figure 4-113. South Bay Residual Circulation, Difference, Year 0, Summer

Figure 4-114. Far South Bay Residual Circulation, Baseline, Summer

Figure 4-115. Far South Bay Residual Circulation, Alt C, Year 0, Summer

Figure 4-116. Far South Bay Residual Circulation, Difference, Year 0, Summer

Figure 4-117. Tidal Bed Shear Stress, South Bay, Alt C, Year 0, Summer

Figure 4-118. Tidal Bed Shear Stress, Eden Landing, Alt C, Year 0, Summer

Figure 4-119. Tidal Bed Shear Stress, Alviso, Alt C, Year 0, Summer

Figure 4-120. Tidal Bed Shear Stress, Ravenswood, Alt C, Year 0, Summer

Figure 4-121. Total Bed Shear Stress, South Bay, Alt C, Year 0, Summer

Figure 4-122. Total Bed Shear Stress, Eden Landing, Alt C, Year 0, Summer

Figure 4-123. Total Bed Shear Stress, Alviso, Alt C, Year 0, Summer

Figure 4-124. Total Bed Shear Stress, Ravenswood, Alt C, Year 0, Summer

5. ALTERNATIVE C, YEAR 0, WINTER CONDITIONS

This section presents the results of the Alternative C, year 0, simulation under winter conditions, including a comparison with baseline winter conditions. The analysis presented utilizes the same approach presented in Section 4 for ease of comparison between simulations, and the results are very similar to those presented for summer conditions. Of note during the winter analysis period is a storm event which begins on February 24 and affects slough hydrodynamics around the whole South Bay. Under winter conditions, the reduction in tidal range is less pronounced in the far South Bay, and the increases in water levels associated with LLW are less asymmetric. During the storm event, the tidal damping in the slough channels is reduced, and the increased mixing between the sloughs and the Bay, coupled with the off-channel pond volume, help keep slough salinities high, thus reducing salinity variability in the tidal sloughs in response to temporarily high freshwater tributary inflows.

An additional dynamic occurring in the model that was not evident in the summer simulation presented in Section 4 was the re-routing of flow observed in the Eden Landing pond complex during the storm event. A portion of the high flows in the ACFCC was captured by the Eden Landing ponds and routed through the ponds and into Old Alameda Creek, increasing the tidal prism and velocities in Old Alameda Creek. This re-routing of flows could have potential flood protection benefit implications in the ACFCC as water levels and velocities did not increase appreciably in the flood control channel in response to the moderate storm event.

As discussed in Section 4, this simulation represents a hypothetical and conservative case where all tidally-restored ponds are restored at year 0 – phasing is not considered. Therefore, the results presented in this section are likely an overstatement of the potential impacts. In reality, the restoration will be phased over many years, thereby reducing the magnitude of the project’s impacts.

The model predictions are analyzed using time series at stations throughout the South Bay. Figure 4-1 through Figure 4-4 show the station locations for the South Bay and three pond complexes. The model predictions are also analyzed at specific snapshots in time for the entire South Bay and the pond complexes. The sections below present the results with respect to water levels, tidal prism, salinity, circulation and bed shear stress.

5.1 Water Levels

This section presents the model results with respect to water levels in the South Bay, the tidal sloughs and the ponds under Alternative C, year 50, winter conditions. The model predictions are compared to baseline winter predictions in order to assess the short-term impacts associated with opening 90 percent of the ponds to tidal action.

5.1.1 South Bay

In the South Bay, the modeled water levels at the San Mateo and Dumbarton Bridges under Alternative C exhibit minimal change when compared with the baseline. Table 5-1 shows the water surface elevations

and phase difference for the South Bay under Alternative C winter conditions. Positive water surface elevation values in Table 5-1 represent an increase in water surface elevation when compared with baseline conditions, and negative values represent a decrease in water surface elevation. Positive phase values correspond to a slower arrival time under Alternative C, or a phase lag when compared with baseline conditions, whereas negative values represent that modeled water levels under Alternative C are leading baseline conditions.

At the San Mateo Bridge (Figure 5-1), LLW increases by approximately 1 cm under both neap and spring conditions (see Table 5-1), and higher high water (HHW) decreases by approximately 1 cm. At the Dumbarton Bridge (Figure 5-2), LLW increases by approximately 2 cm under neap tide and 1 cm under spring tide, and HHW decreases by approximately 3 cm under neap tide and 4 cm under spring tide. The water level changes are relatively negligible north of the Dumbarton Bridge, and the differences are similar to the level of accuracy of the model calibration with respect to tidal amplitudes. The model predicts no noticeable change in phase relative to baseline conditions at either bridge station.

Within the far South Bay, water level and phase changes under Alternative C become more pronounced. At Channel Marker 17 (Figure 5-3), located near the mouth of Coyote Creek, LLW increases by approximately 5 cm under neap tide and 11 cm under spring tide, and HHW decreases by approximately 6 cm under neap tide and 8 cm under spring tide. When compared with summer conditions under Alternative C (see Table 4-1), the far South Bay experiences a smaller reduction in tidal amplitude, and the increase in water level associated with LLW is less pronounced.

Although the tidal amplitude changes are small, the long-term trend in reduced tidal amplitude (decrease in high water levels and increase in low water levels) would lead to an increase in the MLLW tidal datum, and a decrease in the MHHW tidal datum. Figure 5-4 depicts the change in MLLW in response to the tidal restoration. The increase in MLLW is most pronounced in the far South Bay, with the change trending toward zero just north of the San Mateo Bridge. Similar changes are seen with respect to MHHW (Figure 5-5), with the largest reduction occurring in the far South Bay, and the reduction trending toward zero just north of the San Mateo Bridge.

Harmonic analysis was performed on water levels at several stations along the main South Bay channel, and the computed phase and amplitudes of the M_2 and K_1 tidal constituents for baseline and Alternative C year 0 conditions are compared (Figure 5-6). By comparing the phase and amplitude of the two primary harmonic constituents along the centerline of the South Bay, it is possible to assess how the tidal restoration is affecting the tidal propagation within the South Bay. Figure 5-6a presents the computed phase of the M_2 and K_1 tidal constituents. Little difference is observed in the South Bay as a result of the restoration project, which is consistent with Table 5-1. Figure 5-6b presents the computed amplitude of the M_2 and K_1 tidal constituents. As the tides propagate into the South Bay, the amplitude of both tidal constituents is decreased, with a more marked difference observed in the M_2 tidal constituent in the far South Bay.

Table 5-1. South Bay Tidal Water Surface Elevation and Phase Differences under Alt C, Year 0, Winter
(Water surface elevation differences in cm, phase differences in minutes. Feb 27 = neap tide, Mar 12 = spring tide.)

Station Name	Feb 27 LLW		Feb 27 HHW		Mar 12 LLW		Mar 12 HHW	
	WSE	Phase	WSE	Phase	WSE	Phase	WSE	Phase
San Mateo Bridge, Figure 5-1	1	0	-1	0	1	0	-2	0
Dumbarton Bridge, Figure 5-2	1	0	-3	0	2	0	-4	0
Channel Marker 17, Figure 5-3	5	10	-6	10	39	30	-8	0

5.1.2 Tidal Sloughs

As with the summer condition simulation (Section 4), Alternative C has a significant effect on modeled tidal slough water levels within all the three pond complexes under winter conditions. This is expected as the tidally-restored ponds are breached directly to the tidal sloughs, and the volume of water exchanged through the breach represents a considerable increase over the existing, or baseline, tidal prism in the slough regardless of the increased freshwater inflow contributions occurring during winter. The overall magnitude of the effect on water levels within each slough is dependent on the baseline tidal prism, the tributary freshwater inflow, and the tidal prism added to the slough by the restored ponds. The bathymetry of the sloughs also plays an important role in determining the change in water levels. As described in Section 3.2, the bathymetry of the tidal sloughs was not altered under this simulation; therefore the sloughs are undersized relative to the newly restored flow conditions. As discussed in Section 2.3.5, some of the sloughs, particularly those in the Eden Landing and Ravenswood pond complex, are modeled with larger than actual channel widths due to limitations with respect to the grid resolution; therefore, the model results for these sloughs may underestimate the potential short-term changes in water levels.

Table 5-2 shows the water surface elevation and phase difference for the water levels under Alternative C at both upstream (landward) and downstream (near the mouth) stations in each tidal slough. Positive water surface elevation values in Table 5-2 represent an increase in water level when compared with baseline conditions, and negative values represent a decrease in water level. Positive phase values correspond to a slower arrival time under Alternative C, or a phase lag when compared with baseline conditions, whereas negative values represent that modeled water levels under Alternative C are leading baseline conditions. The neap tide period corresponds with a moderate storm event beginning February 24 and extending through February 28 when freshwater tributary inflows are higher. During this period, the change in water levels between baseline and Alternative C conditions is lessened; therefore the short-term impact of Alternative C on tidal slough water levels is less pronounced during high flow events.

Near slough mouths (downstream stations), the water level trends are similar to that seen under summer conditions (Table 4-2). For most sloughs, there is a moderate reduction of the water surface elevation at high water, and a larger increase in the water surface elevation at LLW when compared to baseline conditions. The larger increase in water levels at LLW reflects the influence of the channel geometry on the water level dynamics. At low water levels, the wetted cross-section area of the channel is small, yet it is draining a large surface area (e.g., the tidally-restored ponds). Therefore, in order to convey the larger volume of water, LLW is increased relative to baseline conditions. The relative difference between the

wetted cross-sectional area under baseline and Alternative C, year 0 conditions is not as great at HHW, therefore a smaller difference is observed. Water levels downstream in Alviso Slough (Figure 5-17) provide an example of this response pattern. At both high water marks and higher low water (HLW), Alternative C predicts damping on the order of 20 – 60 cm during spring tide and by 10 – 30 cm during neap tide. In contrast, LLW is predicted to dampen by 60 – 90 cm during spring tide. The upstream stations experience similar changes in tidal amplitude relative to the downstream stations.

Phasing changes are relatively small at the downstream stations in the Eden Landing pond complex, with Alternative C lagging behind baseline conditions by approximately 30 – 40 minutes during neap and spring tides. In the Ravenswood pond complex, Alternative C lags behind baseline conditions on the order of 70 – 110 minutes during neap tide 50 – 90 minutes during spring tide downstream in Ravenswood Slough (Figure 5-28), with smaller phase lags observed upstream (Figure 5-29). In the Alviso pond complex, phase changes vary considerably depending on the volume of the freshwater tributary inflows and the increase in tidal prism. Downstream in Alviso Slough (Figure 5-17), Alternative C lags winter baseline conditions on the order of 40 – 70 minutes on spring and neap tides. In Guadalupe Slough (Figure 5-19), Alternative C lags baseline conditions on the order of 10 – 20 minutes under neap tides, with a phase lag of approximately 90 minutes on LLW under spring tide conditions.

Table 5-2. Tidal Slough Water Surface Elevation and Phase Differences under Alt C, Year 0, Winter
(Water surface elevation differences in cm, phase differences in minutes. Feb 27 = neap tide, Mar 12 = spring tide.)

Station Name	Feb 27 LLW		Feb 27 HHW		Mar 12 LLW		Mar 12 HHW	
	WSE	Phase	WSE	Phase	WSE	Phase	WSE	Phase
<i>Eden Landing pond complex</i>								
ACFCC Downstream, Figure 5-7	7	30	-14	40	35	30	-28	40
ACFCC Upstream, Figure 5-8	0	-10	-11	60	4	10	-31	20
Old Alameda Creek Downstream, Figure 5-9	6	10	-10	0	38	20	-16	0
Old Alameda Creek Upstream, Figure 5-10	12	30	-21	80	48	40	-38	50
<i>Alviso pond complex</i>								
Coyote Creek Power Tower, Figure 5-11	13	10	-17	10	62	50	-24	0
Coyote Creek Railroad Bridge, Figure 5-12	24	40	-29	70	69	80	-48	0
Coyote Creek/Island Ponds, Figure 5-13	23	40	-30	80	68	70	-53	0
Coyote Creek Upstream, Figure 5-14	24	40	-31	80	68	70	-57	0
Mud Slough Downstream, Figure 5-15	24	30	-32	70	68	70	-48	10
Mud Slough Upstream, Figure 5-16	27	50	-34	110	66	60	-65	0
Alviso Slough Downstream, Figure 5-17	25	40	-29	60	90	70	-43	40
Alviso Slough Upstream, Figure 5-18	26	80	-33	130	86	100	-78	30
Guadalupe Slough Downstream, Figure 5-19	14	20	-11	10	86	90	-16	10
Guadalupe Slough Upstream, Figure 5-20	20	80	-37	120	86	110	-69	10
Moffett Channel, Figure 5-21	20	80	-37	120	86	110	-69	10
Stevens Creek Downstream, Figure 5-22	16	30	-13	40	26	0	-21	30
Stevens Creek Upstream, Figure 5-23	14	60	-16	70	26	10	-25	70
Mountain View Slough Downstream, Figure 5-24	29	90	-10	70	69	40	-18	60
Mountain View Slough Upstream, Figure 5-25	29	90	-10	70	66	30	-17	60
Charleston Slough Downstream, Figure 5-26	16	40	-10	60	51	30	-18	70
Charleston Slough Upstream, Figure 5-27	13	30	-10	80	46	30	-18	70
<i>Ravenswood pond complex</i>								
Ravenswood Slough Downstream, Figure 5-28	23	70	-27	110	69	50	-41	90
Ravenswood Slough Upstream, Figure 5-29	22	40	-8	30	63	30	-12	10

5.1.3 Ponds

Under baseline conditions, only the Island Ponds in the Alviso pond complex and the Eden Landing Ecological Reserve in the Eden Landing pond complex are open to tidal inundation. Restoring additional ponds to tidal action would therefore impact water levels within these existing restoration sites. Figure 5-30 displays the water level in the center of Pond A20. Under winter conditions, Pond A20 experiences a reduction in high water levels. Low water levels remain unchanged as Pond A20 sits relatively high in the tide frame, and the pond is effectively drained under low water conditions.

In the Eden Landing Ecological Reserve, water levels in the north wetlands remain largely unaffected (Figure 5-31). These wetlands are hydraulically connected to the South Bay via Mount Eden Creek, which experiences only a nominal increase in tidal prism under Alternative C. The southern wetlands are hydraulically connected to the South Bay via North Creek. The tidal prism in North Creek is expected to increase by approximately 380percent due to the tidal breaches under Alternative C (Figure 3-15); therefore the water levels in the southern wetlands experience reductions in tidal amplitude (a decrease in high water levels and an increase in low water levels). The increase in low water levels is fairly similar to the decrease in high water levels (Figure 5-32).

Ponds that are not hydraulically connected to the South Bay under baseline conditions (except by culverts and flap gates) would be connected under Alternative C through tidal breaches to the sloughs. The water levels in the ponds are therefore similar to that of the tidal sloughs. In the Eden Landing and Ravenswood ponds complexes, the pond bottom elevations are relatively high in the tide frame; therefore the ponds are only inundated during high tides. Figure 5-33 shows the water level variability in Pond E6B in the Eden Landing pond complex. This pond only experiences diurnal tidal variability during spring tides, and during neap tides, most of the pond area would be effectively drained. However, marsh channels inside the pond would likely exhibit more tidal variability.

In the Alviso pond complex, pond bottom elevations sit lower in the tide frame and the ponds are therefore exposed to diurnal tidal action throughout the spring-neap tide cycle. Ponds A7 and A8 (Figure 5-34 and Figure 5-35, respectively) provide an example of the tide range expected within the subsided ponds. In this case, the water levels are similar to that seen in Alviso Slough. Unlike Pond E6B and similar ponds with higher bottom elevations, Ponds A7 and A8 do not experience cycles of wetting and drying during the diurnal tidal cycle. Instead, the ponds contain water at all times. The tide range within any specific pond will depend on the location of its hydraulic connection to the Bay and the pond's elevation relative to the tides.

5.2 Tidal Prism

A comparison of the estimates of tidal prism between baseline and Alternative C, year 0, winter conditions is summarized in Table 5-3. A conventional definition of tidal prism is the volume of water exchanged over a complete tidal cycle. However, as discussed in Section 4.2, tidal prism has been estimated as the volume of water crossing a cross-section during a flood tide in order to compare the tidal prism estimates with previous studies.

Changes in tidal prism outside of the project area (i.e. at San Mateo Bridge, Dumbarton Bridge and non-project sloughs), are typically five percent or less. Overall, the changes in tidal prism associated with the sloughs within the three pond complexes under winter conditions are similar to those discussed in Section 4.2 for summer conditions.

Figure 5-36 displays the instantaneous modeled flux through San Mateo and Dumbarton Bridge cross-sections under baseline and Alternative C, year 0, winter conditions. At the San Mateo Bridge cross-section, little difference is evident. However, at the Dumbarton Bridge cross-section, the modeled flux decreases slightly under Alternative C conditions. This is consistent with the tidal prism estimates presented in Table 5-3. At a cross-section through Channel Marker 17, the modeled flux is slightly larger under Alternative C conditions when compared to baseline conditions (Figure 5-37). Further south at Calaveras Point, the modeled flux under Alternative C is noticeably larger than under baseline conditions, which is consistent with the 26 percent increase in tidal prism predicted in Table 5-3.

The tidal prism associated with the sloughs in the three pond complexes is predicted to increase. The increase is dependent on the volume of the tidally-restored ponds breached to particular slough and how accurately a slough is represented in the model. For example, the tidal prism in the ACFCC is predicted to increase by approximately 88 percent. In contrast, the tidal prism in Old Alameda Creek is predicted to increase by approximately 15 percent. As discussed in Section 4.2, this is likely an underestimate of the actual percentage increase in tidal prism as a result of the SBSP Restoration Project. The baseline tidal prism in Old Alameda Creek from estimated from GIS is 0.32 million cubic meters (Table 3-6), which is an order or magnitude less than the baseline estimate from the model of 1.6 million cubic meters (Table 5-3). However, the increase in tidal prism of 0.2 million cubic meters is likely representative of the added pond volume due to the restoration; therefore the tidal prism in Old Alameda Creek could increase approximately 67 percent (from 0.32 to 0.52 million cubic meters). Figure 5-38 presents the modeled flux through cross-sections near the mouths of the ACFCC and Old Alameda Creek under both baseline and Alternative C, year 0, summer conditions. The modeled flux is predicted to increase in both sloughs, with a larger increase associated with the ACFCC.

Along Coyote Creek, there is a progression of tidal prism changes (Figure 5-39). Near the mouth, at the Power Tower, the predicted increase is approximately ten million cubic meters. Since Coyote Creek is a large channel, this change represents an increase of only 42 percent over baseline conditions even though several large ponds would breach to this channel. Further up Coyote Creek, at the Railroad Bridge and east of the Island Ponds, the tidal prism decreases as a result of restoration. This decrease occurs because

flows which reach these transects under baseline conditions are deflected into the newly breached ponds under Alternative C.

Alviso Slough and Guadalupe Slough are represented fairly well in the model, and the modeled flux at the downstream transects increases measurably in both sloughs (Figure 5-40), with an increase in tidal prism of approximately 200 percent predicted by the model (Table 5-3). An increase of approximately 310 percent is predicted for Mountain View Slough, a small slough that would connect two large ponds to the Bay. In addition, the large increase associated with Mountain View Slough is caused in part by a portion of Charleston Slough's existing and potential tidal prism being routed through the upstream breach to Pond A1 on Charleston Slough, through Pond A1, and into Mountain View Slough. Mountain View Slough is among those sloughs that are oversized in the model; therefore the actual percent increase in tidal prism may be larger; however, the baseline tidal prism and the Alternative C tidal prism are likely smaller than presented in Table 5-3. The same can be said for Charleston Slough and Stevens Creek. These sloughs have relatively little flow under baseline summer conditions, and the modeled flux at the downstream transects increases markedly under Alternative C, year 0, summer conditions (Figure 5-41 and Figure 5-42).

The model predicts a tidal prism increase of approximately 240 percent for Ravenswood Slough in the Ravenswood pond complex (Figure 5-42). Under baseline conditions, Ravenswood Slough's tidal prism is among the smallest of all the cross-section presented in Table 5-3. Hence, with the addition of nearly the entire complex's pond area to the slough's drainage area, the large increase is expected. Ravenswood Slough is also among those sloughs that are oversized in the model, as discussed in Section 2.3.5; therefore, the actual percent increase in tidal prism may be larger, while the tidal prism values are likely smaller.

The tidal prism within each slough may be larger than presented in Table 5-3 after sloughs scour and deepen and before pond sedimentation raises pond bottom elevations. Due to the subsided nature of the ponds within the Alviso pond complex, this potential increase in tidal prism would be greatest in the Alviso pond complex sloughs.

Table 5-3. Comparison of Tidal Prism between Baseline and Alternative C, Year 0, Winter

Transect location	Tidal prism (millions of cubic meters)		
	Baseline winter	Alternative C year 0, winter	% change baseline to Alt. C
<i>South Bay</i>			
San Mateo Bridge	270	270	-2.6%
Dumbarton Bridge	74	72	-3.0%
<i>Eden Landing pond complex</i>			
ACFCC	1.4	2.7	88%
Old Alameda Creek	1.6	1.8	15%
Mount Eden Creek	0.75	1.0	37%
<i>Ravenswood pond complex</i>			
Ravenswood Slough	0.58	2.0	240%
<i>Alviso pond complex</i>			
Calaveras Point	15	19	26%
Coyote Creek at Power Tower	7.3	10	42%
Coyote Creek at RR Bridge	2.5	1.7	-30%
Coyote Creek east of Island Ponds	0.51	0.38	-26%
Charleston Slough	0.65	1.2	77%
Mountain View Slough	0.24	0.98	310%
Stevens Creek	0.13	0.30	120%
Guadalupe Slough	1.1	3.3	190%
Alviso Slough	1.1	3.3	200%
Artesian Slough	0.50	0.64	27%
Mud Slough	0.86	0.91	5.9%
<i>Non-project Sloughs</i>			
Corkscrew Slough	3.6	3.6	-1.1%
Redwood Creek	17	16	-2.8%
Westpoint Slough	3.1	3.0	-1.3%
Mowry Slough	0.49	0.46	-6.3%
Plummer Slough	0.34	0.33	-2.8%
Newark Slough	0.98	0.95	-3.1%

5.3 Salinity

This section presents the model results with respect to salinity in the South Bay and the tidal sloughs under Alternative C, year 0, winter conditions. The model predictions are compared to baseline winter predictions in order to assess the impact of opening 90 percent of the ponds to tidal action. The SBSP Restoration Project has the potential to alter the salinity regimes within the South Bay, as presented in the sections below.

Modeled salinity within the South Bay is highly dependent on the initial salinity condition, particularly in the summer when residence times in the South Bay are at their longest. Residence times decrease in the winter due to the influence of higher tributary inflows (Walters and others 1985). As discussed in Section 3.2.2, the initial salinity prescribed within the ponds was set by the salinity in the neighboring tidal sloughs, which likely underestimates salinity levels within the ponds at the time of breaching. This

underestimation is most pronounced in the Alviso pond complex where salinities are lowest due to freshwater tributary inflows and the WWTP discharges.

Unlike the simulation for Alternative C under summer conditions (Section 4.3), equilibrium conditions with respect to salinity were met within the tidal sloughs and the far South Bay during the winter analysis period. The high freshwater tributary inflows lowered the residence time in the tidal sloughs, allowing equilibrium conditions to be met fairly rapidly. The analysis period includes both increased tributary freshwater inflows and a high flow event occurring in late February.

5.3.1 South Bay

Under Alternative C, immediately after restoring 90 percent of the ponds to tidal action, little change is seen with respect to salinity north of the Dumbarton Bridge (Table 5-4). Positive values in Table 5-4 represent an increase in salinities relative to the baseline, and negative values represent a decrease in salinities relative to baseline conditions. At the San Mateo and Dumbarton Bridges, there is no significant difference in salinity when compared with baseline conditions (Figure 5-43 and Figure 5-44, respectively).

At Channel Marker 17 (Figure 5-45), little change in salinity is observed at high water levels; however, at higher low water, salinities are 0 – 5 ppt higher than baseline conditions, and at LLW, salinities are 5 – 10 ppt higher. The salinity changes are correlated with the changes in water levels and the increase in tidal prism and mixing observed at this station, with the largest changes occurring at LLW.

Figure 5-46 displays the salinities in the South Bay during spring conditions at HHW, representing peak salinity conditions during the analysis period. As can be seen, little difference in peak South Bay salinities occurs under winter conditions with respect to Alternative C. The largest changes in salinity are confined to the tidal sloughs. Figure 5-47 displays South Bay salinities at LLW during spring tide conditions. At low water, the observed differences are higher downstream of the tidal sloughs under Alternative C, year 0, winter conditions.

Table 5-4. South Bay Salinity Differences under Alt C, Year 0, Winter
(Salinity differences in ppt. Feb 27 = neap tide, Mar 12 = spring tide.)

Station Name	Feb 27 LLW	Feb 27 HHW	Mar 12 LLW	Mar 12 HHW
San Mateo Bridge, Figure 5-43	-0.1	-0.0	-0.0	-0.0
Dumbarton Bridge, Figure 5-44	-0.3	-0.1	-0.2	-0.0
Channel Marker 17, Figure 5-45	4.1	2.0	3.8	0.3

5.3.2 Tidal Sloughs

Within the tidal sloughs, the changes to salinity levels with respect to baseline conditions show similar trends to the changes in water levels. Table 5-5 shows the salinity difference under Alternative C for neap and spring tide winter conditions. Positive values represent an increase in salinities relative to the baseline, and negative values represent a decrease in salinities relative to baseline conditions.

In the Eden Landing pond complex, salinities downstream in the ACFCC increase relative to baseline winter conditions, with the most significant changes occurring at low water levels when salinities are approximately 10 ppt higher than baseline conditions (Figure 5-48). During the moderate storm event when freshwater tributary inflows increase and depress salinities within the slough beginning February 24, the decrease in slough salinities is not as pronounced as observed in the baseline simulation. Under baseline simulation, the entire downstream section of the ACFCC becomes fresh. Under Alternative C, the increased tidal exchange and mixing between the sloughs and the South Bay, coupled with the volume of higher salinity water from the tidally-restored ponds, allows a diurnal salinity signal to remain during the storm event. Salinities fluctuate between 0 and 10 ppt during this period under Alternative C conditions. Upstream in the ACFCC, there is no change in salinities with respect to baseline conditions for the duration of the analysis period as this station is entirely fresh in response to winter tributary inflows (Figure 5-49).

In Old Alameda Creek, salinities are depressed relative to baseline conditions both downstream and upstream under Alternative C (Figure 5-50 and Figure 5-51, respectively). This decrease in salinities is due to freshwater inflows from the ACFCC flowing through the ponds and into Old Alameda Creek. This dynamic can be seen on Figure 5-52 and Figure 5-53 which depict salinities within the Eden Landing pond complex during spring tide at HHW and LLW. This flow path can be prevented during the project-level design phase if desired. This dynamic was not observed during summer conditions (Section 4), therefore it might only occur under storm conditions when flows in the ACFCC are high.

Within the tidal sloughs in the Alviso pond complex, the salinity response is similar to that observed in the ACFCC. Salinities at high water levels experience only minor changes on the order of 1 ppt at the downstream stations near the Bay. At the upstream stations, salinities are largely 0 ppt under baseline conditions due to freshwater tributary inflows. Under Alternative C, increased tidal exchange and mixing in the tidal sloughs and the contribution of higher salinity water from the tidally-restored ponds, pushes the salinity gradient upstream, increasing upstream salinities and providing for a moderate diurnal salinity signal. Figure 5-61 and Figure 5-63 provide an example of this effect in Alviso Slough and Guadalupe South, respectively.

During the moderate flow event beginning February 24, salinities under baseline conditions trend towards zero at low water at the downstream stations in Coyote Creek (Figure 5-54 and Figure 5-55), Mud Slough (Figure 5-58), Alviso Slough (Figure 5-60), and Guadalupe Slough (Figure 5-62). Under Alternative C, salinities are not depressed as significantly due to the increased tidal exchange and mixing. Therefore, the tidally-restored ponds help keep slough salinities high during a moderate storm event, thus reducing salinity variability occurring in response to temporarily high freshwater tributary inflows. At the upstream stations, the effect of the moderate storm can be seen as salinities decrease during the event (e.g., from 10 ppt on Feb 24 upstream in Guadalupe Slough to 4 ppt on Feb 28, Figure 5-63), and slowly increase following the event. Similar trends are seen in Coyote Creek, Alviso Slough, Stevens Creek, Mountain View Slough and Charleston Slough. The magnitude of the response depends on the increase in tidal prism relative to baseline conditions and the magnitude of the freshwater tributary inflows.

Figure 5-71 and Figure 5-72 depict salinities within the Alviso pond complex under Alternative C and baseline conditions during spring tide at both HHW and LLW, respectively. The greatest salinity differences occur within the tidal sloughs in the vicinity of the pond breaches at HHW, and in the downstream reaches of the sloughs and within the subtidal channels in the far South Bay at LLW.

Salinities downstream in Ravenswood Slough in the Ravenswood pond complex (Figure 5-73) are similar under both baseline and Alternative C conditions. At the upstream station (Figure 5-74), the salinity trend is similar to that observed in the Eden landing and Alviso pond complexes, with similar high water salinities when compared with baseline conditions, increased low water salinities, and a reduction in the upstream response to the moderate storm event beginning on February 24.

Figure 5-75 and Figure 5-76 depict salinities within the Ravenswood pond complex under Alternative C and baseline conditions during spring tide at both HHW and LLW, respectively. The greatest salinity differences occur within the tidal sloughs in the vicinity of the pond breaches at HHW, and in the downstream reaches of the sloughs and within the subtidal channels in the far South Bay at LLW.

Table 5-5. Tidal Slough Salinity Differences under Alt C, Year 0, Winter
(Salinity differences in ppt. June 13 = neap tide, June 22 = spring tide.)

Station Name	Feb 27 LLW	Feb 27 HHW	Mar 12 LLW	Mar 12 HHW
<i>Eden Landing pond complex</i>				
ACFCC Downstream, Figure 5-48	0.4	9.7	11.4	0.8
ACFCC Upstream, Figure 5-49	0.0	0.0	0.0	0.0
Old Alameda Creek Downstream, Figure 5-50	-5.0	-3.7	-2.7	-0.8
Old Alameda Creek Upstream, Figure 5-51	-7.7	-7.7	-4.2	-4.0
<i>Alviso pond complex</i>				
Coyote Creek Power Tower, Figure 5-54	4.4	4.4	4.1	0.6
Coyote Creek Railroad Bridge, Figure 5-55	1.5	5.9	2.4	0.8
Coyote Creek/Island Ponds, Figure 5-56	0.1	2.6	2.6	3.7
Coyote Creek Upstream, Figure 5-57	0.2	0.2	1.8	1.9
Mud Slough Downstream, Figure 5-58	3.7	6.8	4.8	3.6
Mud Slough Upstream, Figure 5-59	2.0	1.2	2.1	1.5
Alviso Slough Downstream, Figure 5-60	7.3	8.1	8.8	0.9
Alviso Slough Upstream, Figure 5-61	0.0	0.0	2.1	2.4
Guadalupe Slough Downstream, Figure 5-62	11.8	7.1	8.9	1.0
Guadalupe Slough Upstream, Figure 5-63	3.5	4.1	8.2	8.7
Moffett Channel, Figure 5-64	3.0	3.3	7.0	7.5
Stevens Creek Downstream, Figure 5-65	10.9	6.9	4.5	0.8
Stevens Creek Upstream, Figure 5-66	0.1	2.0	3.9	1.0
Mountain View Slough Downstream, Figure 5-67	12.3	8.4	4.2	1.0
Mountain View Slough Upstream, Figure 5-68	5.8	8.6	8.0	2.8
Charleston Slough Downstream, Figure 5-69	5.9	2.7	0.3	0.2
Charleston Slough Upstream, Figure 5-70	4.2	3.3	0.9	0.1
<i>Ravenswood pond complex</i>				
Ravenswood Slough Downstream, Figure 5-73	-0.5	-0.3	0.1	0.3
Ravenswood Slough Upstream, Figure 5-74	10.1	4.4	3.2	0.3

5.4 Circulation

As with summer conditions, potential changes to South Bay circulation can be evaluated by examining current velocities at specific locations within the Bay and tidal sloughs, and by examining general changes to South Bay residual circulation. The most important factor influencing circulation patterns in South Bay is bathymetry (Cheng and Gartner 1985). At year 0, the only bathymetric change associated with the simulation is hydraulically connecting the ponds to the Bay and re-introducing tidal action. This, in itself, represents a large-scale bathymetric change.

5.4.1 Current Velocity

South Bay

In the South Bay, modeled velocities at the San Mateo and Dumbarton Bridges exhibit little change relative to baseline conditions. Table 5-6 shows the peak modeled velocity magnitudes at the bridge and Channel Marker 17 stations under baseline and Alternative C conditions. Positive values indicate a higher modeled velocity magnitude under Alternative C, and negative values indicate a decrease in current velocity magnitude under Alternative C.

At the San Mateo Bridge (Figure 5-77), velocity magnitudes are slightly higher under Alternative C relative to baseline conditions, although the difference is relatively minor (approximately 2 cm/s). At the Dumbarton Bridge (Figure 5-78), velocity magnitudes decrease slightly relative to baseline conditions. This decrease is due in part to the undersized nature of the tidal sloughs and the potentially undersized nature of the main South Bay channel in the far South Bay which has experienced significant infilling in recent years (Jaffe and Foxgrover 2006b). The undersized channels restrict tidal exchange between the ponds and the northern reaches of the Bay.

In the far South Bay at Channel Marker 17 (Figure 5-79), velocity magnitude increases are more pronounced relative to baseline conditions due to the close proximity of the Alviso pond complex and the location of the station in the main South Bay channel. The peak modeled baseline velocity magnitude at Channel Marker 17 is 109 cm/s, compared with only 67 cm/s under summer conditions, owing to the moderate storm event and the increase in tributary inflows. Under Alternative C, the peak modeled velocity magnitude is 122 cm/s under winter conditions, compared with 119 cm/s under summer conditions. Although the peak velocities are similar under winter and summer conditions, the relative increase over baseline conditions is smaller under winter conditions. Under summer conditions, the velocity magnitude increases are strongest on ebb tides. Under winter conditions, the high tributary inflows contribute to increased winter baseline ebb velocities, therefore the additional effect of increasing the tidal prism is not as significant.

Figure 5-80 and Figure 5-81 depict velocity magnitudes within the South Bay under peak flood and peak ebb conditions under baseline and Alternative C conditions, as well as the difference between the two model predictions. As with summer conditions, the difference is strongest under spring ebb conditions near the mouths of the tidal sloughs and in the main South Bay channel. The differences under spring flood conditions are primarily seen near the mouths of the tidal sloughs.

Table 5-6. South Bay Peak Velocity Magnitude Comparisons: Alternative C, Winter, Year 0 vs. Baseline, Winter

(All velocities in cm/s)

Station Name	Baseline	Alt C	Difference
San Mateo Bridge, Figure 5-77	104	106	2
Dumbarton Bridge, Figure 5-78	35	32	-3
Channel Marker 17, Figure 5-79	109	122	13

Tidal Sloughs

In the South Bay, modeled velocities within the tidal sloughs experience significant changes in response to the restoration. The changes observed under winter conditions are similar to those seen under summer conditions described in Section 4.4.1. The majority of the tidal sloughs exhibit a flood-ebb asymmetry in the velocity increases due to the undersized nature of the sloughs, with a larger increase in modeled velocities observed on ebb tide. This asymmetry is expected to dissipate as the sloughs widen and deepen in response to the increased tidal prism. Table 5-7 shows the peak velocity magnitudes at the downstream stations in the tidal sloughs under baseline and Alternative C conditions. Positive values indicate a higher modeled velocity under Alternative C, and negative values indicate a decrease in current velocity under Alternative C.

In the Eden Landing pond complex, velocity magnitudes in the ACFCC increase significantly in response to the increased tidal prism, with velocity magnitudes increasing by a factor of 2 to 3 on strong ebb tides and a factor of two on flood tides (Figure 5-82). This increase is due to the relatively large increase in tidal prism associated with the restored ponds. Old Alameda Creek experiences a greater increase in velocities under winter conditions than observed under summer conditions, with increases throughout the analysis period on the order of 10 – 30 cm/s (Figure 5-83). A portion of this velocity magnitude increase is attributable to flow from the ACFCC being captured by the Eden Landing ponds and re-routed into Old Alameda Creek. This dynamic was not observed during summer conditions when flows were lower in the ACFCC. Figure 5-84 and Figure 5-85 depict the tidal slough velocities within the Eden Landing pond complex at both strong flood and strong ebb, respectively. At strong ebb, the largest differences are seen in the South Bay just beyond the slough mouth. At strong flood, the largest velocity magnitude differences relative to baseline conditions are seen in the downstream reaches of the sloughs. Unlike summer conditions, the differences in peak velocity magnitude are similar under strong ebb and strong flood conditions.

In the Alviso pond complex, velocity magnitudes at the downstream stations increase relative to baseline conditions. The magnitude of the increase is correlated with the associated increase in tidal prism. In Coyote Creek, stations at the Railroad Bridge (Figure 5-87) and at the upstream edge of the Island Ponds (Figure 5-88) are located upstream of the majority of the pond breaches. At these stations, velocity magnitudes decrease relative to baseline conditions due to the large percentage of the flow captured by the downstream ponds. As with summer conditions, velocities are also predicted to decrease in Charleston Slough (Figure 5-95) because the model predicts that a portion of Charleston Slough's existing and potential tidal prism is routed through the upstream breach to Pond A1 on Charleston Slough, through Pond A1, and into Mountain View Slough.

Figure 6-90 and Figure 6-91 depict the tidal slough velocity magnitudes within the Alviso pond complex at both strong flood and strong ebb, respectively. As with the Eden Landing pond complex, the largest differences under strong ebb conditions are seen in the far South Bay just beyond the slough mouth. At strong flood, the largest velocity differences relative to baseline conditions are seen in the downstream reaches of the tidal sloughs.

In Ravenswood Slough, peak velocity magnitudes increase by a factor of two with respect to baseline conditions under both ebb and flood conditions (Figure 5-98). Figure 5-99 and Figure 5-100 depict the tidal slough velocity magnitudes within the Ravenswood pond complex at both strong flood and strong ebb, respectively. As with the other pond complexes, the largest differences under strong ebb conditions are seen in the far South Bay just beyond the slough mouth, and at strong flood, the largest velocity differences relative to baseline conditions are seen in the downstream reach of the slough.

Table 5-7. Tidal Slough Peak Velocity Comparisons: Alternative C, Winter, Year 0 vs. Baseline, Winter
(All velocities in cm/s)

Station Name	Baseline	Alt C	Difference
ACFCC Downstream, Figure 5-82	48	103	56
Old Alameda Creek Downstream, Figure 5-83	55	77	22
Coyote Creek Power Tower, Figure 5-86	78	105	27
Coyote Creek Railroad Bridge, Figure 5-87	82	59	-23
Coyote Creek/Island Ponds, Figure 5-88	40	29	-11
Mud Slough Downstream, Figure 5-89	48	52	4
Alviso Slough Downstream, Figure 5-90	51	133	82
Guadalupe Slough Downstream, Figure 5-91	46	117	71
Moffett Channel , Figure 5-92	4	1	-3
Stevens Creek Downstream, Figure 5-93	53	102	49
Mountain View Slough Downstream, Figure 5-94	50	75	26
Charleston Slough Downstream, Figure 5-95	79	64	-15
Ravenswood Slough Downstream, Figure 5-98	41	87	46

5.4.2 Residual Circulation

The total residual current observed in the South Bay is a product of tidally-driven residual currents, as well as wind-driven and density-driven circulation patterns. Density-driven currents do exist in the South Bay under winter conditions when freshwater tributary inflows are high, and Delta inflows can intrude into the South Bay causing the main South Bay channel to stratify. However, density-driven processes are not well-represented by the 2D depth-averaged model formulation. Wind-driven circulation in the main South Bay channel is also not well-represented in a 2D model, as the wind can drive a surface flow in the direction of the wind, and a return flow in the deep channel. However, wind-driven flows are not as important to the total South Bay residual circulation patterns in the winter period when winds are typically lower.

The residual currents presented here are a product of tidally-driven and wind-driven circulation. In order to compare the potential impact to residual circulation within the South Bay under winter conditions, the velocities at each point in the model were averaged at two hour intervals over two spring-neap tidal cycles, or approximately 29 days (from February 14 to March 14).

Figure 5-101 displays the 29-day residual circulation under winter baseline conditions. In general, the residual circulation pattern is similar to summer conditions. However, there is a stronger net-northward residual current due to the freshwater tributary inflows in the far South Bay.

Figure 5-102 displays the 29-day residual circulation for Alternative C, with 90 percent of the ponds restored to tidal action, and Figure 5-103 displays the difference between the predicted residual circulation under baseline and Alternative C, winter conditions (Alternative C minus baseline). Little to no change in residual circulation is observed north of the San Mateo Bridge, and little change is observed near the Eden Landing pond complex. The increased tidal prism from the Ravenswood pond complex is observed in the residual currents from Ravenswood Slough.

Figure 5-104 displays the 29-day residual circulation under winter baseline conditions for the far South Bay, and Figure 5-105 displays the same under Alternative C, winter conditions, while Figure 5-106 displays the difference. The increased tidal prism associated with each tidal slough in the Alviso pond complex is evident. In general, the largest changes in residual circulation are seen in the far South Bay, as is expected by the comparatively large area of the Alviso pond complex, and the number of deeply subsided ponds which contribute to the increase in tidal prism.

5.5 Bed Shear Stress

Potential impacts to sediment erosion and deposition patterns are inferred based on comparisons of total bed shear stress both before and after tidal restoration, where total bed shear stress is a function of both tidal currents and locally-generated wind-waves. Section 4.5 provides a description of the methodology used to generate and compare the total combined wind-wave- and tidally-induced bed shear stress. As with the summer analysis period, a one day period corresponding with the peak tidal velocities was chosen to calculate the maximum tidally-induced bed shear stress. The one-day period corresponding to the highest wind conditions was chosen to calculate the maximum combined wind-wave- and tidally-induced bed shear stress. However, winds rarely exceeded 7 m/s for any significant duration within the analysis period, as is typical under winter conditions.

5.5.1 South Bay

As with summer conditions within the South Bay, the largest changes to the tidally-induced bed shear stress are seen in the subtidal channels and in the regions downstream of the tidal sloughs (Figure 5-107). The difference map shown on Figure 5-107 depicts red regions where the erosive potential increases (bed shear stresses are higher under Alternative C relative to baseline conditions), and the areas depicted in blue correspond to regions with a potential for increased deposition. As the critical shear stresses for erosion are not well known within the South Bay, and they vary spatially depending on the sediment characteristics and level of compaction of the substrate, the red and blue areas are for illustrative purposes only and do not predict erosion or deposition under Alternative C.

When the combined wind-wave- and tidally-induced shear stress is considered in the South Bay, additional changes become apparent. MLLW is higher and MHHW is lower under Alternative C (Figure

5-4 and Figure 5-5, respectively). Because wind-wave-driven shear stress is a function of water depth, and the erosive potential decreases with increasing water depth, the reduction in tidal amplitude leads to a slight reduction in the total bed shear stresses in the far South Bay (Figure 5-113). This reduction in total bed shear stress is not apparent along the eastern and western shoals north of the Dumbarton Bridge (Figure 5-112 and Figure 5-114, respectively). The reduction in tidal amplitude could lead to less erosion of the intertidal mudflats and increased erosion of the South Bay shoreline.

In general, the difference between the tidally-induced bed shear stresses and the combined wind-wave- and tidally-induced shear stresses are not as dramatic as under summer conditions due to the lessened influence of the wind under winter conditions. Summer wind conditions in the South Bay are typically more conducive to sediment resuspension and redistribution.

5.5.2 Tidal Sloughs

Within and adjacent to the Eden Landing pond complex (Figure 5-108), the maximum tidally-induced bed shear stress is increased downstream of tidal breaches, corresponding to the increased tidal prism, and decreased upstream of the tidal breaches because a portion of the flow upstream in the tidal slough under baseline conditions is captured within the downstream tidally-restored ponds under restored conditions. Within and adjacent to the Alviso pond complex (Figure 5-109) and the Ravenswood pond complex (Figure 5-110), the dynamic is similar to that observed in the Eden Landing pond complex. Tidally-induced bed shear stresses increase downstream of tidal breaches and decrease upstream of tidal breaches.

The primary effect of the combined wind-wave- and tidally-induced shear stress is evident in the South Bay, rather than in the tidal sloughs, as wind-induced waves require sufficient fetch to develop.

Figure 5-1. Water Levels, San Mateo Bridge, Alt C, Year 0, Winter

Figure 5-2. Water Levels, Dumbarton Bridge, Alt C, Year 0, Winter

Figure 5-3. Water Levels, Channel Marker 17, Alt C, Year 0, Winter

Figure 5-4. Changes in MLLW, Alt C, Year 0, Winter

Figure 5-5. Changes in MHHW, Alt C, Year 0, Winter

Figure 5-6. Changes in Tidal Propagation, Alt C, Year 0, Winter

Figure 5-7. Water Levels, ACFCC Downstream, Alt C, Year 0, Winter

Figure 5-8. Water Levels, ACFCC Upstream, Alt C, Year 0, Winter

Figure 5-9. Water Levels, Old Alameda Creek Downstream, Alt C, Year 0, Winter

Figure 5-10. Water Levels, Old Alameda Creek Upstream, Alt C, Year 0, Winter

Figure 5-11. Water Levels, Coyote Creek Power Tower, Alt C, Year 0, Winter

Figure 5-12. Water Levels, Coyote Creek Railroad Bridge, Alt C, Year 0, Winter

Figure 5-13. Water Levels, Coyote Creek/Island Ponds, Year 0, Winter

Figure 5-14. Water Levels, Coyote Creek Upstream, Year 0, Winter

Figure 5-15. Water Levels, Mud Slough Downstream, Alt C, Year 0, Winter

Figure 5-16. Water Levels, Mud Slough Upstream, Alt C, Year 0, Winter

Figure 5-17. Water Levels, Alviso Slough Downstream, Alt C, Year 0, Winter

Figure 5-18. Water Levels, Alviso Slough Upstream, Alt C, Year 0, Winter

Figure 5-19. Water Levels, Guadalupe Slough Downstream, Alt C, Year 0, Winter

Figure 5-20. Water Levels, Guadalupe Slough Upstream, Alt C, Year 0, Winter

Figure 5-21. Water Levels, Moffett Channel, Alt C, Year 0, Winter

Figure 5-22. Water Levels, Steven Creek Downstream, Alt C, Year 0, Winter

Figure 5-23. Water Levels, Stevens Creek Upstream, Alt C, Year 0, Winter

Figure 5-24. Water Levels, Mountain View Slough Downstream, Alt C, Year 0, Winter

Figure 5-25. Water Levels, Mountain View Slough Upstream, Alt C, Year 0, Winter

Figure 5-26. Water Levels, Charleston Slough Downstream, Alt C, Year 0, Winter

Figure 5-27. Water Levels, Charleston Slough Upstream, Alt C, Year 0, Winter

Figure 5-28. Water Levels, Ravenswood Slough Downstream, Alt C, Year 0, Winter

Figure 5-29. Water Levels, Ravenswood Slough Upstream, Alt C, Year 0, Winter

Figure 5-30. Water Levels, Pond A20, Alt C, Year 0, Winter

Figure 5-31. Water Levels, ELER North, Alt C, Year 0, Winter

Figure 5-32. Water Levels, ELER South, Alt C, Year 0, Winter

Figure 5-33. Water Levels, Pond E6B, Alt C, Year 0, Winter

Figure 5-34. Water Levels, Pond A7, Alt C, Year 0, Winter

Figure 5-35. Water Levels, Pond A8, Alt C, Year 0, Winter

Figure 5-36. Tidal Prism, San Mateo and Dumbarton Bridges, Alt C, Year 0, Winter

Figure 5-37. Tidal Prism, Channel Marker 17 and Calaveras Point, Alt C, Year 0, Winter

Figure 5-38. Tidal Prism, ACFCC and Old Alameda Creek, Alt C, Year 0, Winter

Figure 5-39. Tidal Prism, Coyote Creek, Alt C, Year 0, Winter

Figure 5-40. Tidal Prism, Alviso and Guadalupe Sloughs, Alt C, Year 0, Winter

Figure 5-41. Tidal Prism, Stevens Creek and, Mountain View Sloughs, Alt C, Year 0, Winter

Figure 5-42. Tidal Prism, Charleston and Ravenswood Sloughs, Alt C, Year 0, Winter

Figure 5-43. Salinity, San Mateo Bridge, Alt C, Year 0, Winter

Figure 5-44. Salinity, Dumbarton Bridge, Alt C, Year 0, Winter

Figure 5-45. Salinity, Channel Marker 17, Alt C, Year 0, Winter

Figure 5-46. Salinity at Spring HHW, Alt C, Year 0, Winter

Figure 5-47. Salinity at Spring LLW, Alt C, Year 0, Winter

Figure 5-48. Salinity, ACFCC Downstream, Alt C, Year 0, Winter

Figure 5-49. Salinity, ACFCC Upstream, Alt C, Year 0, Winter

Figure 5-50. Salinity, Old Alameda Creek Downstream, Alt C, Year 0, Winter

Figure 5-51. Salinity, Old Alameda Creek Upstream, Alt C, Year 0, Winter

Figure 5-52. Salinity at Spring HHW, Eden Landing, Alt C, Year 0, Winter

Figure 5-53. Salinity at Spring LLW, Eden Landing, Alt C, Year 0, Winter

Figure 5-54. Salinity, Coyote Creek Power Tower, Alt C, Year 0, Winter

Figure 5-55. Salinity, Coyote Creek Railroad Bridge, Alt C, Year 0, Winter

Figure 5-56. Salinity, Coyote Creek/Island Ponds, Year 0, Winter

Figure 5-57. Salinity, Coyote Creek Upstream, Year 0, Winter

Figure 5-58. Salinity, Mud Slough Downstream, Alt C, Year 0, Winter

Figure 5-59. Salinity, Mud Slough Upstream, Alt C, Year 0, Winter

Figure 5-60. Salinity, Alviso Slough Downstream, Alt C, Year 0, Winter

Figure 5-61. Salinity, Alviso Slough Upstream, Alt C, Year 0, Winter

Figure 5-62. Salinity, Guadalupe Slough Downstream, Alt C, Year 0, Winter

Figure 5-63. Salinity, Guadalupe Slough Upstream, Alt C, Year 0, Winter

Figure 5-64. Salinity, Moffett Channel, Alt C, Year 0, Winter

Figure 5-65. Salinity, Steven Creek Downstream, Alt C, Year 0, Winter

Figure 5-66. Salinity, Stevens Creek Upstream, Alt C, Year 0, Winter

Figure 5-67. Salinity, Mountain View Slough Downstream, Alt C, Year 0, Winter

Figure 5-68. Salinity, Mountain View Slough Upstream, Alt C, Year 0, Winter

Figure 5-69. Salinity, Charleston Slough Downstream, Alt C, Year 0, Winter

Figure 5-70. Salinity, Charleston Slough Upstream, Alt C, Year 0, Winter

Figure 5-71. Salinity at Spring HHW, Alt C, Alviso, Year 0, Winter

Figure 5-72. Salinity at Spring LLW, Alt C, Alviso, Year 0, Winter

Figure 5-73. Salinity, Ravenswood Slough Downstream, Ravenswood, Alt C, Year 0, Winter

Figure 5-74. Salinity, Ravenswood Slough Upstream, Ravenswood, Alt C, Year 0, Winter

Figure 5-75. Salinity at Spring HHW, Ravenswood, Alt C, Year 0, Winter

Figure 5-76. Salinity at Spring LLW, Ravenswood, Alt C, Year 0, Winter

Figure 5-77. Velocity, San Mateo Bridge, Alt C, Year 0, Winter

Figure 5-78. Velocity, Dumbarton Bridge, Alt C, Year 0, Winter

Figure 5-79. Velocity, Channel Marker 17, Alt C, Year 0, Winter

Figure 5-80. Velocity at Spring Flood, Alt C, Year 0, Winter

Figure 5-81. Velocity at Spring Ebb, Alt C, Year 0, Winter

Figure 5-82. Velocity, ACFCC Downstream, Alt C, Year 0, Winter

Figure 5-83. Velocity, Old Alameda Creek Downstream, Alt C, Year 0, Winter

Figure 5-84. Velocity at Spring Flood, Eden Landing, Alt C, Year 0, Winter

Figure 5-85. Velocity at Spring Ebb, Eden Landing, Alt C, Year 0, Winter

Figure 5-86. Velocity, Coyote Creek Power Tower, Alt C, Year 0, Winter

Figure 5-87. Velocity, Coyote Creek Railroad Bridge, Alt C, Year 0, Winter

Figure 5-88. Velocity, Coyote Creek/Island Ponds, Year 0, Winter

Figure 5-89. Velocity, Mud Slough Downstream, Alt C, Year 0, Winter

Figure 5-90. Velocity, Alviso Slough Downstream, Alt C, Year 0, Winter

Figure 5-91. Velocity, Guadalupe Slough Downstream, Alt C, Year 0, Winter

Figure 5-92. Velocity, Moffett Channel, Alt C, Year 0, Winter

Figure 5-93. Velocity, Steven Creek Downstream, Alt C, Year 0, Winter

Figure 5-94. Velocity, Mountain View Slough Downstream, Alt C, Year 0, Winter

Figure 5-95. Velocity, Charleston Slough Downstream, Alt C, Year 0, Winter

Figure 5-96. Velocity at Spring Flood, Alviso, Alt C, Year 0, Winter

Figure 5-97. Velocity at Spring Ebb, Alviso, Alt C, Year 0, Winter

Figure 5-98. Velocity, Ravenswood Slough Downstream, Alt C, Year 0, Winter

Figure 5-99. Velocity at Spring Flood, Ravenswood, Alt C, Year 0, Winter

Figure 5-100. Velocity at Spring Ebb, Ravenswood, Alt C, Year 0, Winter

Figure 5-101. South Bay Residual Circulation, Baseline, Winter

Figure 5-102. South Bay Residual Circulation, Alt C, Year 0, Winter

Figure 5-103. South Bay Residual Circulation, Difference, Year 0, Winter

Figure 5-104. Far South Bay Residual Circulation, Baseline, Winter

Figure 5-105. Far South Bay Residual Circulation, Alt C, Year 0, Winter

Figure 5-106. Far South Bay Residual Circulation, Difference, Year 0, Winter

Figure 5-107. Tidal Bed Shear Stress, South Bay, Alt C, Year 0, Winter

Figure 5-108. Tidal Bed Shear Stress, Eden Landing, Alt C, Year 0, Winter

Figure 5-109. Tidal Bed Shear Stress, Alviso, Alt C, Year 0, Winter

Figure 5-110. Tidal Bed Shear Stress, Ravenswood, Alt C, Year 0, Winter

Figure 5-111. Total Bed Shear Stress, South Bay, Alt C, Year 0, Winter

Figure 5-112. Total Bed Shear Stress, Eden Landing, Alt C, Year 0, Winter

Figure 5-113. Total Bed Shear Stress, Alviso, Alt C, Year 0, Winter

Figure 5-114. Total Bed Shear Stress, Ravenswood, Alt C, Year 0, Winter

6. ALTERNATIVE A, YEAR 50, SUMMER CONDITIONS

This section presents the results of the Alternative A, year 50, simulation under summer conditions, including a comparison with baseline summer conditions. The year 50 simulation includes large-scale bathymetric change in response to unplanned levee failures, tidal conversions occurring throughout the 50-year horizon, and sea-level rise, as described in Section 3.3. The analysis presented utilizes the same approach presented in Section 4 for ease of comparison between simulations. The model predictions are analyzed using time series at stations throughout the South Bay. Figure 4-1 through Figure 4-4 show the station locations for the South Bay and three pond complexes. The model predictions are also analyzed at specific snapshots in time for the entire South Bay and the pond complexes. Figure 4-5 shows where in the analysis period the snapshots were taken with respect to the spring-neap tidal cycle. The sections below present the results with respect to water levels, tidal prism, salinity, circulation, and bed shear stress.

6.1 Water Levels

This section presents the model results with respect to water levels in the South Bay, the tidal sloughs, and the ponds under Alternative A, year 50, summer conditions. The model predictions are compared to baseline summer predictions in order to assess the long-term impacts associated with the No Action Alternative.

6.1.1 South Bay

Table 6-1 shows the water surface elevation and phase difference for the South Bay under Alternative A, long-term, summer conditions. Positive values in Table 6-1 represent an increase in water surface elevation when compared with baseline conditions, and negative values represent a decrease in water surface elevation. Positive phase values correspond to a slower arrival time under Alternative A, long-term conditions, or a phase lag when compared with baseline conditions, whereas negative values represent that modeled water levels under Alternative A are leading baseline conditions.

In the South Bay, the modeled water levels at the San Mateo Bridge increase on all phases of the daily tidal cycle relative to baseline conditions, and the increase is largely representative of the modeled rate of sea-level rise of 15 cm over 50 years (Figure 6-1). At the Dumbarton Bridge (Figure 6-2), the water level increase under Alternative A, year 50 conditions is approximately equal to sea-level rise throughout the analysis period with the exception of LLW during spring tide. Water levels decrease by approximately 25 to 30 cm at LLW during spring tide conditions. The Dumbarton Bridge station is located on the eastern edge of the main South Bay channel, and this station is completely dry at approximately -0.4 m NAVD88 under baseline conditions. At year 50, scour is predicted to occur along the edges of the main South Bay channel to a depth of approximately 6 feet below MLLW (PWA 2006b), therefore the water level at LLW would no longer be constrained by the bed elevation.

At Channel Marker 17 (Figure 6-3), located near the mouth of Coyote Creek, water levels increase on all phases of the tide. The increases at HHW are largely associated with sea-level rise, however, the

unplanned tidal conversions under Alternative A temper the water level increase. In other words, the increase in HHW could be larger in the absence of the unplanned tidal conversions. LLW increases by approximately 20 cm under neap tide and 25 cm under spring tide conditions in response to sea-level rise, mudflat accretion in the far South Bay (see Section 3.3.3), and to a lesser extent, the small increase in tidal prism associated with the unplanned tidal conversions in the Alviso pond complex.

The long-term trend in increased water levels leads to an increase in the MLLW and MHHW tidal datums. Figure 6-4 depicts the change in MLLW at year 50. The increase in MLLW is most pronounced in the far South Bay; however, the increase is on-the-order of sea-level rise north of the Dumbarton Bridge. With respect to MHHW (Figure 6-5), the smallest increases occur in the far South Bay, and as a whole, the increase in MHHW is approximately 10 – 15 cm throughout the South Bay.

Harmonic analysis was performed on water levels at several stations along the main South Bay channel, and the computed phase and amplitudes of the M_2 and K_1 tidal constituents for baseline and Alternative A, year 50 conditions are compared in order to assess how the alternative is affecting tidal propagation within the South Bay (Figure 6-6). Figure 6-6a presents the computed phase of the M_2 and K_1 tidal constituents, and little difference is observed in the South Bay between Alternative A, year 50 and baseline conditions. Figure 6-6b presents the computed amplitude of the M_2 and K_1 tidal constituents, and again, little difference is observed.

Table 6-1. South Bay Tidal Water Surface Elevation and Phase Differences under Alt A, Year 50, Summer

(Water surface elevation differences in cm, phase differences in minutes. June 13 = neap tide, June 22 = spring tide.)

Station Name	June 13 LLW		June 13 HHW		June 22 LLW		June 22 HHW	
	WSE	Phase	WSE	Phase	WSE	Phase	WSE	Phase
San Mateo Bridge, Figure 6-1	15	0	13	0	17	0	15	0
Dumbarton Bridge, Figure 6-2	16	0	12	-10	-27	-40	14	0
Channel Marker 17, Figure 6-3	19	0	12	10	25	10	10	0

6.1.2 Tidal Sloughs

Under Alternative A, approximately 35 percent of the SBSP Restoration Project Area is assumed to convert to tidal action in an unplanned manner in response to levee failures and erosion occurring over the 50-year horizon. The ponds assumed to convert to tidal marsh are shown in Figure 3-18, Figure 3-19 and Figure 3-20 for each pond complex, with the majority of the tidally-converting ponds located in the Eden Landing pond complex. In response to the increase in tidal prism associated with this conversion, the tidal sloughs are expected to scour and deepen as they approach equilibrium conditions, potentially removing the tidal damping effect seen under the Alternative C, year 0 simulations in the absence of channel scour (Section 4). Table 3-5 presents the predicted increase in channel depth for ACFCC, Old Alameda Creek, Alviso Slough and Guadalupe Slough. The remaining sloughs are assumed to retain their existing bathymetry. As discussed in Section 2.3.5, some of the sloughs, particularly those in the Eden Landing and Ravenswood pond complex, are modeled with larger than actual channel widths due to limitations

with respect to the grid resolution; therefore, the model results for these sloughs may underestimate the potential long-term changes in water levels.

Table 6-2 presents the water surface elevation and phase difference under Alternative A at both upstream and downstream stations in each tidal slough. Positive water surface elevation values in Table 6-2 represent an increase in water surface elevation when compared with baseline conditions, and negative values represent a decrease in water surface elevation. Positive phase values correspond to a slower arrival time under Alternative A, or a phase lag when compared with baseline conditions, whereas negative values represent that modeled water levels under Alternative A, long-term conditions are leading baseline conditions.

Water levels downstream in ACFCC change in response to the predicted slough scour and sea-level rise (Figure 6-7). The increase in high water levels appears to be on-the-order of sea-level rise. At LLW, water levels decrease nearly 80 cm on spring tides, with smaller decreases occurring on neap tides. This decrease is associated with the 1.2 to 1.4 m of slough scour predicted to occur. The magnitude of the water level changes at LLW could be associated with an over-prediction of potential channel scour. Upstream, no channel scour is predicted because the upstream levees are assumed to be maintained for flood control. The trend in water levels changes is similar to that observed at the downstream station, although the associated amplitude changes are larger and more symmetric across spring and neap tides (Figure 6-8). Water level changes are similar in Old Alameda Creek, although the relative changes are smaller owing to the smaller increase in tidal prism (Figure 6-9).

In Alviso Slough and Guadalupe Slough, water levels increase on all phases of the tidal cycle, and the increases are roughly on the order of sea-level rise (Figure 6-17 and Figure 6-19, respectively). The effect of the increased tidal prism resulting from unplanned upstream tidal conversions is minimal as only Ponds A5, A6 and A7 are assumed to convert to tidal action, and the equilibrium predictions of channel scour appear to properly account for the increased tidal prism.

The remaining sloughs within the SBSP Restoration Project Area, including Ravenswood Slough in the Ravenswood pond complex and the remaining sloughs within the Alviso pond complex experience water level changes that are largely attributable to sea-level rise, with increases at LLW roughly twice those at HHW. One exception is Coyote Creek, which continues to accrete sediment over the 50-year horizon. This decrease in tidal prism is associated with minor decreases in LLW during spring tides.

Phasing changes are relatively small (on the order of 10 to 30 minutes) throughout the SBSP Restoration Project Area. The largest changes are observed in the ACFCC where Alternative A at year 50 leads baseline conditions by more than 60 minutes at LLW. As with the water level changes, this may be attributable to an over-prediction of channel scour relative to the increased upstream tidal prism.

Table 6-2. Tidal Slough Water Surface Elevation and Phase Differences under Alt A, Year 50, Summer (Water surface elevation differences in cm, phase differences in minutes. June 13 = neap tide, June 22 = spring tide.)

Station Name	June 13 LLW		June 13 HHW		June 22 LLW		June 22 HHW	
	WSE	Phase	WSE	Phase	WSE	Phase	WSE	Phase
<i>Eden Landing pond complex</i>								
ACFCC Downstream, Figure 6-7	-28	-100	16	-10	-77	-80	17	0
ACFCC Upstream, Figure 6-8	-58	-50	35	-90	-60	-160	23	-60
Old Alameda Creek Downstream, Figure 6-9	-12	-70	14	0	-36	-40	13	0
Old Alameda Creek Upstream, Figure 6-10	30	40	18	10	17	30	13	40
<i>Alviso pond complex</i>								
Coyote Creek Power Tower, Figure 6-11	24	-20	13	10	34	-30	14	0
Coyote Creek Railroad Bridge, Figure 6-12	10	-10	25	-20	-8	-20	26	-20
Coyote Creek/Island Ponds, Figure 6-13	8	-20	26	-20	-10	-30	28	-30
Coyote Creek Upstream, Figure 6-14	8	-20	26	-20	-10	-40	28	-40
Mud Slough Downstream, Figure 6-15	13	0	21	0	-1	-10	24	-20
Mud Slough Upstream, Figure 6-16	11	-10	24	-10	-1	-20	28	-30
Alviso Slough Downstream, Figure 6-17	20	0	12	0	19	10	11	10
Alviso Slough Upstream, Figure 6-18	23	10	2	30	30	20	2	50
Guadalupe Slough Downstream, Figure 6-19	22	10	12	0	31	20	13	0
Guadalupe Slough Upstream, Figure 6-20	36	30	1	70	44	40	-7	20
Moffett Channel, Figure 6-21	36	30	1	70	45	40	-6	40
Stevens Creek Downstream, Figure 6-22	28	10	12	10	27	10	13	-10
Stevens Creek Upstream, Figure 6-23	23	-30	12	10	24	-10	14	10
Mountain View Slough Downstream, Figure 6-24	19	10	13	0	20	0	14	-10
Mountain View Slough Upstream, Figure 6-25	17	-10	13	0	18	0	14	-10
Charleston Slough Downstream, Figure 6-26	-3	-30	17	-20	-7	-20	14	10
Charleston Slough Upstream, Figure 6-27	-4	20	17	-20	-5	0	14	0
<i>Ravenswood pond complex</i>								
Ravenswood Slough Downstream, Figure 6-28	-16	60	12	-10	-21	-40	14	-10
Ravenswood Slough Upstream, Figure 6-29	21	10	13	0	22	0	14	-10

6.2 Tidal Prism

A comparison of the estimates of modeled tidal prism between baseline conditions and Alternative A, year 50 with summer boundary conditions is summarized in Table 6-3. As discussed in Section 4.2, tidal prism has been estimated as the volume of water crossing a cross-section during a flood tide for the basis of comparing tidal prism estimates with previous studies. Overall, the unplanned levee breaches and sea-level rise combine to alter the tidal prism across many of the South Bay cross-sections. Although the exact location of the levee breaches is impossible to predict, this comparison between baseline and

Alternative A, long-term conditions provides an indication of the magnitude of tidal prism changes regardless of the specific breach locations.

The cross-sections at the San Mateo and Dumbarton Bridges exhibit small changes in tidal prism. At the San Mateo Bridge, a four percent increase in tidal prism is predicted and is largely in response to sea-level rise and the mudflat erosion predicted north of the Dumbarton Bridge (see Section 3.3.3). At the Dumbarton Bridge, a five percent decrease in tidal prism is predicted under Alternative A, long-term conditions. This decrease in tidal prism is likely largely associated with the continuing trend of mudflat accretion predicted to occur in the far South Bay (PWA 2006b). Figure 6-30 presents the modeled flux of water across both bridge cross-sections under baseline and Alternative A, long-term conditions, and the relative increase and decrease in tidal prism are evident. In the far South Bay, slight decreases in the modeled flux of water across cross-sections near Channel Marker 17 and Calaveras Point are predicted to occur under Alternative A, long-term conditions (Figure 6-31).

Sloughs in the Eden Landing pond complex have the largest predicted changes in tidal prism under Alternative A, long-term conditions. The magnitude of the changes ranges from 80 percent in the ACFCC to 360 percent in Mount Eden Creek. The tidal prism increases are consistent with the assumption that this complex would have the largest extent of unplanned breaches due to levee erosion and failures. Along Mount Eden Creek, the large increase in tidal prism is associated with several factors. First, Ponds E12 and E13 are assumed to convert to tidal marsh in an unplanned manner and breach to Mount Eden Creek. In response to this tidal conversion, the slough is expected to scour, as discussed Section 3.3.2. In addition, mudflat erosion is predicted to occur adjacent to the Eden Landing pond complex. This large-scale geomorphic change enables better tidal propagation into the Eden Landing Complex, thereby increasing tidal prism. A final factor which contributes to the tidal prism increase is an artifact of the model's grid cell sizing in this region. As discussed in Section 2.3.5, the grid resolution limitations cause the sloughs to be represented in the model at a larger than actual width. All of these factors together account for the large increase in tidal prism observed in Mount Eden Creek. Lesser tidal prism increases are predicted for Old Alameda Creek and the ACFCC. Figure 6-32 presents the modeled flux of water near the mouth of Old Alameda Creek and the ACFCC; the relative increases in tidal prism are evident.

Along Coyote Creek, the tidal prism changes are influenced by the bathymetric changes that occur to the adjacent ponds. Nearly the same tidal prism enters the mouth of Coyote Creek at the Power Tower in year 50 as in year 0 (Figure 6-33). However, because of the unplanned tidal conversions, a greater portion of this tidal prism is drawn into Alviso Slough than under baseline conditions. The reduced tidal prism remaining in the main stem of Coyote Creek registers as decreased tidal prism at the Railroad Bridge (Table 6-3). However, further upstream from the Railroad Bridge, east of the Island Ponds and in the creek's tributary, Artesian Slough, tidal prism is predicted to increase. This increase occurs because the Island Ponds are assumed to develop into mature marsh by year 50, thus reducing the tidal prism introduced by the ponds under baseline conditions. Therefore, more water is available for propagation up Coyote Creek east of the ponds and into Artesian Slough.

Within the Alviso pond complex, the only ponds which are assumed to undergo unplanned tidal conversions are Ponds A5, A6 and A7 between Guadalupe and Alviso Slough. As a result of these tidal conversions, the tidal prism in these two sloughs is predicted to increase approximately 30 – 50 percent. Figure 6-34 presents the modeled flux of near the mouth of both sloughs, and the relative increases in tidal prism are evident. The smaller sloughs in the Alviso pond complex, such as Stevens Creek, Charleston Slough and Mountain View Slough exhibit minimal change in tidal prism in the absence of any ponds breached along their length (see Figure 6-35 and Figure 6-36). The decrease in tidal prism associated with these sloughs is likely a function of the reduced tidal range and mudflat accretion predicted in the far South Bay.

Ravenswood Slough in the Ravenswood pond complex exhibits a modest increase of tidal prism on the order of 20 percent (Figure 6-36). This is likely a result of the large-scale mudflat erosion predicted to occur between the San Mateo and Dumbarton Bridges (PWA 2006b), as well as the assumed rate of sea-level rise. A similar dynamic is likely associated with the non-project sloughs north of Dumbarton Bridge (Corkscrew Slough, Redwood Slough and Westpoint Slough).

Table 6-3. Comparison of Tidal Prism between Baseline and Alternative A, year 50, summer

Transect Location	Tidal Prism (millions of cubic meters)		
	Baseline summer	Alternative A year 50, summer	% change baseline to yr 50
<i>South Bay</i>			
San Mateo Bridge	270	280	3.9%
Dumbarton Bridge	71	68	-5.2%
<i>Eden Landing pond complex</i>			
ACFCC	1.4	2.6	84%
Old Alameda Creek	1.4	3.5	150%
Mount Eden Creek	0.58	2.7	360%
Ravenswood pond complex			
Ravenswood Slough	0.53	0.64	19%
<i>Alviso pond complex</i>			
Calaveras Point	14	14	-1.2%
Coyote Creek at Power Tower	6.8	6.9	1.2%
Coyote Creek at RR Bridge	2.2	1.8	-17%
Coyote Creek east of Island Ponds	0.53	0.73	39%
Charleston Slough	0.55	0.51	-6.2%
Mountain View Slough	0.21	0.21	-3.0%
Stevens Creek	0.11	0.10	-11%
Guadalupe Slough	1.1	1.5	33%
Alviso Slough	1.1	1.7	50%
Artesian Slough	0.48	0.54	12%
Mud Slough	0.79	0.78	-1.4%
<i>Non-project Sloughs</i>			
Corkscrew Slough	3.4	3.9	12%
Redwood Creek	16	18	14%
Westpoint Slough	2.9	3.3	14%
Mowry Slough	0.41	0.43	5.3%
Plummer Slough	0.32	0.31	-3.2%
Newark Slough	0.86	0.92	6.6%

6.3 Salinity

This section presents the model results with respect to salinity in the South Bay and the tidal sloughs under Alternative A, year 50, summer conditions. The model predictions are compared to baseline summer predictions in order to assess the long-term impact of unplanned tidal conversion occurring under the No Action Alternative on the South Bay and the tidal sloughs, as presented below.

6.3.1 South Bay

Under Alternative A, long-term conditions, little change is observed with respect to salinity within the South Bay (Table 6-4). Positive values in Table 6-4 represent an increase in salinities relative to the baseline, and negative values represent a decrease in salinities relative to baseline conditions. At the San Mateo and Dumbarton Bridges, there is no significant difference in salinity when compared with baseline

conditions (Figure 6-37 and Figure 6-38, respectively). Slightly higher salinity differences are observed at Channel Marker 17 (Figure 6-39), with salinity increases on the order of 0 – 2 ppt the observed at LLW.

Figure 6-40 displays the salinities in the South Bay during spring conditions at HHW, representing peak salinity conditions during the analysis period. As can be seen, little difference in peak South Bay salinities occurs under summer conditions with respect to long-term Alternative A conditions. The largest changes in salinity are confined to the tidal sloughs. Figure 6-41 displays South Bay salinities at LLW during spring tide conditions. At low water, the observed differences are greatest downstream of the tidal sloughs and in the subtidal channels in the South Bay.

Table 6-4. South Bay Salinity Differences under Alt A, Year 50, Summer
(Salinity differences in ppt. June 13 = neap tide, June 22 = spring tide.)

Station Name	June 13 LLW	June 13 HHW	June 22 LLW	June 22 HHW
San Mateo Bridge, Figure 6-37	0.1	0.0	0.1	0.0
Dumbarton Bridge, Figure 6-38	0.4	0.1	0.2	0.0
Channel Marker 17, Figure 6-39	0.8	0.3	1.7	0.4

6.3.2 Tidal Sloughs

Table 6-5 shows the salinity difference between Alternative A long-term conditions and baseline conditions in the tidal sloughs during neap and spring tide summer conditions. Positive values represent an increase in salinities relative to the baseline, and negative values represent a decrease in salinities relative to baseline conditions.

In the Eden Landing pond complex, salinities increase in the downstream reach of the ACFCC in response to the increased tidal exchange and mixing associated with the deeper channel (Figure 6-42). At high water levels, only a moderate salinity increase of 0 – 2 ppt is observed; however low water salinities increase up to 8 ppt. This increase in downstream salinities shifts the salinity gradient upstream, and salinities at the upstream station in ACFCC are 5 – 10 ppt higher throughout the analysis period (Figure 6-43). Salinities in Old Alameda Creek exhibit little change with respect to baseline salinities (Figure 6-44 and Figure 6-45). Due to the oversized representation of the Old Alameda Creek in the model (see Section 2.3.5), salinity changes in Old Alameda Creek may be underestimated.

Figure 6-46 and Figure 6-47 present the peak salinities in the Eden Landing pond complex during spring HHW and LLW conditions, respectively. As can be seen, the largest salinity changes are observed in the ACFCC and the South Bay directly downstream of the slough mouths.

The most significant change in the Alviso pond complex can be seen in Coyote Creek and Mud Slough. At the Power Tower (Figure 6-48), little change is seen between Alternative A, long-term and baseline conditions. However, at the Railroad Bridge (Figure 6-49), salinities decrease approximately 3 – 5 ppt throughout the analysis period, and the decrease in salinity is slightly higher at the upstream stations at

the eastern end of Pond A19 (Figure 6-50) and near Warm Springs (Figure 6-51). A similar decrease in salinity is observed in Mud Slough (Figure 6-52 and Figure 6-53). Coyote Creek is assumed to continue accreting sediment over the 50-year horizon (PWA 2006b). This leads to a reduction in the tidal exchange between the upstream reaches of Coyote Creek and the South Bay and reduced velocities along Coyote Creek. This trend leads to an increased residence time in the upper reaches of Coyote Creek, increasing the effect of the City of San Jose's WWTP freshwater discharge on upstream salinities.

In Alviso Slough, Guadalupe Slough and Moffett Channel, salinities increase 1 – 6 ppt in response to the unplanned tidal conversion of Ponds A5, A6 and A7. The remaining slough channels within the SBSP Restoration Project Area exhibit relatively little change with respect to salinities. In general, salinities increase less than 1 ppt throughout the analysis period. This may at least partially be due to the oversized representation of the sloughs in the model, particularly with respect to Stevens Creek, Mountain View and Charleston Sloughs.

Figure 6-65 and Figure 6-66 present the peak salinities in the Alviso pond complex during spring HHW and LLW conditions, respectively. The decreased salinities in Coyote Creek and increased salinities in Alviso Slough, Guadalupe Slough and the Moffett Channel are evident. In the Ravenswood pond complex, all pond levees are assumed to be maintained due to the presence of the PG&E substation, therefore no ponds are converted to tidal action due to levee failure and little salinity differences are observed between long-term, Alternative A and baseline conditions (Figure 6-69 and Figure 6-70).

Table 6-5. Tidal Slough Salinity Differences under Alt A, Year 50, Summer
(Salinity differences in ppt. June 13 = neap tide, June 22 = spring tide.)

Station Name	June 13 LLW	June 13 HHW	June 22 LLW	June 22 HHW
<i>Eden Landing pond complex</i>				
ACFCC Downstream, Figure 6-42	6.7	0.9	4.9	0.1
ACFCC Upstream, Figure 6-43	7.6	7.3	10.0	5.0
Old Alameda Creek Downstream, Figure 6-44	0.1	0.0	0.0	0.0
Old Alameda Creek Upstream, Figure 6-45	-0.2	-0.2	-0.2	-0.3
<i>Alviso pond complex</i>				
Coyote Creek Power Tower, Figure 6-48	-0.1	0.5	-1.3	0.5
Coyote Creek Railroad Bridge, Figure 6-49	-3.2	-4.9	-5.3	-3.2
Coyote Creek/Island Ponds , Figure 6-50	-4.4	-4.3	-5.1	-4.9
Coyote Creek Upstream, Figure 6-51	-3.9	-4.1	-4.2	-4.4
Mud Slough Downstream, Figure 6-52	-3.6	-1.4	-4.2	-2.5
Mud Slough Upstream, Figure 6-53	-4.0	-3.9	-4.2	-5.0
Alviso Slough Downstream, Figure 6-54	2.3	0.8	3.4	0.7
Alviso Slough Upstream, Figure 6-55	1.5	1.7	1.8	1.9
Guadalupe Slough Downstream, Figure 6-56	2.0	1.0	3.2	0.9
Guadalupe Slough Upstream, Figure 6-57	4.1	5.6	4.9	6.7
Moffett Channel, Figure 6-58	3.6	4.4	4.4	5.5
Stevens Creek Downstream, Figure 6-59	0.6	0.2	0.9	0.5
Stevens Creek Upstream, Figure 6-60	0.7	0.6	0.9	0.8
Mountain View Slough Downstream, Figure 6-61	0.3	0.3	0.4	0.4
Mountain View Slough Upstream, Figure 6-62	0.4	0.3	0.5	0.4
Charleston Slough Downstream, Figure 6-63	0.4	0.4	0.2	0.1
Charleston Slough Upstream, Figure 6-64	0.0	0.5	-0.4	0.2
<i>Ravenswood pond complex</i>				
Ravenswood Slough Downstream, Figure 6-67	0.1	0.1	0.2	0.1
Ravenswood Slough Upstream, Figure 6-68	0.3	0.3	0.4	0.3

6.4 Circulation

Potential changes to South Bay circulation can be evaluated by examining current velocities at specific locations within the Bay and tidal sloughs, and by examining general changes to South Bay residual circulation. The most important factor influencing circulation patterns in South Bay is bathymetry (Cheng and Gartner 1985). At year 50, significant large-scale bathymetric change is assumed to have occurred under the No Action Alternative. Mudflat accretion is assumed in the far South Bay, mudflat erosion occurs between the San Mateo and Dumbarton Bridges, the unplanned, tidally-converted ponds have developed into mature salt marsh with a corresponding marsh channel network, and the tidal sloughs have scoured in response to the associated increased tidal prism.

6.4.1 Current Velocity

South Bay

In the South Bay, modeled velocities at the San Mateo and Dumbarton Bridges exhibit little change relative to baseline conditions. Table 6-6 shows the peak velocity magnitudes at the bridge and Channel Marker 17 stations under baseline and Alternative A, long-term conditions. Positive values indicate a higher modeled velocity under Alternative A, and negative values indicate a decrease in current velocity under Alternative A.

At the San Mateo and Dumbarton Bridges, velocity magnitudes exhibit little change with respect to baseline conditions (Figure 6-71 and Figure 6-72, respectively). At Channel Marker 17 (Figure 6-73), velocities are increased under Alternative A, long-term conditions. This increase in velocities is due to the sediment accretion on the far South Bay mudflats. The mudflat elevations increased at a rate greater than sea-level rise, which leads to more mudflat area being exposed at LLW and more flow being directed through the subtidal channels on ebb tides.

Figure 6-74 and Figure 6-75 present velocity magnitudes within the South Bay under peak flood and peak ebb conditions under baseline and Alternative A, long-term conditions, as well as the difference between the two model predictions. The differences are minor under spring flood conditions, and the greatest change occurs in the subtidal channels under ebb tide conditions.

Tidal Sloughs

Table 6-7 shows the peak velocity magnitudes at the downstream stations in the tidal sloughs under baseline and Alternative A conditions. Positive values indicate a higher modeled velocity under Alternative A, and negative values indicate a decrease in current velocity under Alternative A. Little change in tidal slough velocities is observed when comparing Alternative A, long-term and baseline conditions. The largest changes are seen downstream in Old Alameda Creek in the Eden Landing pond complex, in Coyote Creek near the Railroad Bridge, and downstream in Alviso Slough in the Alviso pond complex.

The velocity increases in Old Alameda Creek are a result of unplanned tidal conversion of Ponds E8A, E8, E6B and E6A to the north, and Ponds E5, E6, and E7 to the south (Figure 6-77). Figure 6-78 and Figure 6-79 present peak velocity magnitude within the South Bay under flood and ebb conditions under baseline and Alternative A, long-term conditions. On flood, the primary changes are observed within the tidal channels, and on ebb tide, the largest differences are observed downstream of the channel mouths.

Velocities decrease near the Railroad Bridge in Coyote Creek (Figure 6-81) due to the assumption of continuing sediment accretion within Coyote Creek, as discussed in Section 6.3.2. This velocity magnitude decrease is observed at both peak flood (Figure 6-90) and peak ebb conditions (Figure 6-91). Also evident are the increased velocities in the main South Bay subtidal channel and Alviso and Guadalupe Sloughs under both flood and ebb conditions.

No velocity increases are expected or observed within the Ravenswood pond complex as all ponds levees are assumed to be maintained, therefore no unplanned tidal conversions are assumed to occur within the 50-year horizon (Figure 6-93 and Figure 6-94).

Table 6-6. South Bay Peak Velocity Magnitude Comparisons: Alt A, Year 50, Summer vs. Baseline, Summer

(All velocities in cm/s)

Station Name	Baseline	Alt A	Difference
San Mateo Bridge, Figure 6-71	102	100	-2
Dumbarton Bridge, Figure 6-72	34	36	2
Channel Marker 17, Figure 6-73	67	81	14

Table 6-7. Tidal Slough Peak Velocity Magnitude Comparisons: Alt A, Year 50, Summer vs. Baseline, Summer

(All velocities in cm/s)

Station Name	Baseline	Alt A	Difference
ACFCC Downstream, Figure 6-76	45	38	-7
Old Alameda Creek Downstream, Figure 6-77	53	80	27
Coyote Creek Power Tower, Figure 6-80	76	78	3
Coyote Creek Railroad Bridge, Figure 6-81	82	68	-14
Coyote Creek/Island Ponds, Figure 6-82	39	46	7
Mud Slough Downstream, Figure 6-83	46	46	0
Alviso Slough Downstream, Figure 6-84	49	72	23
Guadalupe Slough Downstream, Figure 6-85	46	49	3
Moffett Channel, Figure 6-86	5	3	-2
Stevens Creek Downstream, Figure 6-87	51	46	-6
Mountain View Slough Downstream, Figure 6-88	4	49	0
Charleston Slough Downstream, Figure 6-89	77	64	-13
Ravenswood Slough Downstream, Figure 6-92	38	40	2

6.4.2 Residual Circulation

The total residual current observed in the South Bay is a product of tidally-driven residual currents, as well as wind-driven and density-driven circulation patterns. The long-term conditions under Alternative A, including large-scale bathymetric change and sea-level rise, have the potential to alter residual circulation patterns within the South Bay.

Figure 6-95 displays the 29-day residual circulation under summer baseline conditions. Figure 6-96 displays the 29-day residual circulation for long-term, Alternative A conditions, and Figure 6-97 displays the difference between the predicted residual circulation under baseline and Alternative A conditions

(Alternative A, year 50 minus baseline). Little change is observed in the South Bay north of the Dumbarton Bridge.

More noticeable changes are observed in the far South Bay, south of the Dumbarton Bridge. Figure 6-98 displays the 29-day residual circulation under summer baseline conditions for the far South Bay, Figure 6-99 displays the same for long-term, Alternative A conditions, and Figure 6-100 displays the difference. The largest difference in residual circulation pattern is observed in the main South Bay subtidal channel and Coyote Creek. A net-northward residual current is still present under Alternative A, long-term conditions; however, its magnitude has lessened, resulting in an increased residence time in the upper reaches of Coyote Creek, as discussed under Section 6.3.2.

6.5 Bed Shear Stress

Potential impacts to sediment erosion and deposition patterns are inferred based on comparisons of total bed shear stress both before and after tidal restoration, where total bed shear stress is a function of both tidal currents and locally-generated wind-waves. Section 4.5 provides a description of the methodology used to generate and compare the total combined wind-wave- and tidally-induced bed shear stress.

6.5.1 South Bay

The increase in water levels and tidal datums associated with sea-level rise result in minor decreases in tidally-induced bed shear stresses in much of the South Bay (Figure 6-101). The difference map shown on Figure 6-101 depicts red regions where the erosive potential increases (bed shear stresses are higher under Alternative A relative to baseline conditions), and the areas depicted in blue correspond to regions with a potential for increased deposition. As the critical shear stresses for erosion are not well known within the South Bay, and they vary spatially depending on the sediment characteristics and level of compaction of the substrate, the red and blue areas are for illustrative purposes only and do not predict erosion or deposition under Alternative A.

Slight decreases in tidally-induced bed shear stress are observed in the main South Bay channel and the shallow mudflat areas in the far South Bay and on the western and eastern shores, with little change observed in the shallow subtidal areas. Slight increases in tidally-induced bed shear stresses are observed downstream of Alviso Slough and Guadalupe Slough in the far South Bay, and Old Alameda Creek and Mt. Eden in the Eden Landing pond complex.

More significant changes are observed when the combined wind-wave- and tidally-induced bed shear stresses are considered (Figure 6-105). Both MLLW and MHHW are higher under Alternative A, long-term conditions. Because wind-wave-driven bed shear stress is a function of water depth, and the erosive potential decreases with increasing water depth, the overall increase in water levels leads to a reduction in the total bed shear stresses in the shallow areas of the South Bay. This dynamic is primarily seen along the eastern and western shoals north of the Dumbarton Bridge. Within the far South Bay, mudflat accretion was assumed to outpace sea-level rise, therefore mean water depths are actually lower under

Alternative A in the long term when compared with baseline conditions. This leads to an increase in total bed shear stress in the far South Bay and an increase in the erosive potential.

6.5.2 Tidal Sloughs

Within and adjacent to the Eden Landing pond complex (Figure 6-102), the maximum tidally-induced bed shear stress is increased downstream of the unplanned tidal breaches, corresponding to the increased tidal prism, and decreased upstream of the tidal breaches because a portion of the flow upstream in the tidal slough under baseline conditions is captured within the tidally-restored ponds under restored conditions. Within and adjacent to the Alviso pond complex (Figure 6-103), the dynamic is similar to that observed in the Eden Landing pond complex. Tidally-induced bed shear stresses increase downstream of tidal breaches and decrease upstream of tidal breaches. No change is observed within the Ravenswood pond complex because no levee failures are assumed to occur (Figure 6-104).

The primary effect of the combined wind-wave- and tidally-induced shear stress is evident in the South Bay rather than in the tidal sloughs as wind-induced waves require sufficient fetch to develop.

Figure 6-1. Water Levels, San Mateo Bridge, Alt A, Year 50, Summer

Figure 6-2. Water Levels, Dumbarton Bridge, Alt A, Year 50, Summer

Figure 6-3. Water Levels, Channel Marker 17, Alt A, Year 50, Summer

Figure 6-4. Changes in MLLW, Alt A, Year 50, Summer

Figure 6-5. Changes in MHHW, Alt A, Year 50, Summer

Figure 6-6. Changes in Tidal Propagation, Alt A, Year 50, Summer

Figure 6-7. Water Levels, ACFCC Downstream, Alt A, Year 50, Summer

Figure 6-8. Water Levels, ACFCC Upstream, Alt A, Year 50, Summer

Figure 6-9. Water Levels, Old Alameda Creek Downstream, Alt A, Year 50, Summer

Figure 6-10. Water Levels, Old Alameda Creek Upstream, Alt A, Year 50, Summer

Figure 6-11. Water Levels, Coyote Creek Power Tower, Alt A, Year 50, Summer

Figure 6-12. Water Levels, Coyote Creek Railroad Bridge, Alt A, Year 50, Summer

Figure 6-13. Water Levels, Coyote Creek/Island Ponds, Year 50, Summer

Figure 6-14. Water Levels, Coyote Creek Upstream, Year 50, Summer

Figure 6-15. Water Levels, Mud Slough Downstream, Alt A, Year 50, Summer

Figure 6-16. Water Levels, Mud Slough Upstream, Alt A, Year 50, Summer

Figure 6-17. Water Levels, Alviso Slough Downstream, Alt A, Year 50, Summer

Figure 6-18. Water Levels, Alviso Slough Upstream, Alt A, Year 50, Summer

Figure 6-19. Water Levels, Guadalupe Slough Downstream, Alt A, Year 50, Summer

Figure 6-20. Water Levels, Guadalupe Slough Upstream, Alt A, Year 50, Summer

Figure 6-21. Water Levels, Moffett Channel, Alt A, Year 50, Summer

Figure 6-22. Water Levels, Steven Creek Downstream, Alt A, Year 50, Summer

Figure 6-23. Water Levels, Stevens Creek Upstream, Alt A, Year 50, Summer

Figure 6-24. Water Levels, Mountain View Slough Downstream, Alt A, Year 50, Summer

Figure 6-25. Water Levels, Mountain View Slough Upstream, Alt A, Year 50, Summer

Figure 6-26. Water Levels, Charleston Slough Downstream, Alt A, Year 50, Summer

Figure 6-27. Water Levels, Charleston Slough Upstream, Alt A, Year 50, Summer

Figure 6-28. Water Levels, Ravenswood Slough Downstream, Alt A, Year 50, Summer

Figure 6-29. Water Levels, Ravenswood Slough Upstream, Alt A, Year 50, Summer

Figure 6-30. Tidal Prism, San Mateo and Dumbarton Bridges, Alt A, Year 50, Summer

Figure 6-31. Tidal Prism, Channel Marker 17 and Calaveras Point, Alt A, Year 50, Summer

Figure 6-32. Tidal Prism, ACFCC and Old Alameda Creek, Alt C, Year A, Summer

Figure 6-33. Tidal Prism, Coyote Creek, Alt A, Year 50, Summer

Figure 6-34. Tidal Prism, Alviso and Guadalupe Sloughs, Alt A, Year 50, Summer

Figure 6-35. Tidal Prism, Stevens Creek and, Mountain View Sloughs, Alt A, Year 50, Summer

Figure 6-36. Tidal Prism, Charleston and Ravenswood Sloughs, Alt A, Year 50, Summer

Figure 6-37. Salinity, San Mateo Bridge, Alt A, Year 50, Summer

Figure 6-38. Salinity, Dumbarton Bridge, Alt A, Year 50, Summer

Figure 6-39. Salinity, Channel Marker 17, Alt A, Year 50, Summer

Figure 6-40. Salinity at Spring HHW, Alt A, Year 50, Summer

Figure 6-41. Salinity at Spring LLW, Alt A, Year 50, Summer

Figure 6-42. Salinity, ACFCC Downstream, Alt A, Year 50, Summer

Figure 6-43. Salinity, ACFCC Upstream, Alt A, Year 50, Summer

Figure 6-44. Salinity, Old Alameda Creek Downstream, Alt A, Year 50, Summer

Figure 6-45. Salinity, Old Alameda Creek Upstream, Alt A, Year 50, Summer

Figure 6-46. Salinity at Spring HHW, Eden Landing, Alt A, Year 50, Summer

Figure 6-47. Salinity at Spring LLW, Eden Landing, Alt A, Year 50, Summer

Figure 6-48. Salinity, Coyote Creek Power Tower, Alt A, Year 50, Summer

Figure 6-49. Salinity, Coyote Creek Railroad Bridge, Alt A, Year 50, Summer

Figure 6-50. Salinity, Coyote Creek/Island Ponds, Year 50, Summer

Figure 6-51. Salinity, Coyote Creek Upstream, Year 50, Summer

Figure 6-52. Salinity, Mud Slough Downstream, Alt A, Year 50, Summer

Figure 6-53. Salinity, Mud Slough Upstream, Alt A, Year 50, Summer

Figure 6-54. Salinity, Alviso Slough Downstream, Alt A, Year 50, Summer

Figure 6-55. Salinity, Alviso Slough Upstream, Alt A, Year 50, Summer

Figure 6-56. Salinity, Guadalupe Slough Downstream, Alt A, Year 50, Summer

Figure 6-57. Salinity, Guadalupe Slough Upstream, Alt A, Year 50, Summer

Figure 6-58. Salinity, Moffett Channel, Alt A, Year 50, Summer

Figure 6-59. Salinity, Steven Creek Downstream, Alt A, Year 50, Summer

Figure 6-60. Salinity, Stevens Creek Upstream, Alt A, Year 50, Summer

Figure 6-61. Salinity, Mountain View Slough Downstream, Alt A, Year 50, Summer

Figure 6-62. Salinity, Mountain View Slough Upstream, Alt A, Year 50, Summer

Figure 6-63. Salinity, Charleston Slough Downstream, Alt A, Year 50, Summer

Figure 6-64. Salinity, Charleston Slough Upstream, Alt A, Year 50, Summer

Figure 6-65. Salinity at Spring HHW, Alt A, Alviso, Year 50, Summer

Figure 6-66. Salinity at Spring LLW, Alt A, Alviso, Year 50, Summer

Figure 6-67. Salinity, Ravenswood Slough Downstream, Ravenswood, Alt A, Year 50, Summer

Figure 6-68. Salinity, Ravenswood Slough Upstream, Ravenswood, Alt A, Year 50, Summer

Figure 6-69. Salinity at Spring HHW, Ravenswood, Alt A, Year 50, Summer

Figure 6-70. Salinity at Spring LLW, Ravenswood, Alt A, Year 50, Summer

Figure 6-71. Velocity, San Mateo Bridge, Alt A, Year 50, Summer

Figure 6-72. Velocity, Dumbarton Bridge, Alt A, Year 50, Summer

Figure 6-73. Velocity, Channel Marker 17, Alt A, Year 50, Summer

Figure 6-74. Velocity at Spring Flood, Alt A, Year 50, Summer

Figure 6-75. Velocity at Spring Ebb, Alt A, Year 50, Summer

Figure 6-76. Velocity, ACFCC Downstream, Alt A, Year 50, Summer

Figure 6-77. Velocity, Old Alameda Creek Downstream, Alt A, Year 50, Summer

Figure 6-78. Velocity at Spring Flood, Eden Landing, Alt A, Year 50, Summer

Figure 6-79. Velocity at Spring Ebb, Eden Landing, Alt A, Year 50, Summer

Figure 6-80. Velocity, Coyote Creek Power Tower, Alt A, Year 50, Summer

Figure 6-81. Velocity, Coyote Creek Railroad Bridge, Alt A, Year 50, Summer

Figure 6-82. Velocity, Coyote Creek/Island Ponds, Year 50, Summer

Figure 6-83. Velocity, Mud Slough Downstream, Alt A, Year 50, Summer

Figure 6-84. Velocity, Alviso Slough Downstream, Alt A, Year 50, Summer

Figure 6-85. Velocity, Guadalupe Slough Downstream, Alt A, Year 50, Summer

Figure 6-86. Velocity, Moffett Channel, Alt A, Year 50, Summer

Figure 6-87. Velocity, Steven Creek Downstream, Alt A, Year 50, Summer

Figure 6-88. Velocity, Mountain View Slough Downstream, Alt A, Year 50, Summer

Figure 6-89. Velocity, Charleston Slough Downstream, Alt A, Year 50, Summer

Figure 6-90. Velocity at Spring Flood, Alviso, Alt A, Year 50, Summer

Figure 6-91. Velocity at Spring Ebb, Alviso, Alt A, Year 50, Summer

Figure 6-92. Velocity, Ravenswood Slough Downstream, Alt A, Year 50, Summer

Figure 6-93. Velocity at Spring Flood, Ravenswood, Alt A, Year 50, Summer

Figure 6-94. Velocity at Spring Ebb, Ravenswood, Alt A, Year 50, Summer

Figure 6-95. South Bay Residual Circulation, Baseline, Summer

Figure 6-96. South Bay Residual Circulation, Alt A, Year 50, Summer

Figure 6-97. South Bay Residual Circulation, Difference, Year 50, Summer

Figure 6-98. Far South Bay Residual Circulation, Baseline, Summer

Figure 6-99. Far South Bay Residual Circulation, Alt A, Year 50, Summer

Figure 6-100. Far South Bay Residual Circulation, Difference, Year 50, Summer

Figure 6-101. Tidal Bed Shear Stress, South Bay, Alt A, Year 50, Summer

Figure 6-102. Tidal Bed Shear Stress, Eden Landing, Alt A, Year 50, Summer

Figure 6-103. Tidal Bed Shear Stress, Alviso, Alt A, Year 50, Summer

Figure 6-104. Tidal Bed Shear Stress, Ravenswood, Alt A, Year 50, Summer

Figure 6-105. Total Bed Shear Stress, South Bay, Alt A, Year 50, Summer

Figure 6-106. Total Bed Shear Stress, Eden Landing, Alt A, Year 50, Summer

Figure 6-107. Total Bed Shear Stress, Alviso, Alt A, Year 50, Summer

Figure 6-108. Total Bed Shear Stress, Ravenswood, Alt A, Year 50, Summer

7. ALTERNATIVE C, YEAR 50, SUMMER CONDITIONS

This section presents the results of the Alternative C, year 50, simulation under summer conditions, including a comparison with baseline summer conditions, where baseline represents present conditions, not the Alternative C, year 0 conditions presented in Section 4. The analysis presented utilizes the same approach presented in Section 4 for ease of comparison between simulations. The model predictions are analyzed using time series at stations throughout the South Bay. Figure 4-1 through Figure 4-4 show the station locations for the South Bay and the three pond complexes. The model predictions are also analyzed at specific snapshots in time for the entire South Bay and the pond complexes. Figure 4-5 shows where in the analysis period the snapshots were taken with respect to the spring-neap tidal cycle. The sections below present the results with respect to water levels, tidal prism, salinity, circulation and bed shear stress.

7.1 Water Levels

This section presents the model results with respect to water levels in the South Bay and the tidal sloughs under Alternative C, year 50, summer conditions (a.k.a. Alternative C, long-term conditions). The model predictions are compared to baseline summer predictions in order to assess the long-term impacts associated with opening 90 percent of the ponds to tidal action.

7.1.1 South Bay

Table 7-1 shows the water surface elevation and phase difference for the South Bay under Alternative C, long-term, summer conditions. Positive values in Table 7-1 represent an increase in water surface elevation when compared with baseline conditions, and negative values represent a decrease in water surface elevation. Positive phase values correspond to a slower arrival time under Alternative C, long-term conditions, or a phase lag when compared with baseline conditions, whereas negative values represent that modeled water levels under Alternative C are leading baseline conditions.

In the South Bay, the modeled water levels at the San Mateo Bridge increase on all phases of the daily tidal cycle relative to baseline conditions, and the increase is largely representative of the modeled rate of sea-level rise of 15 cm over 50 years (Figure 7-1). The change in water surface elevation is greatest at LLW when the water surface increases approximately 20 cm. Compared with Alternative A, long-term conditions (Figure 6-1), the water surface elevation is approximately 1 cm higher under Alternative C, long-term conditions for much of the diurnal tidal cycle, and approximately 3 cm higher at LLW.

At the Dumbarton Bridge (Figure 7-2), the water level increase under Alternative C, long-term conditions, when compared with baseline conditions, is approximately equal to sea-level rise throughout the analysis period with the exception of LLW during spring tide. Water levels decrease by approximately 25 to 30 cm at LLW during spring tide conditions. The Dumbarton Bridge station is located on the eastern edge of the main South Bay channel, and this station is completely dry when the water surface elevation drops below approximately -0.4 m NAVD88 under baseline conditions. At year 50, scour is predicted to occur along the edges of the main South Bay channel; therefore the water level at LLW is no longer

constrained by the bed elevation. The change in water surface elevation at the Dumbarton Bridge is slightly lower (-1 cm) than that predicted under Alternative A long-term conditions at low water, with slightly higher water levels (+ 2 cm) predicted at HHW under neap tide conditions.

At Channel Marker 17 (Figure 7-3), located near the mouth of Coyote Creek, water levels increase on all phases of the tide when compared with baseline conditions. The increases at HHW are of similar magnitude to the rate of sea-level rise; however, the tidal restoration under Alternative C tempers the water level increase. In other words, the increase in HHW could be larger in the absence of the tidal restoration. The increase in HHW water surface elevations is slightly higher (+ 2 to 3 cm) under Alternative C, long-term conditions than predicted under Alternative A, long-term conditions. LLW increases by approximately 20 cm under neap tide and 25 cm under spring tide conditions in response to sea-level rise, the increase in tidal prism associated with the tidal restoration in the Alviso pond complex, and the erosion of the intertidal mudflats predicted to occur in the far South Bay.

The long-term trend in increased water levels leads to an increase in the MLLW and MHHW tidal datums. Table 7-2 presents the increase in MLLW and MHHW tidal datums relative to baseline conditions for both Alternative C and Alternative A, long-term conditions. Figure 7-4 depicts the change in MLLW at year 50. The increase in MLLW is most pronounced in the far South Bay where MLLW increases approximately 18 – 19 cm. This trend is similar to that observed under Alternative A, long-term conditions; however, the increase in MLLW in the far South Bay is approximately 1 cm greater under Alternative C. Conversely, the increase in MHHW is approximately 1 cm less under Alternative C, long-term conditions than predicted under Alternative A. MHHW increases by approximately 15 cm throughout most of the South Bay (Figure 7-5), with a slightly smaller increase on the order of 12 cm occurring in the far South Bay.

Harmonic analysis was performed on water levels at several stations along the main South Bay channel, and the computed phase and amplitudes of the M_2 and K_1 tidal constituents for baseline and Alternative C year 50 conditions are compared in order to assess how the alternative is affecting tidal propagation within the South Bay (Figure 7-6). Figure 7-6a presents the computed phase of the M_2 and K_1 tidal constituents. There is a small reduction in phase relative to baseline conditions for both tidal constituents under Alternative C, year 50 conditions. Figure 7-6b presents the computed amplitude of the M_2 and K_1 tidal constituents. As the tides propagate into the South Bay, the amplitude of both tidal constituents is decreased, with a more marked difference observed in the M_2 tidal constituent in the far South Bay. This difference is smaller than observed under Alternative C, year 0 conditions (Figure 4-11).

Table 7-1. South Bay Water Surface Elevation and Phase Differences under Alt C, Year 50, Summer
(Water surface elevation differences in cm, phase differences in minutes. June 13 = neap tide, June 22 = spring tide.)

Station Name	June 13 LLW		June 13 HHW		June 22 LLW		June 22 HHW	
	WSE	Phase	WSE	Phase	WSE	Phase	WSE	Phase
San Mateo Bridge, Figure 7-1	16	0	15	0	20	0	15	0
Dumbarton Bridge, Figure 7-2	16	10	14	0	-26	-30	14	0
Channel Marker 17, Figure 7-3	19	30	14	0	26	10	13	0

Table 7-2. South Bay Tidal Datums Differences under Alt C, Year 50, Summer and Alt A, Year 50, Summer

(All differences are increases relative to baseline conditions in cm)

South Bay Station	Alternative A, year 50		Alternative C, year 50	
	MLLW	MHHW	MLLW	MHHW
Oakland-Bay Bridge	15.0	15.0	15.0	15.0
San Mateo Bridge	16.2	14.6	18.2	14.9
Dumbarton Bridge	18.1	13.7	17.9	14.0
Channel Marker 17	21.8	13.7	23.0	13.6

7.1.2 Tidal Sloughs

Under Alternative C, approximately 90 percent of the SBSP Restoration Project Area would be restored to tidal action, and over the 50-year horizon, the restored ponds are assumed to develop into mature salt marsh (see Section 3.4). The ponds restored to tidal marsh are shown in Figure 3-7, Figure 3-8 and Figure 3-9 for each pond complex. In response to the increase in tidal prism associated with this conversion, the tidal sloughs are expected to scour and deepen as they approach equilibrium conditions, potentially lessening the tidal damping effect seen under the Alternative C, year 0 simulations in the absence of channel scour (Section 4). Table 3-7 presents the predicted increase in channel depth for the tidal sloughs located within the SBSP Restoration Project Area. The tidal sloughs outside of the project area are assumed to retain their existing bathymetry.

Table 7-3 presents the water surface elevation and phase difference under Alternative C long-term conditions at both upstream and downstream stations in each tidal slough. Positive water surface elevation values in Table 7-3 represent an increase in water level when compared with baseline conditions, and negative values represent a decrease in water level. Positive phase values correspond to a slower arrival time under Alternative C, or a phase lag when compared with baseline conditions, whereas negative values represent that modeled water levels under Alternative C are leading baseline conditions.

The sloughs that are predicted to have the greatest channel scour (downstream in ACFCC, Old Alameda Creek, Charleston Slough, Mountain View Slough, Stevens Creek and Ravenswood Slough) all exhibit an increase in tidal range – low water levels decrease and high water levels increase under Alternative C, long-term conditions. In contrast, under Alternative C, year 0 conditions where no channel scour was assumed, tidal damping was predicted in these sloughs. In the sloughs predicted to have a lesser amount

of channel scour (upstream in ACFCC, Coyote Creek, downstream in Alviso and Guadalupe Sloughs, and Mud Slough), water levels increase on all phases of the tide – low water levels and high water levels increase, with the increase in low water levels greater than the increase in high water levels.

Upstream in Alviso Slough (Figure 7-18), Guadalupe Slough (Figure 7-20) and the Moffett Channel (Figure 7-21), tidal damping is predicted – low water levels increase and high water levels decrease. Compared with the year 0 simulation (Section 4), the increase in low water levels under long-term conditions is approximately half that predicted at year 0, and the increase in high water levels is approximately one-half to three-quarters of the year 0 prediction. In general for all tidal sloughs, the increase in high water levels is less than the predicted rate of sea-level rise of 15 cm, and the increase is smaller than that predicted for Alternative A, long-term conditions.

Phasing changes are relatively small in most tidal sloughs, with a phase lag on the order of 30 minutes throughout the SBSP Restoration Project Area. Larger phase changes are observed in the tidal sloughs predicted to have the most channel scour, such as ACFCC, Old Alameda Creek, Charleston Slough, Mountain View Slough, Stevens Creek and Ravenswood Slough. In these sloughs, the tide is predicted to arrive one to two hours faster at LLW, with less significant deviations associated with high water levels. However, as discussed in Section 2.3.5, with the exception of the ACFCC, the slough widths associated with these sloughs are oversized in the model due to grid resolution limitations; therefore, the faster arrival times and greater tidal range predicted for these sloughs may be overstated by the model results.

Table 7-3. Tidal Slough Water Surface Elevation and Phase Differences under Alt C, Year 50, Summer (Water surface elevation differences in cm, phase differences in minutes. June 13 = neap tide, June 22 = spring tide.)

Station Name	June 13 LLW		June 13 HHW		June 22 LLW		June 22 HHW	
	WSE	Phase	WSE	Phase	WSE	Phase	WSE	Phase
<i>Eden Landing pond complex</i>								
ACFCC Downstream, Figure 7-7	-33	-90	18	-10	-96	-80	12	10
ACFCC Upstream, Figure 7-8	-4	40	26	-40	7	-90	18	-10
Old Alameda Creek Downstream, Figure 7-9	-7	-60	13	30	-37	-40	12	40
Old Alameda Creek Upstream, Figure 7-10	-14	-60	13	30	-37	-40	12	40
<i>Alviso pond complex</i>								
Coyote Creek Power Tower, Figure 7-11	25	30	11	10	23	80	10	0
Coyote Creek Railroad Bridge, Figure 7-12	21	30	14	0	18	30	13	0
Coyote Creek/Island Ponds, Figure 7-13	21	20	12	10	17	20	11	0
Coyote Creek Upstream, Figure 7-14	22	30	11	10	18	20	8	0
Mud Slough Downstream, Figure 7-15	21	20	7	20	19	20	9	0
Mud Slough Upstream, Figure 7-16	25	20	8	30	24	20	7	0
Alviso Slough Downstream, Figure 7-17	25	30	8	10	36	30	6	10
Alviso Slough Upstream, Figure 7-18	38	80	-13	90	55	90	-19	80
Guadalupe Slough Downstream, Figure 7-19	23	30	13	0	36	30	13	0
Guadalupe Slough Upstream, Figure 7-20	37	40	-9	60	48	50	-11	50
Moffett Channel, Figure 7-21	37	50	-8	60	48	50	-11	50
Stevens Creek Downstream, Figure 7-22	-19	-70	13	10	-15	-50	11	10
Stevens Creek Upstream, Figure 7-23	-23	-90	12	10	-15	-60	10	10
Mountain View Slough Downstream, Figure 7-24	-30	-90	15	0	-33	-60	15	20
Mountain View Slough Upstream, Figure 7-25	-31	-110	15	0	-34	-70	15	20
Charleston Slough Downstream, Figure 7-26	-41	-100	22	-50	-63	-80	14	20
Charleston Slough Upstream, Figure 7-27	-45	-70	21	-60	-56	-50	13	20
<i>Ravenswood pond complex</i>								
Ravenswood Slough Downstream, Figure 7-28	-36	-100	15	10	-38	-60	12	20
Ravenswood Slough Upstream, Figure 7-29	-27	-90	14	0	-30	-50	14	10

7.2 Tidal Prism

A comparison of the estimates of modeled tidal prism between baseline and Alternative C, year 50, summer conditions is summarized in Table 7-4. As discussed in Section 4.2, tidal prism has been estimated as the volume of water crossing a cross-section during a flood tide for the basis of comparing tidal prism estimates with previous studies.

Under Alternative C, long-term conditions, the modeled tidal prism at the San Mateo and Dumbarton Bridge cross-sections is predicted to increase approximately ten to fifteen percent. This increase results from the increase in tidal prism from the tidally-restored ponds and the mudflat erosion predicted to occur in the South Bay (see Section 3.4.3). Figure 7-30 presents the modeled flux of water across both bridge cross-sections under baseline and Alternative C, long-term conditions, and the relative increase and decrease in tidal prism are evident. Within the far South Bay, the tidal prism and the associated modeled flux of water relative to baseline conditions increases, as shown on Figure 7-31. At Calaveras Point, the modeled tidal prism increases approximately 36 percent (Table 7-4).

Within the Eden Landing pond complex, tidal prism is predicted to increase approximately 130 to 250 percent as a result of Alternative C, long-term conditions. This tidal prism increase is associated with the slough scour in response to the tidal restoration (see Section 3.4.2), and the establishment of a mature marsh channel network within the tidally-restored ponds. Although the depth of scour matches the hydraulic geometry estimates, the tidal sloughs in the Eden Landing pond complex are oversized in the model due to the grid resolution limitations discussed in Section 2.3.5; therefore, the volume of scour may be over-estimated in the model. The oversized nature of the sloughs, coupled with an overestimation of the volume of potential slough scour, leads to an over-estimation of the potential long-term increase in tidal prism. Although the magnitudes of tidal prism increase are probably overstated in the Eden Landing pond complex, the trend of increasing tidal prism is consistent with the addition of intertidal area. This trend in increasing tidal prism is also evident in the comparisons of the modeled flux of water under baseline and Alternative C, long-term conditions near the slough mouths of the ACFCC and Old Alameda Creek (Figure 7-32).

All tidal sloughs within the Alviso pond complex are predicted to experience an increase in tidal prism under Alternative C, long-term conditions. The magnitude of the potential increase for a particular slough depends upon the number of tidally-restored ponds along the slough, the location of the slough within the pond complex, and the slough's existing conveyance capacity. Cross-sections in the upper reaches of Coyote Creek, such as at the Railroad Bridge and east of the Island Ponds, exhibit a moderate increase in tidal prism (Figure 7-33). Under Alternative C, year 0 conditions, the tidal prism was predicted to decrease at these cross sections (Section 4.2). However, under Alternative C, long-term conditions, the Island Ponds are assumed to develop into mature salt marsh over the 50-year horizon, therefore water previously captured by the Island Ponds under year 0 conditions can propagate into the upper reaches of Coyote Creek under long-term conditions.

Mud Slough, a tributary of Coyote Creek, exhibits a tidal prism increase of approximately 60 percent under Alternative C, long-term conditions. This increase is associated with the tidal restoration of Ponds A22 and A23 at the upper end of Mud Slough, the development of mature salt marsh within the Island Ponds and sea-level rise.

The remaining sloughs in the Alviso pond complex exhibit increases in tidal prism associated with the development of mature marsh channel networks within the tidally-restored ponds, the sloughs' existing conveyance capacity, estimate of long-term channel scour and sea-level rise. For example, the tidal prism in Guadalupe Slough is predicted to be 62 percent under Alternative C, year 50. Under Alternative C,

year 0 conditions, the tidal prism within Guadalupe Slough is predicted to increase by approximately 160 percent (Table 4-4). The lesser increase under long-term conditions occurs because the tidally-restored ponds develop into mature salt marsh, reducing the volume of added tidal prism associated with the ponds. The tidal prism of Alviso Slough and Artesian Slough evolve similarly with time. Figure 7-34 presents the modeled flux of water near the mouths of Guadalupe and Alviso Sloughs under baseline and Alternative C, long-term conditions. The lesser tidal prism increase than that associated with year 0 conditions is evident upon visual inspection of Figure 7-34 and Figure 4-49, which presents the same results for Alternative C, year 0 conditions.

In contrast, the long-term tidal prism associated with Stevens Creek, Mountain View Slough and Charleston Slough is predicted to increase from year 0 to year 50. These sloughs are oversized in the model, as discussed in Section 2.3.5, therefore the relative increase in tidal prism associated with the predicted increase in channel scour is likely overstated in the model results. The sloughs also experience increases in tidal prism associated with sea-level rise. The predicted tidal prism increase in Ravenswood Slough in the Ravenswood pond complex is likely overstated as well for the same reasons. Although the predicted increases in tidal prism within these sloughs are likely overstated, the general trend of increasing tidal prism is expected. The comparison of modeled flux between baseline and Alternative C, long-term conditions at the mouth of Stevens Creek and Mountain View Slough (Figure 7-35) and Charleston and Ravenswood Sloughs (Figure 7-36) is likely also overstated due to the oversized representation of the sloughs in the model and the associated overestimation of the volume of slough scour.

Non-project sloughs north of the Dumbarton, i.e. Corkscrew Slough, Redwood Creek, and Westpoint Slough exhibit tidal prism increases on the order of 15 percent under Alternative C, long-term conditions. This increase is similar to that predicted for Alternative A, long-term conditions; therefore, this increase is likely largely associated with the predicted rate of sea-level rise.

The non-project sloughs in the far South Bay, i.e. Mowry Slough, Plummer Slough and Newark Slough, exhibit larger increases in tidal prism relative to baseline conditions than predicted for Alternative A, long-term conditions. This increase in tidal prism is therefore likely associated with sea-level rise and the mudflat erosion predicted to occur in the far South Bay. However, the slough mouths were eroded using the same routine applied to the far South Bay, therefore the predicted tidal prism increase is likely overstated. If these sloughs were subject to continued sedimentation over the 50-year horizon, the sloughs would experience a decrease in tidal prism.

Table 7-4. Comparison of Tidal Prism between Baseline and Alternative C, year 50, summer

Transect location	Tidal prism (millions of cubic meters)		
	Baseline summer	Alternative C yr 50, summer	% change baseline to Alt. C
<i>South Bay</i>			
San Mateo Bridge	270	290	9.2%
Dumbarton Bridge	71	80	14%
<i>Eden Landing pond complex</i>			
ACFCC	1.4	3.3	130%
Old Alameda Creek	1.4	4.5	220%
Mount Eden Creek	0.58	2.0	250%
<i>Ravenswood pond complex</i>			
Ravenswood Slough	0.53	2.2	310%
<i>Alviso pond complex</i>			
Calaveras Point	14	19	36%
Coyote Creek at Power Tower	6.8	10	48%
Coyote Creek at RR Bridge	2.2	2.3	1.8%
Coyote Creek east of Island Ponds	0.53	0.81	54%
Charleston Slough	0.55	0.94	73%
Mountain View Slough	0.21	0.85	300%
Stevens Creek	0.11	0.53	380%
Guadalupe Slough	1.1	1.8	62%
Alviso Slough	1.1	2.4	110%
Artesian Slough	0.48	0.63	30%
Mud Slough	0.79	1.3	59%
<i>Non-project Sloughs</i>			
Corkscrew Slough	3.4	3.9	12%
Redwood Creek	16	18	16%
Westpoint Slough	2.9	3.3	14%
Mowry Slough	0.41	0.60	47%
Plummer Slough	0.32	0.36	13%
Newark Slough	0.86	1.1	27%

7.3 Salinity

This section presents the model results with respect to salinity in the South Bay and the tidal sloughs under Alternative C, year 50, summer conditions. The model predictions are compared to baseline summer predictions in order to assess the impact of restoring 90 percent of the SBSP Restoration Project Area to tidal action on the South Bay and the tidal sloughs, as presented below.

7.3.1 South Bay

Under Alternative C, long-term conditions, little change is observed with respect to salinity north of the Dumbarton Bridge (Table 7-5). Positive values in Table 7-5 represent an increase in salinities relative to the baseline, and negative values represent a decrease in salinities relative to baseline conditions. At the San Mateo and Dumbarton Bridges, there is no significant difference in salinity when compared with

baseline conditions (Figure 7-37 and Figure 7-38, respectively). Higher salinity differences are observed at Channel Marker 17 (Figure 7-39), with salinity increases on the order of 3 – 5 ppt observed at LLW.

Figure 7-40 displays the salinities in the South Bay during spring tide conditions at HHW, representing peak salinity conditions during the analysis period. As can be seen, little difference in peak South Bay salinities occurs under summer conditions with respect to long-term, Alternative C conditions. The largest changes in salinity are confined to the tidal sloughs. Figure 7-41 displays South Bay salinities at LLW during spring tide conditions. At low water, the observed differences are higher downstream of the tidal sloughs and in the subtidal channels in the South Bay. The salinity in the tidal sloughs is higher under Alternative C, long-term conditions than baseline conditions; therefore, the water drawn into the Bay from the tidal sloughs on ebb tide is more saline.

Table 7-5. South Bay Salinity Differences under Alt C, Year 50, Summer
(Salinity differences in ppt. June 13 = neap tide, June 22 = spring tide.)

Station Name	June 13 LLW	June 13 HHW	June 22 LLW	June 22 HHW
San Mateo Bridge, Figure 7-37	-0.2	-0.1	-0.1	0.0
Dumbarton Bridge, Figure 7-38	0.0	-0.1	-0.1	-0.1
Channel Marker 17, Figure 7-39	3.0	0.1	4.4	0.4

7.3.2 Tidal Sloughs

Table 6-5 shows the salinity difference between Alternative C, long-term conditions and baseline conditions during neap and spring tide summer conditions. Positive values represent an increase in salinities relative to the baseline, and negative values represent a decrease in salinities relative to baseline conditions.

In the Eden Landing pond complex, salinities increase in the downstream reach of the ACFCC in response to the increased tidal exchange and mixing associated with the deeper channel and the increased tidal prism (Figure 7-42). At high water levels, only a moderate salinity increase of 0 – 2 ppt is observed; however, low water salinities increase up to 10 ppt. This increase in downstream salinities shifts the salinity gradient upstream, and salinities at the upstream station in ACFCC are 4 – 8 ppt higher throughout the analysis period (Figure 7-43). Salinities in Old Alameda Creek exhibit little change with respect to baseline salinities (Figure 7-44 and Figure 7-45). As discussed in the previous sections, the potential changes to the salinity regime in Old Alameda Creek is likely underestimated due to the oversized representation of Old Alameda Creek in the model. The salinity trends in the Eden Landing pond complex are similar to those observed under Alternative A, long-term conditions, although under Alternative C, long-term conditions, salinities downstream are approximately 2 ppt higher, and salinities upstream are approximately 2 ppt lower.

Figure 7-46 and Figure 7-47 present the peak salinities in the Eden Landing pond complex during spring HHW and LLW conditions, respectively. As can be seen, the largest salinity changes are observed in the ACFCC and in the South Bay directly downstream of the ACFCC.

In the Alviso pond complex, salinities increase both upstream and downstream in all tidal sloughs. At the Power Tower downstream in Coyote Creek, salinities increase approximately 5 ppt at LLW and less than 0.5 ppt at HHW on both spring and neap tide (Figure 7-48). Farther upstream in Coyote Creek, salinities increase approximately 3 – 5 ppt on all phases of the tide (Figure 7-49, Figure 7-50, and Figure 7-51). This increase in salinity is due to the increased tidal prism associated with restoring the Pond A9 system (Ponds A9 through A17), as well as the estimates of long-term bathymetric change. Moderate channel scour is predicted to occur in Coyote Creek (Table 3-7), therefore unlike Alternative A, long-term conditions, tidal exchange is not restricted due to continuing channel sedimentation.

Alviso Slough and Guadalupe Slough both experience salinity increases on the order of 4 – 10 ppt. At the downstream stations (Figure 7-54 and Figure 7-56, respectively), salinities at LLW increase 4 – 9 ppt, while salinities at HHW increase approximately 0 – 1 ppt. At the upstream stations, salinities increase across all phases of the tide (Figure 7-55 and Figure 7-57, respectively). Stevens Creek, Mountain View Slough, Charleston Slough and Ravenswood Slough exhibit slight increases in salinity on the order of 0 – 1.5 ppt. As discussed in the previous sections, these sloughs are represented in the model at approximately twice their physical width; therefore they are more hydraulically connected to the Bay in the model. This could result in an underestimation of the potential changes in the salinity regime in these sloughs.

Table 7-6. Tidal Slough Salinity Differences under Alt C, Year 50, Summer
(Salinity differences in ppt. June 13 = neap tide, June 22 = spring tide.)

Station Name	June 13 LLW	June 13 HHW	June 22 LLW	June 22 HHW
<i>Eden Landing pond complex</i>				
ACFCC Downstream, Figure 7-42	9.8	1.1	7.5	0.2
ACFCC Upstream, Figure 7-43	4.6	4.3	7.9	2.8
Old Alameda Creek Downstream, Figure 7-44	0.0	-0.2	0.0	0.0
Old Alameda Creek Upstream, Figure 7-45	-0.4	-0.5	-0.5	-0.5
<i>Alviso pond complex</i>				
Coyote Creek Power Tower, Figure 7-48	5.6	0.2	5.1	0.4
Coyote Creek Railroad Bridge, Figure 7-49	2.8	3.4	3.2	0.4
Coyote Creek/Island Ponds , Figure 7-50	2.7	5.2	3.7	7.3
Coyote Creek Upstream, Figure 7-51	2.4	2.4	3.9	3.8
Mud Slough Downstream, Figure 7-52	3.1	8.3	5.5	2.7
Mud Slough Upstream, Figure 7-53	2.8	3.1	4.6	4.5
Alviso Slough Downstream, Figure 7-54	7.2	0.7	8.9	0.6
Alviso Slough Upstream, Figure 7-55	5.1	5.8	7.1	8.4
Guadalupe Slough Downstream, Figure 7-56	4.4	0.6	5.9	0.9
Guadalupe Slough Upstream, Figure 7-57	6.2	8.1	7.6	10.9
Moffett Channel, Figure 7-58	5.6	6.4	7.0	8.8
Stevens Creek Downstream, Figure 7-59	0.4	0.1	1.1	1.3
Stevens Creek Upstream, Figure 7-60	1.3	1.0	1.0	1.0
Mountain View Slough Downstream, Figure 7-61	0.2	0.0	0.4	0.7
Mountain View Slough Upstream, Figure 7-62	0.6	0.4	0.7	0.7
Charleston Slough Downstream, Figure 7-63	0.1	0.1	0.3	0.3
Charleston Slough Upstream, Figure 7-64	0.2	0.1	0.0	0.2
<i>Ravenswood pond complex</i>				
Ravenswood Slough Downstream, Figure 7-67	-0.2	-0.2	-0.1	0.3
Ravenswood Slough Upstream, Figure 7-68	0.2	0.0	0.4	0.6

7.4 Circulation

As discussed previously, the most important factor influencing circulation patterns in South Bay is bathymetry (Cheng and Gartner 1985). At year 50, significant large-scale bathymetric change is assumed to have occurred under Alternative C. Mudflat erosion is assumed to have occurred in both the far South Bay and in the region between the San Mateo and Dumbarton Bridges, the tidally-restored ponds are assumed to have developed into mature salt marsh with corresponding marsh channel networks, and the tidal sloughs within the SBSP Restoration Project Area are assumed to have scoured in response to restoration efforts.

7.4.1 Current Velocity

South Bay

Table 7-7 shows the peak velocity magnitudes at the San Mateo and Dumbarton Bridge stations and Channel Marker 17 under baseline and Alternative C long-term conditions. Positive values indicate a higher modeled velocity under Alternative C, and negative values indicate a decrease in current velocity under Alternative C. At the San Mateo Bridge station, velocities increase approximately 0 – 10 cm/s on strong flood tides (Figure 7-71). At the Dumbarton Bridge station, velocities increase less than 10 cm/s on all phases of the tide. These velocity increases are in response to the tidal restoration, and the predicted estimates of mudflat erosion and sea-level rise.

At Channel Marker 17 (Figure 7-73), velocity magnitudes increase 5 – 15 cm/s on strong ebb tide and decrease 0 – 5 cm/s on weak ebb tide. The increase in velocities under Alternative C, long-term conditions is less than predicted under Alternative A, long-term conditions due to the predictions of mudflat erosion rather than mudflat accretion. A larger cross-sectional area is available to carry the ebbing flow due to the higher elevation of MLLW relative to the bathymetry.

Figure 7-74 and Figure 7-75 present velocity magnitudes within the South Bay under peak flood and peak ebb conditions under baseline and Alternative C long-term conditions, as well as the difference between the two model predictions. The differences are minor, and the greatest change occurs in the subtidal channels under ebb tide conditions.

Table 7-7. South Bay Peak Velocity Magnitude Comparisons: Alt C, Year 50, Summer vs. Baseline, Summer

(All velocities in cm/s)

Station Name	Baseline	Alt C	Difference
San Mateo Bridge, Figure 7-71	102	104	2
Dumbarton Bridge, Figure 7-72	34	37	3
Channel Marker 17, Figure 7-73	67	79	12

Tidal Sloughs

In the South Bay, modeled velocities within the tidal sloughs experience significant changes in response to the restoration, estimates of large-scale bathymetric change, and sea-level rise. Table 7-8 shows the peak velocity magnitudes at the downstream stations in the tidal sloughs under baseline and Alternative C, long-term conditions. Positive values indicate a higher modeled velocity under Alternative C, and negative values indicate a decrease in current velocity under Alternative C.

In the Eden Landing pond complex, velocity magnitudes in both the ACFCC and Old Alameda Creek increase on all phases of the tide. In the ACFCC, the velocity magnitude increase on ebb and flood tides is similar (Figure 7-76). In Old Alameda Creek, the velocity magnitude increase is largest on strong ebb tide under spring tide conditions (Figure 7-77). Figure 7-78 and Figure 7-79 depict the tidal slough velocity magnitudes within the Eden Landing pond complex at both strong flood and strong ebb, respectively. At strong flood, the largest velocity magnitude differences relative to baseline conditions are

seen in the downstream reaches of the sloughs. At strong ebb, the largest differences are seen in the South Bay just beyond the slough mouth.

In the Alviso pond complex, velocity magnitudes increase in the Coyote Creek/Mud Slough region, with the exception of the Coyote Creek Railroad Bridge station (Figure 7-81). A portion of the tidal prism in this region under baseline conditions is captured by the tidally-restored ponds along Alviso Slough and the Pond A9 system (Ponds A9 through A 17) under Alternative C long-term conditions. Channel scour is also predicted to occur in Coyote Creek under Alternative C, long-term conditions, compared with continued sedimentation under Alternative A, long-term conditions, and therefore the cross-sectional area under Alternative C is larger, leading to the potential for a velocity decrease.

Velocity magnitudes increase in both Alviso Slough (Figure 7-84) and Guadalupe Slough (Figure 7-85), with a larger increase predicted in Alviso Slough due to the larger increase in tidal prism. In Stevens Creek (Figure 7-87), Mountain View Slough (Figure 7-88) and Charleston Slough (Figure 7-89), velocity magnitudes exhibit lesser differences when compared with baseline conditions. These sloughs are predicted to scour in response to the tidal restoration (see Table 3-6 and Table 3-7 for the respective increases in tidal prism and channel depth), and the increase in channel cross-sectional area nearly compensates for the increase in tidal flows. However, under baseline conditions, the sloughs exhibit a higher degree of flood-ebb asymmetry (higher velocities on flood tide) than predicted under Alternative C long-term conditions.

Figure 7-90 and Figure 7-91 depict the tidal slough velocity magnitudes within the Alviso pond complex at both strong flood and strong ebb, respectively. As with the Eden Landing pond complex, the largest differences under strong ebb conditions are seen in the far South Bay just beyond the slough mouth. At strong flood, the largest velocity differences relative to baseline conditions are seen in the downstream reaches of the tidal sloughs.

In Ravenswood Slough in the Ravenswood pond complex, velocities decrease 0 – 5 cm/s on flood tide, and increase 0 – 15 cm/s on ebb tide, decreasing some of the flood-ebb asymmetry observed under baseline conditions (Figure 7-92). Figure 7-93 and Figure 7-94 depict the tidal slough velocity magnitudes within the Ravenswood pond complex at both strong flood and strong ebb, respectively. As with the other pond complexes, the largest differences under strong ebb conditions are seen in the far South Bay just beyond the slough mouth. At strong flood, the largest velocity magnitude differences relative to baseline conditions are seen in the downstream reach of the slough.

Table 7-8. Tidal Slough Peak Velocity Magnitude Comparisons: Alt C, Year 50, Summer vs. Baseline, Summer

(All velocities in cm/s)

Station Name	Baseline	Alt C	Difference
ACFCC Downstream, Figure 7-76	45	66	21
Old Alameda Creek Downstream, Figure 7-77	53	91	38
Coyote Creek Power Tower, Figure 7-80	76	93	17
Coyote Creek Railroad Bridge, Figure 7-81	82	77	-5
Coyote Creek/Island Ponds, Figure 7-82	39	57	19
Mud Slough Downstream, Figure 7-83	46	67	22
Alviso Slough Downstream, Figure 7-84	49	76	27
Guadalupe Slough Downstream, Figure 7-85	46	53	7
Moffett Channel , Figure 7-86	5	2	-2
Stevens Creek Downstream, Figure 7-87	51	49	-3
Mountain View Slough Downstream, Figure 7-88	49	58	9
Charleston Slough Downstream, Figure 7-89	77	76	-1
Ravenswood Slough Downstream, Figure 7-92	38	35	-3

7.4.2 Residual Circulation

The total residual current observed in the South Bay is a product of tidally-driven residual currents, as well as wind-driven and density-driven circulation patterns. The long-term conditions under Alternative C, including large-scale tidal restoration, bathymetric change and sea-level rise, have the potential to alter residual circulation patterns within the South Bay.

Figure 7-95 displays the 29-day residual circulation under summer baseline conditions. Figure 7-96 displays the 29-day residual circulation for long-term, Alternative C conditions, and Figure 7-97 displays the difference between the predicted residual circulation under baseline and Alternative C conditions (Alternative C, year 50 minus baseline). Little change is observed in the South Bay north of the Dumbarton Bridge.

More noticeable changes are observed in the far South Bay, south of the Dumbarton Bridge. Figure 7-98 displays the 29-day residual circulation under summer baseline conditions for the far South Bay, Figure 7-99 displays the same for long-term, Alternative C conditions, and Figure 7-100 displays the difference. The largest difference in residual circulation pattern is observed in the main South Bay subtidal channel near the mouth Coyote Creek. Under Alternative C, long-term conditions, there is a stronger net-northward residual current in the downstream reach of Coyote Creek, and there is a small increase in the net-northward flux through the Dumbarton Narrows.

7.5 Bed Shear Stress

Potential impacts to sediment erosion and deposition patterns are inferred based on comparisons of total bed shear stress both before and after tidal restoration, where total bed shear stress is a function of both tidal currents and locally-generated wind-waves. Section 4.5 provides a description of the methodology used to generate and compare the total combined wind- and tidally-induced bed shear stress.

7.5.1 South Bay

The changes in water levels and tidal datums associated with sea-level rise and large-scale bathymetric change result in minor decreases in tidally-induced bed shear stresses in the shallow regions of the South Bay, including the eastern and western shoals. The increase in tidal prism and tidal flows also leads to slight increases in the tidally-induced bed shear stress in the subtidal areas and in the main South Bay channel (Figure 7-101). The difference map shown on Figure 7-101 depicts red regions where the erosive potential increases (bed shear stresses are higher under Alternative C long-term conditions relative to baseline conditions), and the areas depicted in blue correspond to regions with a potential for increased deposition. However, the red and blue areas are for illustrative purposes only and do not predict erosion or deposition under Alternative C long-term conditions. The critical shear stresses for erosion are not well known within the South Bay, and they vary spatially and temporally depending on the sediment characteristics and level of compaction of the substrate. In addition, such an inference would assume that the erodibility of the bed remains constant over the 50-year horizon. The benthic community strongly affects erodibility and the benthic community is likely to change in the next 50 years, therefore an assumption of constant erodibility would be poor.

When the combined wind-wave- and tidally-induced shear stress is considered in the South Bay, additional changes become apparent. MLLW and MHHW are higher under Alternative C long-term conditions (Figure 7-4 and Figure 7-5, respectively). Because wind-wave-driven bed shear stress is a function of water depth, and the erosive potential decreases with increasing water depth, the reduction in tidal amplitude leads to additional reductions in the total bed shear stress in the shallow areas of the South Bay (Figure 7-105), including the shallows in the far South Bay (Figure 7-107) and the eastern and western shoals north of the Dumbarton Bridge (Figure 7-108 and Figure 7-106, respectively).

7.5.2 Tidal Sloughs

Within and adjacent to the Eden Landing pond complex (Figure 7-102), the maximum tidally-induced bed shear stress is increased downstream of tidal breaches, corresponding to the increased tidal prism, and decreased upstream of the tidal breaches because a portion of the flow upstream in the tidal slough under baseline conditions is captured within the tidally-restored ponds under restored conditions. Within and adjacent to the Alviso pond complex (Figure 7-103) and the Ravenswood pond complex (Figure 7-104), the dynamic is similar to that observed in the Eden Landing pond complex. Tidally-induced bed shear stresses increase downstream of tidal breaches and decrease upstream of tidal breaches.

The primary effect of the combined wind-wave- and tidally-induced shear stress is evident in the South Bay rather than in the tidal sloughs as wind-induced waves require sufficient fetch to develop.

Figure 7-1. Water Levels, San Mateo Bridge, Alt C, Year 50, Summer

Figure 7-2. Water Levels, Dumbarton Bridge, Alt C, Year 50, Summer

Figure 7-3. Water Levels, Channel Marker 17, Alt C, Year 50, Summer

Figure 7-4. Changes in MLLW, Alt C, Year 50, Summer

Figure 7-5. Changes in MHHW, Alt C, Year 50, Summer

Figure 7-6. Changes in Tidal Propagation, Alt C, Year 50, Summer

Figure 7-7. Water Levels, ACFCC Downstream, Alt C, Year 50, Summer

Figure 7-8. Water Levels, ACFCC Upstream, Alt C, Year 50, Summer

Figure 7-9. Water Levels, Old Alameda Creek Downstream, Alt C, Year 50, Summer

Figure 7-10. Water Levels, Old Alameda Creek Upstream, Alt C, Year 50, Summer

Figure 7-11. Water Levels, Coyote Creek Power Tower, Alt C, Year 50, Summer

Figure 7-12. Water Levels, Coyote Creek Railroad Bridge, Alt C, Year 50, Summer

Figure 7-13. Water Levels, Coyote Creek/Island Ponds, Year 50, Summer

Figure 7-14. Water Levels, Coyote Creek Upstream, Year 50, Summer

Figure 7-15. Water Levels, Mud Slough Downstream, Alt C, Year 50, Summer

Figure 7-16. Water Levels, Mud Slough Upstream, Alt C, Year 50, Summer

Figure 7-17. Water Levels, Alviso Slough Downstream, Alt C, Year 50, Summer

Figure 7-18. Water Levels, Alviso Slough Upstream, Alt C, Year 50, Summer

Figure 7-19. Water Levels, Guadalupe Slough Downstream, Alt C, Year 50, Summer

Figure 7-20. Water Levels, Guadalupe Slough Upstream, Alt C, Year 50, Summer

Figure 7-21. Water Levels, Moffett Channel, Alt C, Year 50, Summer

Figure 7-22. Water Levels, Steven Creek Downstream, Alt C, Year 50, Summer

Figure 7-23. Water Levels, Stevens Creek Upstream, Alt C, Year 50, Summer

Figure 7-24. Water Levels, Mountain View Slough Downstream, Alt C, Year 50, Summer

Figure 7-25. Water Levels, Mountain View Slough Upstream, Alt C, Year 50, Summer

Figure 7-26. Water Levels, Charleston Slough Downstream, Alt C, Year 50, Summer

Figure 7-27. Water Levels, Charleston Slough Upstream, Alt C, Year 50, Summer

Figure 7-28. Water Levels, Ravenswood Slough Downstream, Alt C, Year 50, Summer

Figure 7-29. Water Levels, Ravenswood Slough Upstream, Alt C, Year 50, Summer

Figure 7-30. Tidal Prism, San Mateo and Dumbarton Bridges, Alt C, Year 50, Summer

Figure 7-31. Tidal Prism, Channel Marker 17 and Calaveras Point, Alt C, Year 50, Summer

Figure 7-32. Tidal Prism, ACFCC and Old Alameda Creek, Alt C, Year 50, Summer

Figure 7-33. Tidal Prism, Coyote Creek, Alt C, Year 50, Summer

Figure 7-34. Tidal Prism, Alviso and Guadalupe Sloughs, Alt C, Year 50, Summer

Figure 7-35. Tidal Prism, Stevens Creek and, Mountain View Sloughs, Alt C, Year50, Summer

Figure 7-36. Tidal Prism, Charleston and Ravenswood Sloughs, Alt C, Year 50, Summer

Figure 7-37. Salinity, San Mateo Bridge, Alt C, Year 50, Summer

Figure 7-38. Salinity, Dumbarton Bridge, Alt C, Year 50, Summer

Figure 7-39. Salinity, Channel Marker 17, Alt C, Year 50, Summer

Figure 7-40. Salinity at Spring HHW, Alt C, Year 50, Summer

Figure 7-41. Salinity at Spring LLW, Alt C, Year 50, Summer

Figure 7-42. Salinity, ACFCC Downstream, Alt C, Year 50, Summer

Figure 7-43. Salinity, ACFCC Upstream, Alt C, Year 50, Summer

Figure 7-44. Salinity, Old Alameda Creek Downstream, Alt C, Year 50, Summer

Figure 7-45. Salinity, Old Alameda Creek Upstream, Alt C, Year 50, Summer

Figure 7-46. Salinity at Spring HHW, Eden Landing, Alt C, Year 50, Summer

Figure 7-47. Salinity at Spring LLW, Eden Landing, Alt C, Year 50, Summer

Figure 7-48. Salinity, Coyote Creek Power Tower, Alt C, Year 50, Summer

Figure 7-49. Salinity, Coyote Creek Railroad Bridge, Alt C, Year 50, Summer

Figure 7-50. Salinity, Coyote Creek/Island Ponds, Year 50, Summer

Figure 7-51. Salinity, Coyote Creek Upstream, Year 50, Summer

Figure 7-52. Salinity, Mud Slough Downstream, Alt C, Year 50, Summer

Figure 7-53. Salinity, Mud Slough Upstream, Alt C, Year 50, Summer

Figure 7-54. Salinity, Alviso Slough Downstream, Alt C, Year 50, Summer

Figure 7-55. Salinity, Alviso Slough Upstream, Alt C, Year 50, Summer

Figure 7-56. Salinity, Guadalupe Slough Downstream, Alt C, Year 50, Summer

Figure 7-57. Salinity, Guadalupe Slough Upstream, Alt C, Year 50, Summer

Figure 7-58. Salinity, Moffett Channel, Alt C, Year 50, Summer

Figure 7-59. Salinity, Steven Creek Downstream, Alt C, Year 50, Summer

Figure 7-60. Salinity, Stevens Creek Upstream, Alt C, Year 50, Summer

Figure 7-61. Salinity, Mountain View Slough Downstream, Alt C, Year 50, Summer

Figure 7-62. Salinity, Mountain View Slough Upstream, Alt C, Year 50, Summer

Figure 7-63. Salinity, Charleston Slough Downstream, Alt C, Year 50, Summer

Figure 7-64. Salinity, Charleston Slough Upstream, Alt C, Year 50, Summer

Figure 7-65. Salinity at Spring HHW, Alt C, Alviso, Year 50, Summer

Figure 7-66. Salinity at Spring LLW, Alt C, Alviso, Year 50, Summer

Figure 7-67. Salinity, Ravenswood Slough Downstream, Ravenswood, Alt C, Year 50, Summer

Figure 7-68. Salinity, Ravenswood Slough Upstream, Ravenswood, Alt C, Year 50, Summer

Figure 7-69. Salinity at Spring HHW, Ravenswood, Alt C, Year 50, Summer

Figure 7-70. Salinity at Spring LLW, Ravenswood, Alt C, Year 50, Summer

Figure 7-71. Velocity, San Mateo Bridge, Alt C, Year 50, Summer

Figure 7-72. Velocity, Dumbarton Bridge, Alt C, Year 50, Summer

Figure 7-73. Velocity, Channel Marker 17, Alt C, Year 50, Summer

Figure 7-74. Velocity at Spring Flood, Alt C, Year 50, Summer

Figure 7-75. Velocity at Spring Ebb, Alt C, Year 50, Summer

Figure 7-76. Velocity, ACFCC Downstream, Alt C, Year 50, Summer

Figure 7-77. Velocity, Old Alameda Creek Downstream, Alt C, Year 50, Summer

Figure 7-78. Velocity at Spring Flood, Eden Landing, Alt C, Year 50, Summer

Figure 7-79. Velocity at Spring Ebb, Eden Landing, Alt C, Year 50, Summer

Figure 7-80. Velocity, Coyote Creek Power Tower, Alt C, Year 50, Summer

Figure 7-81. Velocity, Coyote Creek Railroad Bridge, Alt C, Year 50, Summer

Figure 7-82. Velocity, Coyote Creek/Island Ponds, Year 50, Summer

Figure 7-83. Velocity, Mud Slough Downstream, Alt C, Year 50, Summer

Figure 7-84. Velocity, Alviso Slough Downstream, Alt C, Year 50, Summer

Figure 7-85. Velocity, Guadalupe Slough Downstream, Alt C, Year 50, Summer

Figure 7-86. Velocity, Moffett Channel, Alt C, Year 50, Summer

Figure 7-87. Velocity, Steven Creek Downstream, Alt C, Year 50, Summer

Figure 7-88. Velocity, Mountain View Slough Downstream, Alt C, Year 50, Summer

Figure 7-89. Velocity, Charleston Slough Downstream, Alt C, Year 50, Summer

Figure 7-90. Velocity at Spring Flood, Alviso, Alt C, Year 50, Summer

Figure 7-91. Velocity at Spring Ebb, Alviso, Alt C, Year 50, Summer

Figure 7-92. Velocity, Ravenswood Slough Downstream, Alt C, Year 50, Summer

Figure 7-93. Velocity at Spring Flood, Ravenswood, Alt C, Year 50, Summer

Figure 7-94. Velocity at Spring Ebb, Ravenswood, Alt C, Year 50, Summer

Figure 7-95. South Bay Residual Circulation, Baseline, Summer

Figure 7-96. South Bay Residual Circulation, Alt C, Year 50, Summer

Figure 7-97. South Bay Residual Circulation, Difference, Year 50, Summer

Figure 7-98. Far South Bay Residual Circulation, Baseline, Summer

Figure 7-99. Far South Bay Residual Circulation, Alt C, Year 50, Summer

Figure 7-100. Far South Bay Residual Circulation, Difference, Summer

Figure 7-101. Tidal Bed Shear Stress, South Bay, Alt C, Year 50, Summer

Figure 7-102. Tidal Bed Shear Stress, Eden Landing, Alt C, Year 50, Summer

Figure 7-103. Tidal Bed Shear Stress, Alviso, Alt C, Year 50, Summer

Figure 7-104. Tidal Bed Shear Stress, Ravenswood, Alt C, Year 50, Summer

Figure 7-105. Total Bed Shear Stress, South Bay, Alt C, Year 50, Summer

Figure 7-106. Total Bed Shear Stress, Eden Landing, Alt C, Year 50, Summer

Figure 7-107. Total Bed Shear Stress, Alviso, Alt C, Year 50, Summer

Figure 7-108. Total Bed Shear Stress, Ravenswood, Alt C, Year 50, Summer

8. REFERENCES

- Barnard P, Lescinski J, Hanes D, Eshleman J, Lesser GR. in press. Toward a validated 2-D hydrodynamic model for the mouth of San Francisco Bay. U.S.G.S. Open-File Report. 40 pp p.
- Booij N, Ris R, Holthuijsen L. 1999. A third-generation wave model for coastal regions, 1. Model description and validation. *Journal of Geophysical Research - Oceans* 104(C4):7649-7666.
- California Department of Fish and Game. 2005. 2004 Self-Monitoring Report Baumberg Complex. Order No. R2-2004-0018, WDID No. 2 019438001. Hayward, CA.
- Cheng R, Casulli V. 1982. On lagrangian residual currents with applications in South San Francisco Bay, California. *Water Resources Research* 18(6):1652-1662.
- Cheng RT, Casulli V, Gartner JW. 1993. Tidal, residual, intertidal mudflat (TRIM) model and its applications to San-Francisco Bay, California. *Estuarine, Coastal, and Shelf Science* 36(3):p235-280.
- Cheng RT, Gartner JW. 1985. Harmonic Analysis of tides and tidal Currents in South San Francisco Bay, California. *Estuarine, Coastal, and Shelf Science* 21:p57-74.
- Cloern J, Powell T, Huzzey L. 1989. Spatial and temporal variability in South San Francisco Bay (USA). 2. Temporal changes in salinity, suspended sediments, and phytoplankton biomass and productivity over tidal time scales. *Estuarine, Coastal and Shelf Science* 28(6):599-613.
- Fischer HB, List EJ, Koh RCY, Imberger J, Brooks NH. 1979. *Mixing Inland and Coastal Water*: Academic Press. 483 pp. p.
- Foxgrover AC, Higgins SA, Ingraca MK, Jaffe BE, Smith RE. 2004. Deposition, erosion, and bathymetric change in South San Francisco Bay: 1858-1983.: U.S. Geologic Survey Open-File Report 2004-1192. 25 p.
- Grant WD, Madsen OS. 1979. Combined wave and current interaction with a rough bottom. *Journal of Geophysical Research* 84(C4):1791-1808.
- Gross E. 1997. Numerical modeling of hydrodynamics and scalar transport in an estuary [PhD Thesis]. Stanford, CA: Stanford University. 331 p.
- Gross E, Schaaf & Wheeler. 2003a. Alviso Island Pond Breach Initial Stewardship Plan Study. South Bay Salt Ponds Initial Stewardship Plan, Draft Environmental Impact Report/Environmental Impact Statement, Technical Appendix K.: California Department of Fish and Game and U.S. Fish and Wildlife Service,.
- Gross ES, Schaaf & Wheeler. 2003b. South Bay Salt Ponds Initial Stewardship Plan: South San Francisco Bay Hydrodynamic Model Results Report. Prepared for Cargill Salt.
- IPCC. 2001. *Climate Change 2001: The Scientific Basis*. Contribution of Working Group I to the Third Assessment Report of the Intergovernmental Panel on Climate Change. Houghton JT, Y. Ding, D.J. Griggs, M. Noguer, P.J. van der Linden, X. Dai, K. Maskell, C.A. Johnson (eds.), editor. Cambridge: Cambridge University Press. 881 p.
- Jaffe BE, Foxgrover AC. 2006a. A History of intertidal flat area in South San Francisco Bay, California: 1858 to 2005. U.S. Geological Survey Open-File Report 2006-1262. 32 p.
- Jaffe BE, Foxgrover AC. 2006b. Sediment Deposition and Erosion in South San Francisco Bay, California from 1956 to 2005. U.S. Geological Survey Open-File Report 2006-1287. Report nr Open File Report. 24 p.
- Jaffe BE, Fregoso T. in progress. Bulk density of near-surface sediments of South San Francisco Bay, California. U.S. Geological Survey. Report nr Open File Report.
- Jones & Stokes. 2004a. Napa-Sonoma River Salt Marsh Restoration Project, Final Environmental Impact Report. Prepared for California State Coastal Conservancy, Oakland, CA, and California Department of Fish and Game, Napa, CA. Sacramento, CA.

- Jones & Stokes. 2004b. Napa-Sonoma River Salt Marsh Restoration Project, Final Environmental Impact Statement. Prepared for California State Coastal Conservancy, Oakland, CA, and California Department of Fish and Game, Napa, CA. Sacramento, CA.
- Kamman Hydrology and Engineering. 2004. Technical studies of the Giacomini Restoration Project. Point Reyes, CA: National Park Service, Point Reyes CA.
- Lucas L. 1997. A numerical investigation of coupled hydrodynamic and phytoplankton dynamics in shallow estuaries [PhD Thesis]. Stanford, CA: Stanford University.
- Madsen OS, Wikramanayake PN. 1991. Simple models for turbulent wave-current bottom boundary layer flow. Vicksburg, MS: U.S. Army Corps of Engineers Waterways Experiment Station. Report nr DRP-91-1. 150 p.
- Monsen NE, Cloem JE, Lucas LV. 2002. A comment on the use of flushing time, residence time, and age as transport time scales. *Limnol Oceanogr* 47(5):1545-1553.
- PWA. 2005. Modeling Methods and Strategy Report: Hydrodynamics, Coastal Flood and Fluvial Flood Analyses. San Francisco, CA.: Prepared for: California State Coastal Conservancy, U.S. Fish and Wildlife Service, California Department of Fish and Game.
- PWA. 2006a. Hydrodynamic Modeling Calibration Report. San Francisco, CA.: Prepared for: California State Coastal Conservancy, U.S. Fish and Wildlife Service, California Department of Fish and Game.
- PWA. 2006b. South Bay Geomorphic Assessment. San Francisco, CA.: Prepared for: California State Coastal Conservancy, U.S. Fish and Wildlife Service, California Department of Fish and Game.
- PWA, H. T. Harvey & Associates, EDAW, Brown and Caldwell. 2005. Hydrodynamics and Sediment Dynamics Existing Conditions Report. San Francisco, CA.: Prepared for: California State Coastal Conservancy, U.S. Fish and Wildlife Service, California Department of Fish and Game.
- PWA, H. T. Harvey & Associates, EDAW, Brown and Caldwell. 2006. Final Alternatives Report. San Francisco, CA.: Prepared for: California State Coastal Conservancy, U.S. Fish and Wildlife Service, California Department of Fish and Game.
- Schaaf & Wheeler. 2004. Alviso Slough Tidal Prism Enhancement Project Draft Technical Report. Santa Clara, California: Santa Clara Valley Water District.
- Schemel LE. 1995. Measurements of salinity, temperature, and tides in South San Francisco Bay, California, at Dumbarton Bridge: 1990-1993 water years. US Geological Survey. Report nr Open-File Report 98-650.
- Schoellhamer D. 1996. Factors affecting suspended-solids concentrations in South San Francisco Bay, California. *Journal of Geophysical Research - Oceans* 101(C5):12087-12095.
- Sheldon JE, Alber M. 2006. The calculation of estuarine turnover times using freshwater fraction and tidal prism models: A critical evaluation. *Estuaries and Coasts* 29(1):133-146.
- U.S. Army Corps of Engineers. 1984. Shore Protection Manual. Washington D.C. Vol.1 p.
- U.S. Fish and Wildlife Service. 2005. 2004 Annual Self-Monitoring Report for Alviso Ponds within South San Francisco Bay Low Salinity Salt Ponds. Alameda, Santa Clara, and San Mateo Counties. Order No. R2-2004-0018, WDID No. 2 019438007.
- U.S. Fish and Wildlife Service. 2006. 2005 Self Monitoring Program for Alviso Ponds Within South San Francisco Bay Low Salinity Ponds. Alameda, Santa Clara, & San Mateo Counties, California: California Regional Water Quality Control Board, San Francisco Bay Region. Report nr Order No. R2-2004-0018.
- U.S. Fish and Wildlife Service, California Department of Fish and Game, David J Powers & Associates, H. T. Harvey & Associates, Philip Williams & Associates L. 2004. Draft Environmental Impact Statement, Environmental Impact Report: Bair Island Restoration and Management Plan, Don Edwards San Francisco Bay National Wildlife Refuge, Bair Island Ecological Preserve. San Mateo, California.
- U.S. Fish and Wildlife Service, Santa Clara Valley Water District. 2006. Restoration and mitigation monitoring plan for the Island Ponds Restoration Project.

- van Rijn LC. 1993. Principles of Sediment Transport in Rivers, Estuaries, and Coastal Seas. The Netherlands: Aqua Publications.
- Walters RA, Cheng RT, Conomos TJ. 1985. Time scales of circulation and mixing processes of San Francisco Bay waters. *Hydrobiologia* 129: p13-36.
- Wilcock P, Iverson R. 2003. Prediction in Geomorphology. In: Wilcock P, Iverson, RM, editor. Prediction in Geomorphology. Washington D.C.: American Geophysical Union.
- Williams PB, Orr MK, Garrity NJ. 2002. Hydraulic geometry: A geomorphic design tool for tidal marsh channel evolution in wetland restoration projects. *Restoration Ecology* 10(3):577-590.
- WL | Delft Hydraulics. 2003. Delft3D-FLOW, Simulation of multi-dimensional hydrodynamic flows and transport phenomena, including sediments. Delft, NL.

<This page intentionally left blank>

9. LIST OF PREPARERS

The following Team members assisted in preparation of this document:

Kris May, PWA
Gaurav Misra, PWA
Matt Brennan, PWA
Don Danmeier, PWA
Nick Garrity, PWA
Julie Stephenson, PWA
Matt Wickland, PWA
Phil Williams, PWA
David Brew, PWA

Source files for this report are located at PWA:

\\orca\projects\1750_SBSP\Task03c_Hydrodynamic_Modeling\Modeling_Report\Final_Draft

<This page intentionally left blank>

10. APPENDIX A – MODEL CALIBRATION SUMMARY

This section provides a summary of the calibration and validation results for both the GSFb and South Bay Models. The details with respect to both models and the complete calibration and validation are documented in the Hydrodynamic Model Calibration Report (PWA 2006a)

10.1 GSFb Model Calibration and Validation Summary

Model calibration for the GSFb Model was conducted using data from 2001 and 1980. Water level and salinity calibration was conducted using data from 2001; calibration of current velocities was conducted using data collected during 1980. The model was validated for summer 2000 and winter 2004 conditions. During each period, water levels were analyzed through the use of time series comparisons, statistical correlations and harmonic analysis. Predicted salinity was compared to observed salinity at fixed stations and predicted salinity transects were compared to USGS monitoring data.

During the 2001 calibration period the predicted water levels from the GSFb Model shows very good agreement with observed water levels based on the time series comparisons, correlations and harmonic analysis at all four stations analyzed. Similarly, the predicted salinity at the Oakland-Bay Bridge shows good agreement with observed salinity; slightly higher than observed salinity is predicted at the San Mateo Bridge. The predicted salinity transects show good agreement with observed salinity for the nine days during the simulation period when observation data were available.

During the 1980 simulation period, predicted water levels show a similar level of agreement with observed water levels as shown during the calibration period. Current velocities were compared against observed velocities at eleven stations in the South Bay. The predicted current velocities show good agreement with observed current velocities in terms of speed, direction, spring-neap variability, and trends in current velocity between deeper and shallower stations.

The water level comparisons for the summer 2000 validation period show a similar level of agreement to that achieved for the calibration period. Limited salinity data is available for validation during the summer 2000 period. Based on the limited data available, the GSFb Model tends to slightly under predict salinity relative to observations in summer 2000.

During the 2004 period the correlation between predicted and observed water levels is slightly lower than during the other periods, but relatively good agreement between predicted phase and amplitude of the major harmonic constituents is still achieved. The GSFb Model slightly over predicts salinity at San Mateo Bridge during the analysis period but shows better agreement at Dumbarton Bridge and Channel Marker 17.

Since the GSFb Model is run for a period of two to three months prior to each analysis period to demonstrate that the salinity field is fully spun-up, it is possible to assess the capacity of the GSFb Model to predict longer-term salinity trends. In this regard, the 2001 period shows relatively constant salinity at

the Oakland-Bay Bridge and throughout the South Bay with only a very gradual increase in salinity during the simulation period. The GSFb Model predicts salinity exceptionally well during this period (Figure 10-1 through Figure 10-5). The 2000 simulation period begins with relatively fresh conditions in much of South Bay and salinity increases by more than 5 ppt in much of the South Bay during the simulation period. The GSFb Model captures some of this trend but tends to slightly under predict salinity by the end of the simulation period (Figure 10-6 through Figure 10-9). In contrast, during the 2004 simulation period the salinity in the South Bay starts relatively high and tends to become fresher as the simulation progresses (Figure 10-10 through Figure 10-14) as a result of flow events during the simulation period. Although the model tends to over predict salinity somewhat at the end of the simulation period, much of this freshening trend is captured in the predicted salinity. Given the limited grid resolution—particularly south of Dumbarton Bridge in the GSFb Model (Figure 2-2) with grid cell sizes ranging from 300 to 400 m in this region—the predicted salinity in the far South Bay compares reasonably well with observed salinities.

Overall the GSFb Model shows good agreement with observed water levels, salinity, and current velocities under the range of conditions simulated. In particular, the GSFb Model shows very good agreement with observed water levels near the Oakland-Bay Bridge which demonstrates that it provides a suitable boundary condition for the South Bay Model. The predicted salinity fields from the GSFb Model show reasonable agreement with observed salinity during most periods and can therefore provide a suitable initial salinity condition for the South Bay Model.

10.2 South Bay Model Calibration and Validation Summary

Model calibration for the South Bay Model was conducted using data from 2001 and 1980. Water level and salinity calibration was conducted using data from 2001; calibration of current velocities was conducted using data collected during 1980. The model was validated for summer 2000 and winter 2004 conditions. During each period, water levels were analyzed through the use of time series comparisons, statistical correlations and harmonic analysis. Predicted salinity was compared to observed salinity at fixed stations and predicted salinity transects were compared to USGS monitoring data. The 2001, 2000 and 2004 South Bay simulations span a period of six weeks, with two weeks for spin-up preceding each 29-day analysis period.

During the 2001 calibration period, the predicted water levels from the South Bay period show very good agreement with observed water levels at the Alameda, Redwood City, and Channel Marker 20 stations. At the Railroad Bridge station, the predicted tides tend to lag the observed tides somewhat and there is some damping of tidal amplitude, particularly near low water. Overall the predicted water levels from the South Bay show a similar to better agreement with predicted water levels from the GSFb Model for the same calibration period.

During the South Bay Model 1980 simulation period, predicted water levels show a similar level agreement with observed water levels as during the calibration period. Current velocities were compared against observed velocities at eleven stations in the South Bay. The predicted current velocities show good agreement with observed current velocities in terms of speed, direction, spring-neap variability, and

trends in current velocity between deeper and shallower stations. A similar level of agreement with observed current velocities was achieved in the South Bay Model to that achieved in the GSFb Model for the same period.

The water level comparisons for the South Bay Model during the summer 2000 validation period show a similar level of agreement to that achieved for the calibration period. Based on the limited salinity data available for validation during the summer 2000 period, the South Bay Model shows a similar tendency as the GSFb Model to slightly under predict salinity relative to observations during the summer 2000 analysis period. Much of this may result from the initial condition transferred from the GSFb Model.

During the 2004 period, the correlation between predicted and observed water levels in the South Bay Model is slightly lower than during the other periods, which is the same trend observed in the GSFb Model. Overall, relatively good agreement between predicted phase and amplitude of the major harmonic constituents is achieved. The 2004 validation period offered the most extensive available salinity data in the far South Bay of any of the simulated periods. In addition, two freshwater flow events during this period provide an opportunity to evaluate the model's response to varying flow conditions. Although some differences exist between predicted and observed salinity, overall, the South Bay Model salinity comparisons for the 2004 period (Figure 10-15 through Figure 10-22) demonstrate that the South Bay Model is predicting a reasonable salinity range, similar semi-diurnal variability, and a similar response to flow events in much of the far South Bay. Given the limitations in accurately predicting salinity using a 2D model, a reasonable level of agreement between observed and predicted salinities is achieved over the three different analysis periods.

Overall, the South Bay Model shows very similar results to the GSFb Model in much of the South Bay. However, the South Bay Model provides significantly higher grid resolution in the far South Bay and therefore allows for more accurate predictions in areas not well-resolved in the GSFb Model. As a result, the South Bay Model calibration and validation made use of data in the far South Bay for both water level and salinity comparisons which were not used in the GSFb Model comparisons. In general the South Bay Model agrees favorably with predicted water levels and salinity in the far South Bay. However, the comparisons of observed and predicted water levels at the Railroad Bridge in Coyote Creek highlight that some damping of tidal amplitude occurs in the far South Bay, particularly near low water. In particular, the solution scheme used in DELFT3D appears to result in energy dissipation in channels which are not aligned with the grid (i.e. "stair-step" channels) when the channel is only one cell wide. This effect is most dominant at low water when only a single row of channel cells are wet and can lead to an under prediction of tidal range in narrow sloughs with increasing distance from the Bay. The use of finer grid resolution for project-level modeling would allow for more grid resolution across slough channels and help to reduce this effect.

<This page intentionally left blank>

Figure 10-1. GSFb Summer 2001 Salinity, Pier 24/Bay Bridge

Figure 10-2. GSFb Summer 2001 Salinity, San Mateo Bridge

Figure 10-3. GSFb Summer 2001 Salinity Transect

Figure 10-4. GSFb Summer 2001 Salinity Transect

Figure 10-5. GSFb Summer 2001 Salinity Transect

Figure 10-6. GSFb Summer 2000 Salinity, Pier 24/Bay Bridge

Figure 10-7. GSFb Summer 2000 Salinity, San Mateo Bridge

Figure 10-8. GSFb Summer 2000 Salinity Transect

Figure 10-9. GSFb Summer 2000 Salinity Transect

Figure 10-10. GSFb Winter 2004 Salinity, San Mateo Bridge

Figure 10-11. GSFb Winter 2004 Salinity, Dumbarton Bridge

Figure 10-12. GSFb Winter 2004 Salinity, Channel Marker 17

Figure 10-13. GSFB Winter 2004 Salinity Transect

Figure 10-14. GSFB Winter 2004 Salinity Transect

Figure 10-15. South Bay Winter 2004 Salinity, San Mateo Bridge

Figure 10-16. South Bay Winter 2004 Salinity, Dumbarton

Figure 10-17. South Bay Winter 2004 Salinity, Channel Marker 17

Figure 10-18. South Bay Winter 2004 Salinity, Power Tower

Figure 10-19. South Bay Winter 2004 Salinity, Railroad Bridge

Figure 10-20. South Bay Winter 2004 Salinity, Alviso Slough

Figure 10-21. South Bay Winter 2004 Salinity, ACFCC

Figure 10-22. South Bay Winter 2004 Salinity Transect